IMPROVED CROSS-SHORE SEDIMENT TRANSPORT RELATIONSHIPS AND MODELS

By

JIE ZHENG

A DISSERTATION PRESENTED TO THE GRADUATE SCHOOL
OF THE UNIVERSITY OF FLORIDA IN PARTIAL FULFILLMENT
OF THE REQUIREMENTS FOR THE DEGREE OF
DOCTOR OF PHILOSOPHY

UNIVERSITY OF FLORIDA

1996

ACKNOWLEDGMENTS

I would like to express my deepest gratitude and appreciation to my advisor and the chairman of my supervisory committee Professor Robert G. Dean, for his constructive direction, enthusiasm, advice and unflagging support. His zeal and love for coastal engineering have inspired me throughout this four-year study, which has been a challenging, joyful and unforgettable experience in my life.

My thanks also go to committee members, Professors Daniel M. Hanes, Robert J. Thieke, Hsiang Wang and Ulrich H. Kurzweg, for their valuable advice, suggestions, discussions, comments and patience in reviewing this dissertation.

Appreciation is extended to all other faculty members and staff in the department for supplying various components of knowledge and help during this study. Special thanks go to Becky Hudson, Sandra Bivins, Lucy Hamm, Cynthia Vey, Helen Twedell, John Davis and Dr. Li-Hwa Lin for their help and kindness in the completion of this study. Gratitude is due to my friends in the department, Xu Wang, Yigong Li, Lynda Charles, Emre Otay, Albert Browder, Michael Dombrowski, Taerim Kim, Susan Harr, Michael Krecic, Michael Bootcheck, and Paul Devine, for their friendship and assistance.

My final acknowledgment is reserved for those whom I owe the most, my husband Jian Liu, for his love, support, encouragement and patience through these years, and my parents, who instilled in me the values of life that have made me to go this far, and have supported me all my life.

TABLE OF CONTENTS

Abstract of Dissertation Presented to the Graduate School
of the University of Florida in Partial Fulfillment of the
Requirements for the Degree of Doctor of Philosophy

IMPROVED CROSS-SHORE SEDIMENT TRANSPORT RELATIONSHIPS AND MODELS

By

Jie Zheng

August 1996

Chairperson: Robert G. Dean
Major Department: Coastal and Oceanographic Engineering

A modified nonlinear cross-shore sediment transport relationship is developed based on equilibrium beach profile concepts and dimensional scaling relationships. This nonlinear relationship provides a reasonable explanation for the significantly different time scales of beach evolution evident in various laboratory experiments. To predict a beach profile response under wave action, a finite difference method is applied to solve the sediment transport and continuity equations numerically. The proposed nonlinear model called "CROSS" is calibrated and compared with the commonly employed linear transport relationship using laboratory data. A total of seven large scale wave tank experiments from three different facilities are examined. The results demonstrate that the nonlinear transport model provides overall better predictions than the linear transport equations. The CROSS

model and the three other commonly used models are applied to predict beach erosion at Ocean City, Maryland, during the November 11, 1991, and January 4, 1992, storms. Seven survey lines are available for comparison with the numerical simulations. Two versions (2.0 and 3.0) of SBEACH are applied. Among the four models, the CCCL model is the only one overpredicting average dune erosion and the other three models have different degrees of underprediction with SBEACH version 2.0 underpredicting most. Overall, CROSS, EDUNE and SBEACH version 3.0 present reasonable predictions for both dune erosion and the entire profiles. The sensitivity of CROSS to the transport coefficient, active water depth, storm surge levels and the storm wave heights are studied for the storm erosion at Ocean City. It appears that CROSS is very insensitive to the transport coefficient. The subaqueous part of a profile is quite sensitive to the wave height and the subaerial part is less affected. The CROSS model provides better predictions with the ratio of active water depth to incoming wave height of 1 than with the ratio of 1.28, and the 20% increased storm surge yields a better simulation.

CHAPTER 1
INTRODUCTION

1.1 Motivation

The beaches are the transition zone between land and sea. They protect the shore from damage by coastal storms and hurricanes and provide valuable recreational resources. Their effectiveness as natural barriers depends on their size and shape, sediment characteristics and the severity of storms. Under the seasonal action of waves, currents and winds, beaches often erode during winters and accrete during summers. During storm surges the sea level rises considerably above the normal high water level. As a result the storm driven waves reach the front of the dunes and beach erosion occurs. The eroded sand is moved in an offshore direction and a new beach profile is developed. In fact, the process of storm erosion can be considered as the continuous adjustment of the beach profile to the changing hydrodynamic and meteorological conditions during the storm.

In coastal engineering, accurate estimates of beach profile evolution in response to storm waves and high water levels and the adjustment of beach fill to long term wave action are particularly important for a variety of regulatory and design purposes. The time scale associated with storm induced beach erosion is on the order of hours to days and depends on the duration, water level and wave conditions of the storm, while the time scale of beach fill adjustment is from months to years and depends on the fill material and the wave climate at

the site. Due to the complexities of surf zone hydrodynamics, sediment characteristics, and wave and water level conditions, an analytical treatment of beach profile change is difficult and requires recourse to numerical modeling, which requires an understanding of sediment transport. The objective of this study is to provide a better understanding of cross-shore sediment transport relationships and develop a numerical model to represent beach profile changes associated with variable waves and tides.

1.2 Nearshore Sediment Transport

1.2.1 Transport Processes and Related Problems

Sediment transport at a point in the nearshore zone can be considered in terms of cross-shore and longshore components. It appears that under a number of coastal engineering scenarios of interest, the transport is dominated by either the cross-shore or longshore component and this, in part, has led to a history of separate investigative programs for each of these two components. Longshore sediment transport figures prominently in situations involving loss of sediment supply, such as damming of rivers, and impoundment at structures and inlets. In these cases, longshore sediment transport is the major process governing nearshore topographic change. The cross-shore component determines profile evolution primarily for beaches far away from structures, inlets and river mouths, and under the case of increased water levels, storms and beach nourishment. In contrast to longshore sediment transport modeling, which has been studied for about five decades, a focus on cross-shore sediment transport modeling is relatively recent (about 20 years) and the uncertainty in predicting effects of all variables thus may be considerably greater.

Cross-shore sediment transport encompasses both offshore transport such as occurs during storms and onshore transport which dominates during mild wave conditions. Transport in these two directions appears to occur in significantly distinct modes and with remarkably disparate time scales. The offshore transport moves sand from the dune to the offshore bar in hours to days during a storm, whereas the onshore transport may take months to years to move sand from the offshore bar to the dry beach. The difficulties in predicting transport in the two directions also differ substantially. Offshore transport is simpler and the more predictable of the two with transport more or less in phase over the entire active profile. This is fortunate for coastal engineers since there is considerably greater engineering concern and interest in offshore transport due to the potential for damage to structures and loss of land.

Cross-shore sediment transport is relevant to a number of coastal engineering problems including (a) beach and dune response to storms, (b) the equilibration of a beach project that is placed at a slope steeper than equilibrium, (c) "profile nourishment" in which the sand is placed in the nearshore with the expectation that it will move landward nourishing the beach (this involves the more difficult problem of onshore transport), (d) shoreline response to sea level rise, (e) seasonal changes of shoreline positions, (f) overwash, the process of landward transport due to overtopping of the normal land mass due to high tides and waves, (g) scour immediately seaward of shore parallel structures (e.g. seawalls), and (h) cross-shore and longshore coupled transport around shore normal structures (e.g. jetties and groins) in which the steeper and milder slopes on the updrift and downdrift sides induce seaward and landward components, respectively. These problems are schematized in Figure 1.1.

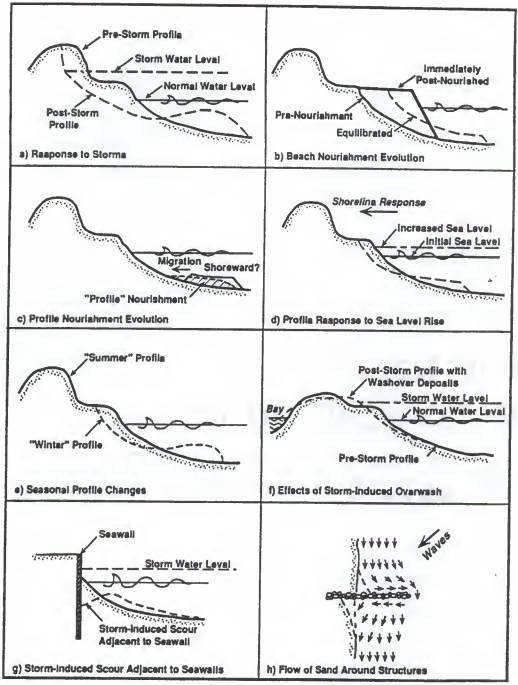

Figure 1.1 Problems and processes in which cross-shore sediment transport is relevant (after Dean, draft of Chapter III of Coastal Engineering Manual).

1.2.2 Bedload and Suspended Load

A complete understanding of cross-shore sediment transport is complicated by the contribution of both bed and suspended load transport components. Bagnold (1956) defined bedload as the part of the total load which is supported by intergranular forces, and the suspended load as the part supported by fluid drag. Usually particles entrained in the bedload exhibit motions of rolling, sliding and sometimes jumping in the bed layer, whereas particles entrained in the suspended load are suspended in the water column. Turbulence is the most important factor in the suspension of sediment. Due to gravity, particles tend to settle to the bottom; however, irregular motions of the fluid introduced by turbulence tend to lift particles from the bed and support them in suspension. For the cross-shore sediment transport, bedload is dominant outside the surf zone because of the relative mild fluid conditions. However, owing to the highly turbulent flow field caused by wave breaking, suspended load prevails inside the surf zone.

Generally bedload is related to the shear stress acting on the bottom. Several researchers have proposed expressions for the transport rate in an oscillatory flow. Bailard and Inman (1981) suggested that bedload transport rate was proportional to the 1.5 power of bottom shear stress. Trowbridge and Young (1989) presented a linear relationship between the transport rate and the bottom shear stress. There are several causes of shear stresses acting on the bottom in the nearshore active zone: (1) shear stress induced by gravity, (2) shear stress due to nonlinear waves, (3) shear stress caused by return flow, and (4) shear stress related to boundary rotation flow. The magnitudes of these stresses can be remarkably

different inside and outside surf zone. A detail discussion of these shear terms will be presented in Chapter 2.

Suspended sediment transport in the cross-shore direction under wave action primally results from the contributions due to the oscillatory first-order velocity (intermittent transport) and the mean cross-shore current. Dean (1973) developed a heuristic model for cross-shore transport in the surf zone based on the intermittent suspension of sand grains by wave breaking and the eventual settling of sand to the bottom. A wave breaking in the surf zone lifts sand from the bottom up into the water column to a particular elevation. The time required for the sand to fall back to the bottom is determined by the ratio of the elevation to the sediment falling velocity. If the fall time is less than half the wave period, the sand grain should move onshore. Alternatively if the fall time is greater, the sand particle would be carried offshore. The elevation is dependent on the wave height, as it seems reasonable that larger waves would lift sand to a higher elevation than smaller waves. Therefore Dean assumed that the elevation is proportional to the breaking wave height. The direction of intermittent transport was determined by the so-called "fall velocity parameter," which is a non-dimensional parameter of breaking wave height divided by wave period and sediment fall velocity. For most ocean wave cases, the mean cross-shore current is caused by the mean mass return flow in the offshore direction. As a result the suspended transport contributed from the mean flow is always in the offshore direction no matter how high the sediment suspended. Because the cross-shore velocity profiles inside the surf zone are different from those outside the surf zone, the contributions of the mean flow to suspended sediment transport inside the surf zone are different from those outside the surf zone. Under unbroken

wave conditions since the upper part of water column has greater return flow velocity but very little suspended sediment, the suspended transport due to the mean flow is almost negligible. By contrast, inside the surf zone the lower part of water column has larger return flow velocities and high sediment concentration, therefore the suspended sediment transport caused by mean flow could be significant.

1.3 Review of Cross-Shore Sediment Transport Relationships and Models

1.3.1 General

Some recent interesting reviews of cross-shore sediment transport models have been reported by Broker Hedegaard et al. (1992), Steetzel (1993), and Schoonees and Theron (1995). Different methods and viewpoints have been applied. Hedegaard et al. made an inter-comparison of six coastal profile models against measured profile evolutions from a large wave flume (under dune erosion conditions). Steetzel classified transport formulae as empirical transport, shear stress related transport, energy dissipation related transport, energy dissipation related suspension and velocity related transport. Schoonees and Theron summarized ten internationally developed transport models according to their theoretical basis and morphological verification data.

In the present review, cross-shore sediment transport models are broadly classified into two groups: "open loop" and "closed loop" models. An "open loop" model is not constrained a priori to the final profile and the sediment transport is determined by sediment concentration and fluid motions. "Closed loop" sediment transport models are based on equilibrium beach profile concepts (Bruun 1954 and Dean 1977) and assume that a profile will eventually achieve equilibrium if exposed to the same conditions for a long time. Cross-shore

transport is caused by deviations of a beach profile from equilibrium. Methodologically "open loop" models are microscale approaches based on detailed physics of the process, while "closed loop" models are more macroscale and utilize conservation laws and heuristic arguments that provide reasonable solutions. Owing to the complexities of highly turbulent flow inside the surf zone, there is considerable uncertainty in the detailed physics of wave breaking processes and related sediment transport. Therefore the macroscale approach is a powerful tool to predict beach profile change at the present time.

1.3.2 "Closed Loop" Models

The earliest relationship between increased water level and profile response was developed by Bruun (1962), which does not require any specific form of the equilibrium profile, but only requires that the form be known. The response is considered in terms of the horizontal recession of the profile and sea level rise. Two requirements must be satisfied by the new profile. First, the profile shape does not change with respect to the sea level. Secondly, the sand volume in the profile must be conserved. One restriction of the Bruun model is that the sea level rise should be much less than the berm height, since the berm height relative to the rising sea level is considered fixed. Edelman (1972) removed the limitation of relative small changes in water level by accounting for the progressive decrease in relative dune elevation. Since the two above assume that a beach profile maintains its equilibrium form immediately in response to the water level rise, no sediment transport relationship is required. However, it is not suitable to apply such static models (no lag) to short-term profile changes.

Following the idea of Bakker (1968), Swart (1974 a, b) schematized the beach profile into 4 zones referred to as backshore, onshore profile, offshore profile and transition area and

developed a time-dependent cross-shore model. With L_1 and L_2 representing the schematized lengths of onshore and offshore profiles, respectively, the transport equation is written as

$$Q = q\,[W-(L_2-L_1)_t] \tag{1.1}$$

where Q is the time dependent cross-shore sediment transport rate, q is a constant for a specific set of boundary conditions, and W and $(L_2-L_1)_t$ are equilibrium and time dependent values of (L_2-L_1), respectively.

Chiu and Dean (1984,1986) developed the CCCL model, which is still used by the State of Florida to establish the location of the State Coastal Construction Control Line associated with the erosion limits of a 100 year return period storm event. Under erosive water level and wave conditions, the time dependent beach recession, R(t), at each depth contour is given by

$$R(t) = R_\infty(1-e^{-Kt}) \tag{1.2}$$

in which R_∞ is the equilibrium recession for the particular condition at that time and K is a decay parameter. Strictly speaking, this is a beach profile change model since there is no sediment transport relationship involved. Compared with Bruun and Edelman models, CCCL is time dependent and can be applied to short-term profile change caused by storms.

Two wave energy dissipation related transport models are EDUNE (Kriebel 1982, 1990, Kriebel and Dean 1985) and SBEACH (Larson and Kraus 1989, Larson et al. 1989). According to equilibrium beach profile concepts, offshore transport continues until the wave energy dissipation per unit volume of water becomes uniform over the entire surf zone. Based

on this consideration, EDUNE expresses the local cross-shore sediment transport rate, Q, in the surf zone as

$$Q = K_e(D - D_*) \tag{1.3}$$

in which K_e is a dimensional transport coefficient, D and D_* are the actual and equilibrium wave energy dissipation per unit volume of water, respectively, and D_* depends on the sand size. Eq. (1.3) was first proposed by Moore (1982) and later modified by Kriebel (1982) and Kriebel and Dean (1985). In SBEACH, the sediment transport rate across the nearshore active zone is calculated by different relationships in four distinct zones identified as pre-breaking zone (extending offshore from the breaking point), transition zone (from the break point to the plunge point), broken wave zone (the plunge point to the seaward limit of the swash zone), and swash zone (from the seaward swash zone to the run-up limit). A transport relationship similar to Eq. (1.3) is applied in the broken wave zone with a term added to account for the effect of local slope and written as

$$\begin{aligned} Q &= K_s\left(D - D_* + \frac{\epsilon}{K_s}\frac{dh}{dx}\right), & D > D_* - \frac{\epsilon}{K_s}\frac{dh}{dx} \\ &= 0, & D < D_* - \frac{\epsilon}{K_s}\frac{dh}{dx} \end{aligned} \tag{1.4}$$

where K_s and ϵ are dimensional coefficients and dh/dx is the local profile slope. The transport rates in the other three ranges are established empirically in accordance with Saville's large wave tank experiments (Kraus 1988).

1.3.3 "Open Loop" Models

"Open loop" models usually relate cross-shore sediment transport to the detailed physics of the flow field such as sediment concentration, fluid velocity, and bottom shear stress. Three different types of formulae will be briefly reviewed here.

(1) Sediment transport rate based on the product of flow velocity and sediment concentration.

The Dally model (Dally 1980, Dally and Dean 1984) presented the net time-averaged flux of suspended sediment past a section in the nearshore zone as

$$Q = \int_{depth} u(z)\, c(z)\, dz \tag{1.5}$$

where u(z) and c(z) are averaged horizontal velocity and sediment concentration at level z, respectively. The flow regime is divided into an upper layer where only mean flow is considered and a lower layer where both mean flow and orbital velocity are taken into account. In the lower layer, the fall time of a sand particle is determined by its elevation and fall velocity. According to linear wave theory, the particle will traverse a horizontal displacement during the fall time. Thus, the average horizontal velocity of the particle during one wave cycle due to the orbital motion is equal to the ratio of the horizontal displacement to the fall time. The interface between the layers is determined by the elevation at which a particle will fall back to the bottom in one wave period.

LITCROSS (Broker Hedegaard et al. 1992) is a coastal profile model developed by the Danish Hydraulic Institute. The net sediment transport is calculated as bed and suspended load. The instantaneous bed load and nearbed boundary condition for the vertical distribution

of suspended sediment are determined as functions of the instantaneous shear stress (Engelund and Fredsoe 1976). The total suspended sediment transport over a wave period is found from

$$Q = \frac{1}{T} \int_{period} \int_{depth} c\, u\, dz\, dt + \int_{depth} u_1 \bar{c}\, dz \qquad (1.6)$$

where the velocity, u, and the concentration, c, in the first integral are functions of time and elevation, u_1 is Lagrangian drift, $\bar{c}$ denotes the time averaged concentration, and T is the wave period. The time varying vertical distribution of suspended concentrations is calculated by the vertical diffusion equation according to Deigaard et al. (1986).

Steetzel (1993) also presented his cross-shore transport model as the integral of the product of concentration and velocity over time and depth. The sediment concentration is solved from a one-dimensional, non-stationary convection-diffusion equation. The reference concentration at the bed is assumed to be related to the kind of breaking and the dissipation of the turbulent kinetic energy. The cross-shore transport rate is calculated in two parts, that is, below and above the trough level. Above the trough level, concentration is a constant and given by that at the mean water level.

(2) Sediment transport rate related to velocity powers

A representation of this type of model was proposed by Bailard (Bailard and Inman 1981, Bailard 1981, 1982) based on the concepts of stream transport developed by Bagnold (1963, 1966). Bagnold assumed that the sediment was transported in two distinct modes, each differing by way of the support of the sediment grains. Sediment transport as bedload

is supported by the bed via grain to grain interactions, while sediment transport as suspended load is supported by the stream fluid via turbulent diffusion. In both modes, energy is expended by the stream in transporting the sediment load. Bagnold, comparing the stream to a machine, defined the sediment transport efficiency as the ratio of the rate of energy expended by sediment load to the total rate of energy produced by the stream. In essence, he assumed that the instantaneous sediment transport rate was directively proportional and reacted immediately to the instantaneous energy dissipation rate per unit bed area.

Bailard (1981) refined Bagnold's work for the cross-shore sediment transport problem and expressed the total load time averaged sediment transport equation as

$$Q = \rho c_f \frac{\epsilon_B}{\tan\phi}\left[<|\vec{u}|^2\vec{u}> - \frac{\tan\beta}{\tan\phi}<|\vec{u}|^3>\vec{i}\right] + \rho c_f \frac{\epsilon_S}{W}\left[<|\vec{u}|^3\vec{u}> - \frac{\epsilon_S}{W}\tan\beta<|\vec{u}|^5>\vec{i}\right] \quad (1.7)$$

where ρ is the density of water, c_f is drag coefficient of the bed, ϵ_B and ϵ_S are bed and suspended load efficiency factors, ϕ is the internal angle of friction for the sediment, $\tan\beta$ is the bottom slope, $\vec{u}$ is the instantaneous velocity vector, $\vec{i}$ is a unit vector in onshore direction, W is the sediment fall velocity, and the $< >$ means time average over a wave period. This formula has been widely applied by others such as Stive (Stive 1986, Roelvink and Stive 1989) and Nairn (1990). Three coastal profile models have been developed based on Bailard transport relationship. They are UNIBEST of Delft Hydraulics, NPM of Hydraulic Reseach, and SEDITEL of Laboratoire National d'Hydraulique.

There are other velocity power related sediment transport relationships. One example was given by Shibayama and Horikawa (1982). The transport rate accounts for bedload and

suspended load. Both bed and suspended loads are proportional to the velocity to the sixth power.

(3) Sediment transport determined by the product of velocity and bottom shear stress

Watanabe (1988) presented a sediment transport rate equation related to local wave-current conditions and bottom shear stress. The total transport rate is the sum of contributions from mean current, Q_c, and waves, Q_w, which are expressed, respectively, by

$$\begin{aligned} Q_c &= A_c(\tau-\tau_c)\vec{U}/\rho g \\ Q_w &= A_w F_D(\tau-\tau_c)\vec{u}_b/\rho g \end{aligned} \tag{1.8}$$

where A_c and A_w are nondimensional coefficients for mean current and wave induced transport, respectively, $\vec{U}$ is the current velocity vector, $\vec{u}_b$ is the amplitude of the near-bottom wave orbital velocity vector, τ is the maximum value of the bottom shear stress in a wave-current coexisting system, τ_c is the critical shear stress, F_D is a direction function for wave-induced net transport, and g is the gravitational acceleration. The coastal profile model WATAN3 developed by University of Liverpool is based on the Watanabe transport equations.

There are some relationships in addition to the above three types such as the one developed by Nishimura and Sunamura (1986), in which the transport rate is related empirically to the Ursell number representing the skewness of water particle velocity profile and the Hallermeier parameter indicating the intensity of sediment movement.

Most "open loop" profile change models include modeling of hydrodynamic processes to different degrees. The sediment transport calculation is related to the properties of

sediment and flow field. A interesting inter-comparison of five coastal profile change models developed in Europe was presented by Broker Hedegaard et al. (1992). The five models are LITCROSS of Danish Hydraulic Institute, UNIBEST of Delft Hydraulics, NPM of Hydraulic Research, WATAN3 of University of Liverpool, and SEDITEL of Laboratory National d'Hydraulique. The associated transport relationships have been described above. The models were tested against measured profile evolution from a large wave flume. The initial profile is a planar beach with a slope of 1:20. The experiment was carried out under regular waves with a wave height of 1.5 m and period of 6 s. The velocities and the transport rates calculated across the planar profile are shown in Figures 1.2 and 1.3. The measured and calculated profiles after 4.3 hours are compared in Figure 1.4. It is noticed that the all five models present quite good fits for the profile although the calculated velocity and transport rates are markedly different. It seems that considerable uncertainty in the understanding of surf zone hydrodynamics and sediment transport process still exists.

1.4 Scope of Study

A major objective of this dissertation is to improve "closed-loop" cross-shore sediment transport relationships. In the following studies, a modified transport equation is proposed according to dimensional arguments. A cross-shore profile change model called CROSS is developed based on the modified transport equation and the conservation of sand. Three sets of different laboratory experiments are applied to the calibration of CROSS. Finally, the model is tested and compared with other three commonly used "closed loop" models against data obtained from field storm erosion.

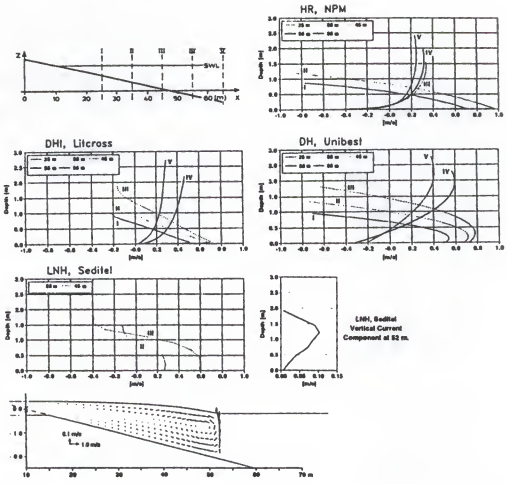

Figure 1.2 Velocity components calculated by NPM, LITCROSS, UNIBEST and SEDITEL and 2-D current field calculated by SEDITEL (after Broker Hedegaard et al., 1992).

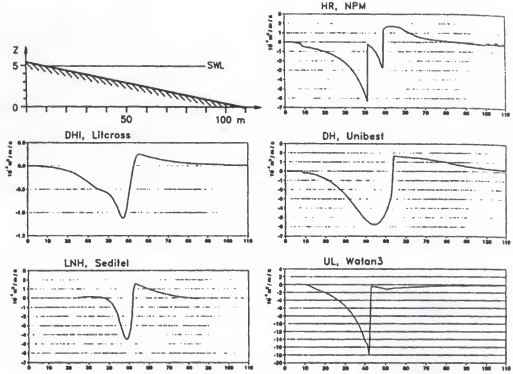

Figure 1.3 Cross-shore sediment transport calculated by NPM, UNIBEST, LITCROSS, SEDITEL and WATAN3 (after Broker Hedegaard et al., 1992).

To better understand the surf zone sediment transport process, Chapter 2 commences with a qualitative description of the time-averaged bottom shear stresses acting in the nearshore. The total shear stress is composed of four components. They are shear stress due to gravity, shear stress induced by non-linear waves, shear stress related to the boundary rotation flow, and shear stress caused by the mean mass return flow.

Chapter 3 is devoted to the development of CROSS based on the concepts of equilibrium beach profiles. The relationship between the transport rate and the deviation of the actual wave energy dissipation per unit volume from equilibrium is discussed according

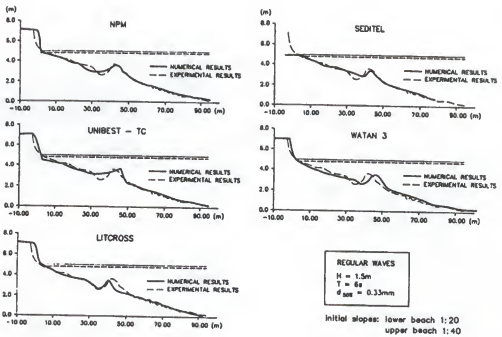

Figure 1.4 Comparison of measured and calculated coastal profiles after 4.3 hours of exposure (after Broker Hedegaard et al. 1992).

to dimensional considerations. The profile change is determined by both the transport and the continuity equations. The two equations are solved by the finite difference method with a staggered grid. A detailed numerical process is presented.

The calibrations of CROSS are described in Chapter 4. Three sets of large wave tank data are utilized, including three cases in the large German wave flume in Hanover (Dette and Uliczka 1987), three cases from Saville's large wave tank experiments (Kraus 1988), and one case from the SUPERTANK experiments at Oregon State University (Kraus and Smith 1994). Among the seven experiments, one of the German set was carried out with a Jonswap-Spectrum of random waves, the Supertank case was run with the combination of random

and regular waves, and the others are conducted under regular waves. The best-fit transport coefficient is determined as the value providing the least squares error for the fitting of eroded volume in each experiment. Based on the calibration results, a transport coefficient is recommended for the applications of CROSS according to the average of the best-fit values in the seven experiments.

In Chapter 5, the CROSS model with the recommended transport coefficient is evaluated by the same experiments used in Chapter 4 for the calibration of CROSS. The predictions of CROSS with the recommended transport coefficient are compared with those with the best-fit values for each experiment. The comparisons include the time history of eroded volume and the profile evolutions.

The applications of CROSS for the November 1991 and January 1992 storm erosion at Ocean City, Maryland, are presented in Chapter 6. The predictions of CROSS are compared with three other models commonly used in the United States. The three models are CCCL (Chiu and Dean 1984,1986), EDUNE (Kriebel and Dean 1985, Kriebel 1989,1990), and SBEACH (Larson and Kraus 1989, Larson et al. 1989). A sensitivity study of CROSS is also included in this chapter to test the sensitivity of the model to changes wave and surge conditions during storms.

Finally, Chapter 7 presents a summary, documents conclusions of the study, and proposes some recommendations for future study.

CHAPTER 2
SHEAR STRESSES ACTING IN THE NEARSHORE

2.1 Introduction

A requirement for a proper understanding of coastal sediment transport is a consideration of forces which act in the nearshore active zone. There are three kinds of forces governing the behavior of sediment particles whether they are resting on the bed or suspended in the water column. These are gravity forces, intergranular forces related to continuous sediment contact, and the wave and current induced fluid forces. The magnitudes of wave induced forces can by remarkably different inside and outside the surf zone. Due to the strong and large scale turbulent flow caused by wave breaking, sediment is typically highly mobilized inside the surf zone. Changes in beach profiles result from intermittent suspension, turbulence, bottom shear stress and gravity. Outside the surf zone, the wave energy dissipation and the turbulence occur mainly within the near-bed wave boundary layer. Within this zone, the bottom shear stress related bedload sediment transport becomes the primary factor in controlling profile change.

Under equilibrium conditions, the forces acting on the sediment particles are in dynamic balance, and, although there is motion of individual particles under even low wave activity, the profile remains more or less static. Cross-shore sediment transport occurs when the nearshore hydrodynamic conditions change thereby modifying one or more of the forces

resulting in an imbalance and causing a sediment transport gradient and profile change. Established terminology is that onshore and offshore directed forces are referred to as "constructive" and "destructive," respectively. It is evident that some forces could behave as constructive under certain conditions and destructive under others. As the result of the combined constructive or destructive forces, sediment is transported onshore or offshore, respectively. For suspended particles, the movement is determined by gravity, drag, lift, added mass force, etc. acting on the particle. For particles resting on the bed, the bottom shear stress is the dominant force. When the bottom shear stress is less than the critical shear stress (friction), particles are under static conditions and no motion occurs. As the bottom shear stress overcomes friction, particles will be moved in the shear stress direction and bedload transport commences. Generally, the bottom shear stresses in the cross-shore direction include contributions from gravity, waves, currents, bottom boundary layer rotation flow, and undertow due to the mass and momentum flux. As waves and currents vary with time, the shear stresses also change temporally. In principle, the sediment transport processes are related directly to the instantaneous shear stresses. However, as a first step, only mean shear stresses averaged over one wave period will be discussed here.

In this chapter, the critical shear stress is discussed first. When the total bottom shear stress is less then the critical shear stress, the intergranular friction will keep sand particles from moving. Under wave conditions, the total bottom shear stress is due to the superposition of four components. These are shear stress induced by gravity, shear stress due to nonlinear waves, shear stress related to the boundary layer rotation flow, and shear stress caused by the mass return flow. Their magnitudes depend on the wave breaking, wind speed, sediment size

and bed slope. To provide a better understand of these forces, a detailed example will be presented to quantify the directions and magnitudes of the four stress terms both inside and outside the surf zone.

2.2 Critical Shear Stresses

The intergranular forces acting on a sediment particle are the normal and frictional forces resulting from the surrounding sediment. For grains at rest, the static angle of repose, ϕ_s, is determined by the friction coefficient, i.e. the ratio between the maximum sustainable shear stress (i.e. critical shear stress), τ_{cr}, and the effective normal stress, σ_e (see Figure 2.1). For mostly sandy materials, the static angle of repose is between 26 and 34 degrees (Nielsen, 1992). For shearing (moving) materials of near maximum concentration, the friction coefficient is only slightly less than the static. Hence the dynamic angle of repose, ϕ_d, is of a similar magnitude to the static angle. Hance and Inman (1985) suggested a typical value of 31 degrees for beach sand.

A different parameter, the Shields parameter, describing the frictional shear stress was suggested by Shields in a study of the incipient motion in steady flow as

$$\theta_s = \frac{\tau}{\rho(s-1)gD} \tag{2.1}$$

where θ_s represents the Shields parameter, ρ is mass density of water, s is relative density of sediment, and D is the sediment diameter. The critical Shields parameter, $\theta_{s,cr}$, which corresponds to the critical shear stress, τ_{cr}, is the effective Shields parameter at which sediment movement starts. For sand grains quiescent under static water, the critical Shields parameter is related to the angle of repose by the relationship, $\theta_{s,cr} = \sin\phi$. Under waves and

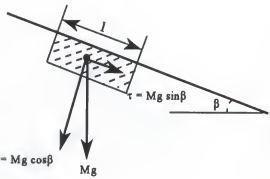

Figure 2.1. The friction coefficient, $(\tau/\sigma)_{max}$, equals $\tan\phi_s$, where ϕ_s is the static angle of repose.

currents, this parameter becomes much less because the fluid lift force and near-bottom turbulence decreases the effective normal stress. Although some laboratory studies (Natarajan 1969, and Hammond & Collins 1979) and field studies (Amos et al. 1988) have been conducted, it is impossible to define a sharp criterion for the initiation of motion under combined wave and current flows. Based on their observations, Amos et al. recommended 0.04 as the critical Shields parameter. Therefore, for the case of bottom shear stress less than 0.04 times the submerged weight of the sand, sediment will remain static on the bottom due to friction effects.

2.3 Gravity

When the sand bed is horizontal, gravity acts normally to the bottom and has no contribution in the shear direction. For a monotonic beach profile, gravity becomes an obvious destructive force which acts downslope, i.e. seaward. However, for the case of a barred profile, gravity can act in the shoreward direction over a portion of the profile. Overall, gravity tends to "smooth" any irregularities that occur in the profile. If gravity were the only force acting , the only possible equilibrium profile would be horizontal and sandy beaches as

we know them would not exist. For particles in the sand bed, the tangent component of gravity force per unit bottom area at a layer of one grain thickness will be determined by the component in the beach slope direction as

$$\tau_b = \alpha \rho g (s-1) d \sin\beta \tag{2.2}$$

Where α is the sediment concentration in the sand bed, d is the mean diameter of the sediment, and β is the beach slope.

2.4 Shear Stress Due to Nonlinear Waves

As noted above, the constructive forces are those that tend to cause onshore sediment transport. For classic nonlinear wave theories (Stokes, Cnoidal, Solitary, Stream Function etc.), the wave crests are higher and of less duration than the troughs. This feature is most pronounced just outside the breaking point. The oscillatory water particle velocities are usually expressed as a sum of phase-locked sinusoids such as for the Stokes and Stream Function wave theories. Although the time averaged water particle velocity is zero, the average bottom shear stress, τ_b , is directed onshore and expressed as

$$\overline{\tau_b} = \rho \frac{f}{8} \overline{|v_b| v_b} \tag{2.3}$$

Where f is Darcy-Weisbach friction coefficient and v_b is the instantaneous wave induced water particle velocity at the bottom. Dean (1987) developed the average bottom shear stress based on the Stream Function nonlinear wave theory and presented the results in the non-dimensional form shown in Figure 2.2.

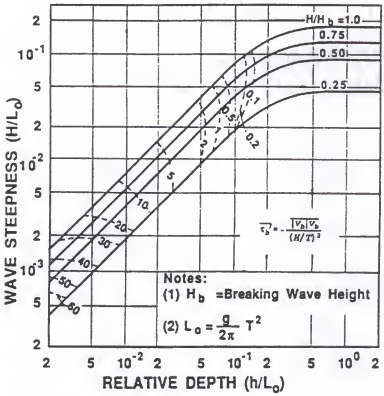

Figure 2.2 Isolines of non-dimensional average bottom shear stress, $\overline{\tau_b}$, versus relative depth and wave steepness (Dean 1987). Note the bottom shear stresses are directed shoreward.

2.5 Boundary Rotation Flow Related Shear Stress

The second constructive force originates from the net mean onshore directed streaming velocity induced by wave motion in the bottom boundary layer. This streaming motion was first observed by Bagnold (1940) in the laboratory and has been studied quantitatively by Longuet-Higgins (1953). The mechanism producing a mean bottom shear stress is reviewed as follows[1]. To satisfy the no-slip bottom boundary condition, the

[1] The following development is a modification of the Longuet-Higgins approach due to James Kirby (personal comminution).

particles of fluid in contact with the boundary must have the same velocity as the boundary itself. But quite near the bottom the fluid is in motion with velocities comparable to that in the interior potential flow of the fluid. This implies that there is strong vorticity in the neighborhood of the bottom. This vorticity modifies the vertical velocity, which is correlated with the streamwise velocity at the outer edge of the boundary layer, so that there is a change in the mean flux of streamwise momentum across the top of boundary layer. This change in the mean momentum flux must be balanced by a mean bottom shear stress.

The case considered here is that of periodic linear waves propagating shoreward above a gently sloping sand bottom with straight and parallel depth contours. The equations governing the water waves flow are the continuity equation and the Navier-Stokes equations

$$\begin{aligned} \frac{\partial v}{\partial y}+\frac{\partial w}{\partial z} &= 0 \\ \frac{\partial v}{\partial t}+\frac{\partial v^2}{\partial y}+\frac{\partial vw}{\partial z} &= -\frac{1}{\rho}\frac{\partial P}{\partial y}+\varepsilon\left(\frac{\partial^2 v}{\partial y^2}+\frac{\partial^2 v}{\partial z^2}\right) \\ \frac{\partial w}{\partial t}+\frac{\partial vw}{\partial y}+\frac{\partial w^2}{\partial z} &= -\frac{1}{\rho}\frac{\partial P}{\partial z}+\varepsilon\left(\frac{\partial^2 w}{\partial y^2}+\frac{\partial^2 w}{\partial z^2}\right)-g \end{aligned} \tag{2.4}$$

where the y axis is positive offshore and coincides with the mean water surface, the z axis is perpendicular to the water surface and positive upward, (v,w) are the corresponding velocity components in (y,z) directions, P is the water pressure, and ε is the kinematic eddy viscosity. It is convenient to divide the flow into two parts with potential and rotational components,

$$\begin{aligned} v &= v_p+v_r = -\frac{\partial \Phi}{\partial y}+v_r \\ w &= w_p+w_r = -\frac{\partial \Phi}{\partial z}+w_r \end{aligned} \tag{2.5}$$

In which, the subscripts p and r represent the potential and rotational components respectively, and Φ is the velocity potential for the interior wave flow. The no-slip boundary condition requires the velocity (v,w) to be equal to zero at the bottom. It is assumed that the conditions at the free surface are unaffected by the viscous flow since the boundary layer is assumed thin. This requires

$$\begin{aligned} v &\to -\frac{\partial \Phi}{\partial y} \quad or \quad v_r \to 0 \quad as \quad (h+z) \to \infty \\ w &\to -\frac{\partial \Phi}{\partial z} \quad or \quad w_r \to 0 \quad as \quad (h+z) \to \infty \end{aligned} \tag{2.6}$$

where h is the mean water depth. The first order potential and viscous velocity components can be solved from the linearized Euler and approximate boundary layer equations,

$$\begin{aligned} \nabla^2 \Phi &= 0 \\ \frac{\partial v_r}{\partial t} &= \varepsilon \frac{\partial^2 v_r}{\partial z^2} \\ \frac{\partial w_r}{\partial t} &= \varepsilon \frac{\partial^2 w_r}{\partial z^2} \end{aligned} \tag{2.7}$$

where ∇ is the Laplace operator. For waves propagating onshore, the solutions of Eqs. (2.7) are of the forms

$$\begin{aligned} \eta &= 0.5 H e^{i(ky+\sigma t)} \\ \Phi &= \bar{\Phi}(z)\, e^{i(ky+\sigma t)} \\ v_r &= \bar{v}_r(z)\, e^{i(ky+\sigma t)} \\ w_r &= \bar{w}_r(z)\, e^{i(ky+\sigma t)} \end{aligned} \tag{2.8}$$

in which i is the imaginary number ($\sqrt{-1}$), η is the instantaneous water elevation, H is the wave height, k is the wave number, and σ is the wave angular frequency. Solving Eqs. (2.7) with the boundary condition (2.6) gives

$$\begin{aligned} \tilde{\Phi}(z) &= A\cosh k(h+z) + B\sinh k(h+z) \\ \tilde{v}_r(z) &= C\exp[-(1+i)\frac{h+z}{\delta}] \\ \tilde{w}_r(z) &= D\exp[-(1+i)\frac{h+z}{\delta}] \end{aligned} \tag{2.9}$$

where $\delta = \sqrt{2\varepsilon/\sigma}$ represents the boundary layer thickness and is very small compared with the water depth, and A, B, C and D are constants to be determined. By substituting (2.9) into the continuity equation and the no-slip bottom boundary condition, the constants B, C and D can be replaced by the constant A. The solution becomes

$$\begin{aligned} \tilde{\Phi}(z) &= A\,[\cosh k(h+z) - \frac{1-i}{2}k\delta\sinh k(h+z)] \\ \tilde{v}_r(z) &= ikA\exp[-(1+i)\frac{h+z}{\delta}] \\ \tilde{w}_r(z) &= -\frac{1-i}{2}k^2\delta A\exp[-(1+i)\frac{h+z}{\delta}] \end{aligned} \tag{2.10}$$

in which, A is related to the wave height through the linearized free surface dynamic and kinematic boundary conditions as

$$\begin{aligned} \frac{H}{2} &= \frac{i\sigma}{g}A\,[\cosh kh - \frac{1-i}{2}k\delta\sinh kh] \\ \frac{H}{2} &= -\frac{kA}{i\sigma}[\sinh kh - \frac{1-i}{2}k\delta\cosh kh] \end{aligned} \tag{2.11}$$

Eliminating H and A in Eqs. (2.11) results in the dispersion relationship

$$\sigma^2 [1 - \frac{1-i}{2} k\delta \tanh kh] = gk \tanh kh [1 - \frac{1-i}{2} k\delta \coth kh] \qquad (2.12)$$

As viscous effects approach zero, (2.12) clearly approaches the classic wave dispersion relationship, $\sigma^2 = gk \tanh kh$, i.e., Dean and Dalrymple (1991). In most cases, $k\delta << 1$, so that the deviations to σ and k determined by (2.12) are small.

Eq. (2.12) generally predicts complex σ and k combinations, which correspond to the wave energy decay temporally and spatially. The two simplest cases are as follows:

(1) σ is real and $k = k_r + ik_i$. Time periodic waves decay with propagation distance.

(2) k is real and $\sigma = \sigma_r + i\sigma_i$. Spatial periodic waves decay in time.

The first case is more generally applicable to ocean waves, while the second case may be used to describe cases such as wave decay in basins, etc. For the problems concerned, we assume $k_i/k_r << 1$ and $kh << 1$ and analyze the first alternative further in detail. Substituting $k = k_r + ik_i$ into Eq. (2.12), retaining only the first order terms, and separating the real and imaginary parts yield

$$\begin{aligned} \sigma^2 [1 - \frac{k_r\delta}{2} \tanh k_r h] &= g k_r [\tanh k_r h - \frac{k_r\delta}{2}] \\ \sigma^2 \frac{k_r\delta}{2} \tanh k_r h &= \frac{g k_r k_i h}{\cosh^2 k_r h} + \frac{g k_r^2 \delta}{2} + g k_i \tanh k_r h \end{aligned} \qquad (2.13)$$

Assuming $k_r = k + \Delta k$, where k is determined by $\sigma^2 = gk \tanh kh$, we obtain

$$k_r = k + \frac{k^2\delta}{2kh + \sinh 2kh}$$
$$k_i = -\frac{k^2\delta}{2kh + \sinh 2kh} \tag{2.14}$$

Thus waves of fixed frequency are shortened by friction, and their phase speed is reduced. The constant A can be solved from (2.11) as

$$A = -i\frac{H\sigma}{2k\sinh kh}\left[1 + \frac{k\delta}{\sqrt{2}}\coth kh \exp(-i\frac{\pi}{4})\right] \tag{2.15}$$

Combing Eqs. (2.8), (2.10) and (1.15) together, the real parts of potential and rotational velocities are presented as

$$\Phi(z) = \frac{H\sigma\cosh k(h+z)}{2k\sinh kh}\sin\theta + \frac{H\sigma\delta\cosh kz}{2\sqrt{2}\sinh^2 kh}\sin(\theta-\frac{\pi}{4})$$
$$v_p(z) = -\frac{H\sigma\cosh k(h+z)}{2\sinh kh}\cos\theta - \frac{H\sigma k\delta\cosh kz}{2\sqrt{2}\sinh^2 kh}\cos(\theta-\frac{\pi}{4}) \tag{2.16}$$
$$w_p(z) = -\frac{H\sigma\sinh k(h+z)}{2\sinh kh}\sin\theta - \frac{H\sigma k\delta\sinh kz}{2\sqrt{2}\sinh^2 kh}\sin(\theta-\frac{\pi}{4})$$

and

$$v_r(z) = e^{-\xi}\left[\frac{H\sigma}{2\sinh kh}\cos(\theta-\xi) + \frac{H\sigma k\delta\cosh kh}{2\sqrt{2}\sinh^2 kh}\cos(\theta-\xi-\frac{\pi}{4})\right]$$
$$w_r(z) = -e^{-\xi}\frac{H\sigma k\delta}{2\sqrt{2}\sinh kh}\sin(\theta-\xi-\frac{\pi}{4}) \tag{2.17}$$

where $\theta = ky + \sigma t$ and $\xi = \frac{h+z}{\delta}$. Since δ/h is very small, the higher order terms are neglected.

We now consider the streamwise mean momentum flux in the bottom boundary layer and the possibility of mean flows. Neglecting the effects of wave height damping and wave length shortening caused by bottom friction, averaging the second equation of (2.4) over a wave period yields a second order mean flow in the boundary layer

$$\frac{\partial \overline{vw}}{\partial z} = \varepsilon \frac{\partial^2 \bar{v}_r}{\partial z^2} \tag{2.18}$$

where the over bar means the time average over a wave period. The mean shear stress caused by the boundary viscous flow is obtained by integrating (2.18) from an arbitrary depth, z, to the surface

$$\tau(z) = \rho\varepsilon \frac{\partial \bar{v}_r}{\partial z} = \rho \overline{vw}\big|_z - \rho \overline{vw}\big|_\infty \tag{2.19}$$

where the velocities v and w include both the potential and rotational parts. Applying Eqs. (2.16) and (2.17) into the term $\overline{vw}$ yields

$$\overline{vw} = \overline{v_p w_p} + \overline{v_p w_r} + \overline{v_r w_p} + \overline{v_r w_r} \tag{2.20}$$

with the terms in the right hand side are expanded as

$$
\begin{aligned}
\overline{v_p w_p}|_z &= \frac{H^2\sigma^2 k\delta}{16\sinh^2 kh} \\
\overline{v_p w_r}|_z &= -e^{-\xi}\frac{H^2\sigma^2 k\delta\cosh k(h+z)}{8\sqrt{2}\sinh^2 kh}\sin(\xi+\frac{\pi}{4}) \\
\overline{v_r w_p}|_z &= -e^{-\xi}\frac{H^2\sigma^2 sinhk(h+z)}{8\sinh^2 kh}\sin\xi \\
&\quad -e^{-\xi}\frac{H^2\sigma^2 k\delta}{8\sqrt{2}\sinh^3 kh}[sinhk(h+z)\,coshkh\sin(\xi+\frac{\pi}{4})+\sinh kz\sin(\xi-\frac{\pi}{4})] \\
\overline{v_r w_r}|_z &= e^{-2\xi}\frac{H^2\sigma^2 k\delta}{16\sinh^2 kh}
\end{aligned}
\tag{2.21}
$$

Therefore the mean shear stress caused by the boundary layer rotation flow is

$$
\tau(z) = -\frac{\rho H^2\sigma^2}{8\sinh^2 kh}\left[\sinh k(h+z)\sin\xi + k\delta[\frac{\sinh k(h+z)}{\tanh kh}\sin\xi+\cosh k(h+z)\cos\xi-\frac{e^{-\xi}}{2}]\right]e^{-\xi} \tag{2.22}
$$

which decays exponentially outside the boundary layer. The corresponding bottom shear stress is given by (2.22) with z=-h as

$$
\tau_b = -\frac{\rho H^2\sigma^2 k\delta}{16\sinh^2 kh} \tag{2.23}
$$

For shallow water conditions, kh <<1, substituting (2.22) into (2.19) and integrating from the bottom to an arbitrary depth, z, with the no-slip bottom boundary condition, the time mean flow in the boundary layer is given as

$$
\bar{v}_r = -\frac{H^2\sigma k}{16\sinh^2 kh}[3-2(\xi+3+\frac{z}{h})\cos\xi\, e^{-\xi}-2(\xi+\frac{z}{h})\sin\xi\, e^{-\xi}+e^{-2\xi}] \tag{2.24}
$$

which is usually referred to as the "streaming velocity" and is directed in the onshore direction. It is seen that just outside the boundary layer, this time averaged rotational related velocity is independent of the value of the viscosity and is given by

$$\bar{v}_r\big|_\infty = -\frac{3H^2\sigma k}{16\sinh^2 kh} \tag{2.25}$$

which is 1.5 times the average of the return flow due to the mass transport.

2.6 Shear Stress Related to Undertow

The seaward return flow of wave mass transport induces a seaward stress on the bottom sediment particles. In a real beach, a net onshore or offshore mass flux may exist in the presence of three dimensional circulations, therefore an additional shoreward or seaward bottom shear stress can result from the non-zero net onshore or offshore mass flux. It is well known that associated with the wave propagation toward shore is a shoreward linear momentum flux (Longuet-Higgins & Stewart 1964) and wave energy damping. Outside the surf zone, wave energy damps slowly with distance due to dissipation in the bottom boundary layer. Inside the surf zone, the waves decay relatively rapidly due to turbulent dissipation caused by wave breaking. As a result of wave energy damping, the momentum is transferred to the water column causing a shoreward directed thrust and thus a wave induced set-up, the gradient of which is proportional to the gradient of wave energy dissipation. This momentum flux is distributed over depth as shown as Figure 2.3. In shallow water, linear wave theory predicts that one third of the momentum flux originates between the trough and the crest levels and has its centroid at the mean water level and that the remaining two thirds, which

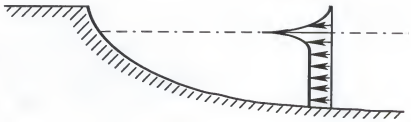

Figure 2.3 Distribution of the onshore component of momentum flux over depth.

originates between the bottom and the mean water level, is uniformly distributed over this dimension and thus has its centroid at the mid-depth of the water column. Because of the momentum contribution within the free surface, wave energy dissipation by breaking induces an equivalent shear force on the water surface which will be quantified later. This surface stress causes a seaward bottom shear stress, which does not exist outside the breaking zone and will become very significant within the breaking zone. The magnitude of the induced bottom shear stress is dependent on the rate of wave energy dissipation and the relationship of the velocity gradient and shear stress. Over the water column, this effect of surface shear stress caused by the momentum transfer must be balanced by the bottom shear stress and the pressure gradient due to the slope of the water surface.

2.6.1 Linear Shear Stress Relationship

The linear Boussineq shear stress relationship with eddy viscosity, ε, is applied as

$$\tau = \rho\varepsilon\frac{\partial\bar{v}}{\partial z} \tag{2.26}$$

Considering linear wave theory, the momentum equation for cross-shore flow is given by the second equation of (2.4). Assuming shallow water waves, kh<<1, averaging over one wave period and integrating from the free surface, $z = 0$, to an arbitrary elevation, z, yield

$$\frac{\partial}{\partial y}\left(\frac{E}{2}\right) - \frac{z}{h}\frac{\partial E}{\partial y} - \rho g z \frac{\partial \bar{\eta}}{\partial y} - (\tau_\eta - \tau(z)) = 0 \qquad (2.27)$$

where $E = \frac{\rho g H^2}{8}$ is wave energy density per unit surface area, and $\bar{\eta}$ is mean water level. The first two terms of Eq. (2.27) represent the so-called radiation stress components with the first being the contribution between trough and crest and the second below the mean water surface. The third term is the effect of the slope of the mean water level. The τ_η in the fourth term is the wind shear stress on the free surface. Applying Eq. (2.26) into (2.27) and integrating from the bottom, $z = -h$, to an arbitrary depth, z, with the no-slip bottom boundary condition yield

$$\rho\varepsilon\bar{v}(z) = \left[\tau_\eta - \frac{\partial(E/2)}{\partial y}\right](h+z) + \frac{z^2 - h^2}{2}\left[\rho g \frac{\partial \bar{\eta}}{\partial y} + \frac{1}{h}\frac{\partial E}{\partial y}\right] \qquad (2.28)$$

Integrating the above equation over the entire water depth results in the volumetric flux, which is equal to the sum of the net volumetric flux, q_{net}, and the wave mass transport flux, $\frac{E}{\rho c}$, where c is the wave celerity. The slope of the mean water surface is therefore determined as

$$\frac{\partial \bar{\eta}}{\partial y} = \frac{1}{\rho g h}\left[\frac{3}{2}\tau_\eta - \frac{7}{4}\frac{\partial E}{\partial y} - \frac{3\rho\varepsilon}{h^2}\left(\frac{E}{\rho c} + q_{net}\right)\right] \qquad (2.29)$$

Substituting (2.29) into (2.28), we obtain the final expression for the velocity

$$\bar{v}(z) = \frac{h}{\rho\varepsilon}\left(2\tau_\eta - \frac{\partial E}{\partial y}\right)\left[\frac{3}{8}\left(\frac{z}{h}\right)^2 + \frac{1}{2}\frac{z}{h} + \frac{1}{8}\right] + \frac{3}{2h}\left(\frac{E}{\rho c} + q_{net}\right)\left[1 - \left(\frac{z}{h}\right)^2\right] \qquad (2.30)$$

The corresponding bottom shear stress is given as

$$\tau_b = \rho\varepsilon\frac{\partial\bar{v}}{\partial z}\Big|_{z=-h} = -\frac{\tau_\eta}{2} + \frac{1}{4}\frac{\partial E}{\partial y} + \frac{3\rho\varepsilon}{h^2}\left(\frac{E}{\rho c} + q_{net}\right) \qquad (2.31)$$

The first term on the above right hand side is the contribution of the surface wind. Onshore winds cause a shoreward directed surface flow and a seaward directed bottom flow as shown in Figure 2.4. Of course, offshore winds would cause a shoreward directed flow near bottom. Thus landward and seaward directed winds result in destructive (offshore) and constructive (onshore) forces, respectively. The second term is related to the part of momentum flux originating between the wave trough and crest. Since the gradient of momentum flux is due

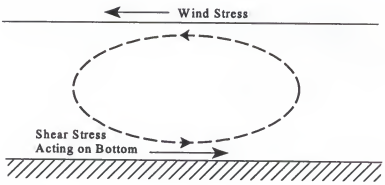

Figure 2.4 Bottom stresses caused by surface winds.

to the rate of wave energy dissipation, this term is vary important for breaking waves but almost negligible outside surf zone. The third term results from the mass flux. The seaward return flow of the wave mass flux induces a seaward bottom shear stress. A net offshore or onshore volumetric flux may exist when the return flow is enhanced or weakened due to gradients in the longshore current. In storm events in which there is overtopping of the barrier island, a portion or all of the potential return flow due to mass transport can be relieved. A net onshore volumetric flux induced by the weakened return flow causes an onshore directed bottom shear stress, while a net offshore volumetric flux acts oppositely and results in a offshore directed bottom shear stress.

2.6.2 Quadratic Shear Stress Relationship

As waves propagate into shallow water, the wave related flow becomes more turbulent. After wave breaking, the turbulence near the free surface is much stronger than that near the bottom. Figures 2.5 and 2.6 present variations of mean turbulent kinetic energy, $\bar{k}$, from experiments of Ting and Kirby (1994), and Stive and Wind (1982) for spilling and plunging breakers, respectively. In the figures, h/h_b represents the ratio of local water depth to the breaking water depth, and $\frac{z-\bar{\zeta}}{h}$ denotes the relative elevation. It appears that the turbulent level decays in both types of wave breakers. The assumption of constant eddy viscosity is not suitable anymore. Following Prandtl and Von Karman, the shear stress under conditions of turbulent flow is related to the velocity shear as follows

$$\tau = \rho l^2 \left|\frac{\partial v}{\partial z}\right| \frac{\partial v}{\partial z} \tag{2.32}$$

where l is the mixing length for an open channel flow. The form presented by Reid (1957)

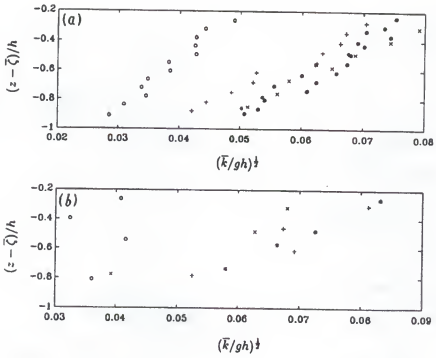

Figure 2.5 Variation of turbulent kinetic energy with depth in spilling breakers. (a) Ting and Kirby (1994); h/h_b = 0.879 (o), 0.809 (•), 0.744 (+), 0.668 (∗), 0.563 (×). (b) Test 1 of Stive and Wind (1982); h/h_b = 0.882 (o), 0.765 (+), 0.647 (∗), 0.529 (×).

is applied here

$$l = \frac{\kappa_0}{h}(z_0+h+z)(z_1-z) \tag{2.33}$$

where z_0 and z_1 are roughness lengths at the bottom and the free surface, respectively. Given a surface stress and nearshore beach profile, the momentum equation (2.27) is solved by equating return flow to the sum of Stoke's drift, $\frac{E}{\rho c}$, and net volumetric flux, q_{net}.

A comparison of cross-shore velocity variation with depth associated with the linear and quadratic shear stress relationships is presented in Figures 2.7 and 2.8 for breaking and

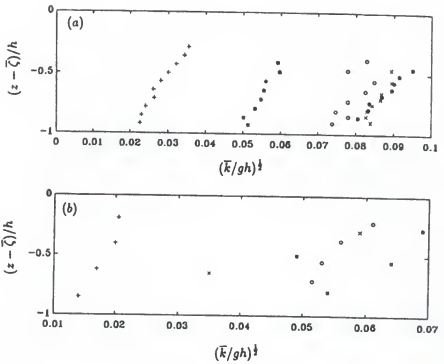

Figure 2.6 Variation of turbulent kinetic energy with depth in plunging breakers. (a) Ting and Kirby (1994); h/h_b = 0.929 (+), 0.857 (∗), 0.773 (o), 0.675 (×), 0.584 (•). (b) Test 2 of Stive and Wind (1982); h/h_b = 0.905 (+), 0.709 (∗), 0.544 (o), 0.381 (×), 0.143 (•).

non-breaking waves, respectively. Bottom streaming is not included in this model. In the figures, the following wave conditions have been considered: water depth h = 1 m, beach slope = 0.02, wave height H = 0.78 m, and wave period T = 6 s. In the quadratic relationship, the bottom roughness is 1 cm for both breaking and non-breaking waves. Since breaking waves cause a very rough water surface, the surface roughness is taken as half the wave height for breaking waves and 1 cm for non-breaking waves, respectively. Generally, the eddy viscosity in the linear stress relationship is difficult to determine and may vary with the water and wave conditions. For the comparisons presented here, the eddy viscosities are given

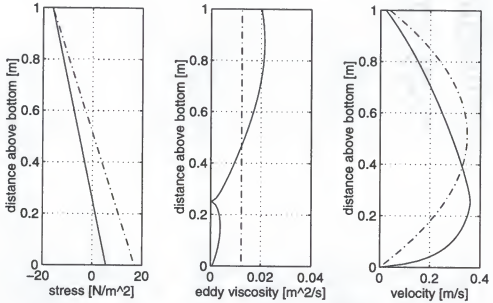

Figure 2.7 Comparisons of the linear (dashed line) and the quadratic (solid line)shear stress relationships for breaking waves. Note: the net seaward transport is equal to the shoreward mass transport.

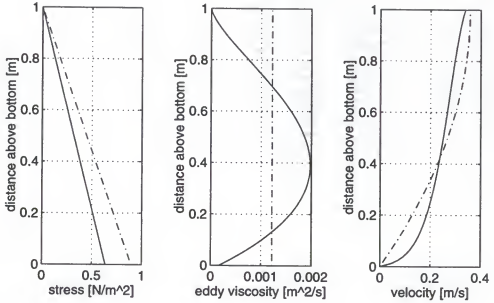

Figure 2.8 Comparisons of the linear (dashed line) and the quadratic (solid line)shear stress relationships for non-breaking waves. Note: the net seaward transport is equal to the shoreward mass transport.

by the average values of the quadratic shear stress relationship as 1.23×10^{-2} m^2/s and 1.22×10^{-3} m^2/s for the breaking and non-breaking waves, respectively. As shown in Figure 2.7, the magnitudes of velocity predicted by two methods are about the same order, but the profiles are quite different. The position for the maximum velocity is at an elevation of 50% and 25% above the bottom in the linear and quadratic relationships, respectively. In both models, the shear stress varies linearly with the elevation and the surface value is equal to one half the local wave energy gradient due to the wave breaking; but the bottom shear stress predicted by the linear model is about three times large as that predicted by the quadratic model. As shown in Eqs. (2.30) and (2.31) for the linear stress model, the velocity is inversely proportional to the eddy viscosity and the bottom stress varies directly with eddy viscosity. It is difficult to determine a proper value of eddy viscosity to satisfy both the velocity distribution and the bottom shear stress under such conditions. For the non-breaking wave case shown in Figure 2.8, the two methods yield much closer results. Due to the turbulence caused by wave breaking, the eddy viscosity is much larger inside the surf zone. Since the velocity profile is independent of eddy viscosity in the linear model for non-breaking waves, a better fitting between the two methods for the shear stress can be achieved by decreasing the eddy viscosity in the linear model. In the following, the predictions of the two methods are compared with measurements from the literature.

Hansen and Svendsen (1984) measured the velocity distributions for undertow on a planar bed with a slope of 1:34.3. The incident wave height was 12 cm in the uniform depth portion of tank with a water depth of 36 cm, and a wave period of 2 seconds. Breaking occurs at an approximate depth of 20 cm. The velocity distributions were measured in one

position outside the surf zone with a water depth of 22.5 cm and four different positions inside the surf zone with water depths of 7.6 cm, 9.5 cm, 12 cm and 14.9 cm, respectively.

Figure 2.9 shows the comparison between the measured and the predicted results at a water depth of 22.5 cm for non-breaking waves. The relative bottom and surface roughnesses are 0.01 for the quadratic stress model. The eddy viscosity in the linear stress model is taken as 0.609 cm^2/s based on the average of the quadratic model. It appears that the linear shear stress relationship presents a better velocity agreement than the quadratic. However the difficulty in determine an approximate eddy viscosity in the linear stress model should be noticed. Under non-breaking wave condition without winds, the velocity is independent of eddy viscosity, but the shear stress is linearly proportional to it.

The velocity profiles of Hansen and Svendsen at the four positions inside the surf zone are compared with the model predictions in Figure 2.10. The h/h_b values shown in the figure are the ratios of the local water depth to the depth at the initial breaking point. The relative bottom roughnesses, z_0/h, are 0.01 for all cases. Due to the wave breaking effects, the surface roughness is given as half of the local wave height for each position. It appears that the linear shear stress relationship is not suitable inside the surf zone anymore. The measured velocities and these predicted by the quadratic shear stress relationship are in quite good agreement except the case with 14.9 cm of water depth, which is a position very close to the breaking point with a quite uniform velocity distribution.

Figures 2.11 and 2.12 compare the shear stresses, eddy viscosities and the velocities computed from the quadratic stress model with those measured in Case 2 of Okayasu et al (1988). The experiments were carried out with a bed slope of 1:20, incident wave height of

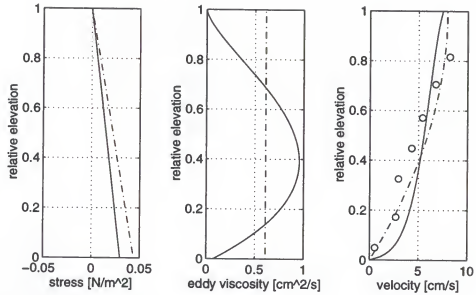

Figure 2.9 Comparisons of the measurements (circles, Hansen and Svendsen 1984) with the predictions of the linear (dashed line) and the quadratic (solid line)shear stress relationships for non-breaking waves at water depth of 22.5 cm.

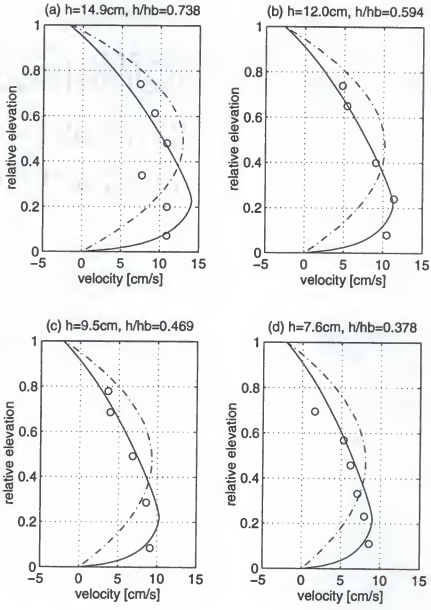

Figure 2.10 Comparisons of the measured velocities (circles, Hansen and Svendsen 1984) with the predictions of the linear shear stress model (dashed lines) and the quadratic shear stress model (solid lines). Four different positions are presented.

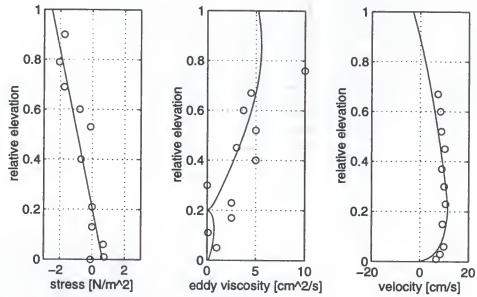

Figure 2.11 Comparisons of the measurements (circles, Okayasu et al 1988) with the predictions of the quadratic (solid line)shear stress relationships for breaking waves at water depth of 6.5 cm and wave height of 5.1 cm.

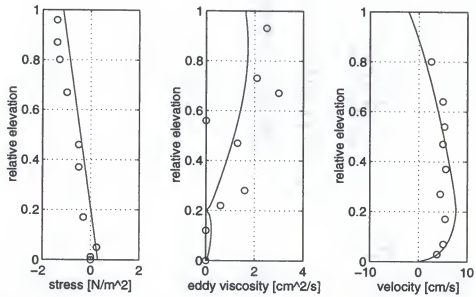

Figure 2.12 Comparisons of the measurements (circles, Okayasu et al 1988) with the predictions of the quadratic (solid line)shear stress relationships for breaking waves at water depth of 3.0 cm and wave height of 2.34 cm.

5.63 cm and period of 2 seconds at the uniform depth portion of the tank with a water depth of 40 cm. The measurements inside the surf zone at two different locations are presented here. In the experimental data, the Reynold stresses were calculated by Okayasu from the measured turbulent fluctuating velocity; the mean shear stresses shown in the figures was obtained by averaging the Reynold stresses over one wave period, and the mean eddy viscosity was calculated from the mean shear stress and the gradient of the mean velocity. As expected, the shear stresses varied quite linearly from the bottom to the surface. Since waves broke at the surface, the eddy viscosity in the upper part of the water was greater than that in the lower part. The turbulent level of flow decreased from the water surface to the bottom. In both locations, the measurements and the predictions of the quadratic stress model agree well for the shear stresses and the velocities. The predictions for the eddy viscosity are acceptable.

2.7 Comparison of Magnitude of Shear Stress Terms

In the field, all the bottom shear stress components mentioned in sections 2.3, 2.4, 2.5 and 2.6 exist however their relative magnitudes differed with some terms being much more important than others. The momentum flux related shear stresses are remarkably different for breaking and non-breaking waves. To provide an estimate of the relative magnitudes of these shear stresses, the following conditions have been considered:

- Water depth, $h = 1$ m, and density, $\rho = 1025$ kg/m^3.
- Beach slope of 0.02.
- Wave height, $H = 0.78$ m, and period $T = 6$ s.
- Mean sand diameter, $D = 0.2$ mm, and relative density, $s = 2.65$.
- Wind speed at 10 m above the water level, $u_{10} = 20$ m/s.

Because of the relative strong turbulence levels, the eddy viscosities are larger for breaking waves than those for non-breaking waves. Under the water and wave conditions listed above, the shear stresses will be calculated for both breaking and non-breaking wave cases.

(1) Critical shear stress

Generally, the critical shear stress inside the surf zone is much smaller than that outside the surf zone due to the turbulence caused by wave breaking. Since very few studies have been conducted under breaking wave conditions, the results from Amos et al. (1988) are applied to determine the critical shear stress outside the surf zone as

$$\tau = 0.04\rho(s-1)gD = 0.13\ N/m^2 \tag{2.34}$$

Inside the surf zone, the critical shear stress is considered as zero.

(2) Gravitation contribution

In Eq. (2.2), the sediment concentration, α, in the equation is assumed to be 0.66, therefore the gravity induced shear stress is 0.04 N/m^2.

(3) Shear stress due to non-linear waves

For the wave conditions given above, the wave length in the deep water, L_0, is 56.2 meters. The corresponding wave steepness, H/L_0, and the relative depth, h/L_0, are 0.0139 and 0.0178, respectively. From Figure 2.2, the non-dimensional average bottom shear stress is 5.4. Considering a Darcy-Weisbach friction coefficient of 0.08, the shear stress will be given by Eq.(2.3) as 0.94 N/m^2 directed shoreward.

(4) Shear stress due to streaming velocity

The shear stress due to the boundary layer streaming velocity is presented by Eq. (2.23). The negative sign in the equation means the shear stress is acting in the onshore direction. The bottom eddy viscosities computed by the quadratic shear stress relationship are applied here for the calculations. For non-breaking wave conditions, the bottom eddy viscosity is 1.66×10^{-4} m^2/s, the boundary layer thickness, δ, is calculated as 1.86 cm, and therefore the shear stress is 2.17 N/m^2. Under breaking waves, the bottom eddy viscosity is 6.69×10^{-4} m^2/s, the corresponding boundary layer thickness and shear stress are calculated as 3.74 cm and 4.36 N/m^2, respectively.

(5) Shear stress due to the wave mass flux

The case considered here assumes no net mass flux in the cross-shore direction, which means the seaward return flow balances the wave mass transport. The bottom shear stresses are computed by the quadratic stress model as 0.64 N/m^2 and 1.38 N/m^2 for the non-breaking and breaking wave conditions, respectively. The difference between the two conditions is caused by the different eddy viscosities, which result from the different turbulence levels.

(6) Shear stress due to momentum flux

As seen from Eq.(2.31), the contribution of momentum flux is related to the gradient of wave energy. Outside the surf zone, the change of wave energy can be neglected, therefore the shear stress due to the momentum flux is almost zero. Inside the surf zone, there is a substantial wave energy dissipation due to wave breaking. The shear stress caused by the momentum flux becomes a very important term. For the wave and water conditions listed

above, the bottom stress computed by the quadratic stress model is 4.2 N/m^2, which is the total value presented in Figure 2.7 reduced by the contribution due to the mass flux.

(7) Shear stress due to winds

Winds blowing over water cause a wind shear stress and a slope of water surface. As a result, a surface flow in the wind direction and a bottom flow in the opposite direction are generated. The wind shear stress is expressed by a friction factor, f_w (assumed as 0.005 here), and the the wind speed at 10 m elevation

$$\tau_\eta = \frac{\rho_a}{2} f_w u_{10}^2 \tag{2.35}$$

where ρ_a is the density of air and equal to 1.20 kg/m^3 under the temperature of 20 °C. For the given wind speed of 20 m/s, the surface stress is calculated as 1.20 N/m^2. In the quadratic stress model, the magnitude of bottom shear stress induced by this wind depends on the wind direction and wave breaking. An onshore directed wind will cause an additional offshore directed bottom stress of 0.549 and 0.255 N/m^2 for the non-breaking and breaking wave conditions, respectively. An offshore directed wind will induce an onshore directed bottom stress of 0.31 and 0.26 N/m^2 for the non-breaking and breaking wave conditions, respectively.

A summary of all shear stress terms discussed above is presented in Table 2.1. The stresses due to the momentum flux transport and streaming velocity are the two dominant terms. The critical shear stress is quite small compared with other terms. Because winds are the only source of the surface shear stress outside the surf zone, they have the most significant effects on bottom stress in this region.

Table 2.1 Constructive and destructive bottom shear stresses.

Type	Description of Force	Magnitude N/m^2	
		Outside Surf Zone	Inside Surf Zone
Critical Shear Stress	Friction	0.13	0
Constructive	Nonlinear Wave	0.94	0.94
	Streaming Velocity	2.17	4.36
	Wind* in Offshore Direction	0.31	0.26
Destructive	Gravity	0.04	0.04
	Mass Flux	0.64	1.38
	Momentum Flux	0	4.16
	Wind* in Onshore Direction	0.55	0.26

* Wind speed at 10 m above the water level, $u_{10} = 20$ m/s.

CHAPTER 3
DEVELOPMENT OF CROSS-SHORE TRANSPORT MODEL — CROSS

The "closed loop" cross-shore sediment transport relationships, which are studied in this chapter, are based on wave energy dissipation and implicitly "capture" the dominant destructive shear stress mechanism (i.e. wave momentum flux) discussed in Chapter 2. Since these models do not represent any constructive mechanisms, they would not be expected to perform well for beach accretion. Based on equilibrium beach profile concepts (Dean 1977), sediment transport is caused by deviations of a beach from its equilibrium form. According to scale analysis, the linear transport relationship proposed by Moore (1982) should be modified and a non-linear model is developed. In the non-linear model, the transport rate is proportional to the cube of the difference of the local wave energy dissipation per unit volume from the equilibrium value at each location across the surf zone. It appears that the non-linearity of this transport relationship can reasonably explain the time scale difference in the beach profile evolution in different experiments. A finite difference method is applied to solve the transport and the continuity equations numerically. Beach profile response at different times is determined by the numerical solutions.

3.1 Equilibrium Beach Profile

An equilibrium beach profile represents a dynamic balance of destructive and constructive forces acting on the beach. A change of these two competing types of forces will

result in a disequilibrium. Considering wave energy dissipation per unit water volume to represent the dominant destructive force, Dean (1977) has proposed that a sediment of a given size will be stable in the presence of a particular level of wave energy dissipation per unit volume, D_*. This can be expressed in terms of wave energy conservation as

$$D_* = \frac{1}{h}\frac{d(Ec_g)}{dy} \tag{3.1}$$

in which y is the shore-normal coordinate directed offshore, E is the wave energy, and c_g is the wave group velocity. As a first approximation, D_* is assumed to be a function only of sediment size (Moore, 1982), or equivalent sediment fall velocity (Dean, 1987). With linear wave theory and shallow water assumption, Eq. (3.1) can be integrated to

$$h = \left(\frac{24D_*}{5\rho g\sqrt{g}\kappa^2}\right)^{2/3} y^{2/3} = A y^{2/3} \tag{3.2}$$

where κ is the ratio of breaking wave height to water depth, and A is defined as a profile scale parameter. The relationship between A values and the median sediment size is shown in Table 3.1 (Dean and Dalrymple 1996). Since the profile scale parameter, A, is only a function of sediment size, wave conditions are not included in the above relationship.

The two-thirds power law profile formula of Eq. (3.2) was first empirically identified by Bruun (1954) as an appropriate representation of the profiles in a field study of beach profiles at Monterey Bay, CA and along the Denmark coast. Dean (1977) examined 502 beach profiles from the east coast and Gulf shoreline of the United States by a least square

fit to each profile with a generalized power law profile, $h = Ay^m$. It was found that the average value of the exponent was 0.66, in very good accord with the result derived in Eq. (3.2). Hughes and Chiu (1978) carried out a study of beach profiles and associated sediment characteristics at different locations in the state of Florida and Lake Michigan and found that Eq. (3.2) described the beach profiles reasonably well.

Table 3.1 Summary of Recommended A values, units of A parameter are $m^{1/3}$ (after Dean and Dalrymple 1996).

D (mm)	0.00	0.01	0.02	0.03	0.04	0.05	0.06	0.07	0.08	0.09
0.1	0.063	0.067	0.071	0.076	0.080	0.084	0.087	0.090	0.094	0.097
0.2	0.100	0.103	0.106	0.109	0.112	0.115	0.117	0.119	0.121	0.123
0.3	0.125	0.127	0.129	0.131	0.133	0.135	0.137	0.139	0.141	0.143
0.4	0.145	0.147	0.148	0.150	0.151	0.153	0.155	0.156	0.158	0.159
0.5	0.161	0.162	0.163	0.165	0.166	0.167	0.168	0.169	0.171	0.172
0.6	0.173	0.174	0.175	0.177	0.178	0.179	0.180	0.181	0.183	0.184
0.7	0.185	0.186	0.187	0.188	0.189	0.190	0.190	0.191	0.192	0.193
0.8	0.194	0.195	0.196	0.196	0.197	0.198	0.199	0.200	0.200	0.201
0.9	0.202	0.203	0.204	0.204	0.205	0.206	0.207	0.208	0.208	0.209
1.0	0.210	0.211	0.212	0.212	0.213	0.214	0.215	0.216	0.216	0.217

Two disadvantages of Eq. (3.2) are the infinite beach slope at the water line and the monotonic form of the profile. The first shortcoming is overcome by including gravity as a significant destructive force when a profile becomes steep. In this case, Eq. (3.2) is modified to include the beach face slope, m_0,

$$y = \frac{h}{m_0} + \left(\frac{h}{A}\right)^{3/2} \tag{3.3}$$

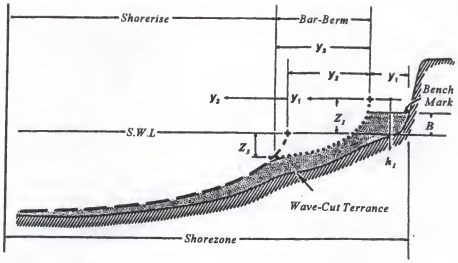

Figure 3.1 Definition sketch for Inman's curve fitting. Crosses denote the origin for bar-berm (dotted) and shorerise (dashed) curves, with y coordinates, y_1, y_2, and vertical coordinates, h_1, h_2 (from Inman et al. 1993).

Larson (1988) modified Dean's approach and developed an equation of similar form by replacing the spilling breaker assumption with the wave breaking model of Dally et al. (1985) and retaining the requirement of uniform wave energy dissipation per unit volume.

Inman et al. (1993) developed an equilibrium beach profile that treats a profile as two parts, the inner (bar-berm) and the outer (shorerise) portions. The two portions are matched at the breakpoint-bar and fit by curves of the form

$$h = By^m \tag{3.4}$$

The coordinates of Inman's curve fitting are shown in Figure 3.1 with the subscripts 1 and 2 corresponding to bar-berm and shorerise curves respectively. In addition to B and m in Eq. (3.4), the origins of two curves must be determined from the profile data. In total, seven

variables, y_1, z_1, B_1, m_1, y_2, B_2, and m_2 are required to fit a profile. This method is diagnostic and generally useful for a beach with measured data available. Comparatively, the method described by Eq. (3.2) is prognostic and needs only a description of sediment size.

3.2 Scale Analysis

A beach which is steeper than equilibrium has a smaller volume of water over which the incident wave energy is dissipated. This causes the energy dissipation per unit volume to be greater than the equilibrium value. As a result, the total destructive forces are greater than the constructive forces. The profile will respond to the imbalance of forces through redistribution of the sediments. Over time, sand will be carried from onshore to offshore and deposited near the breakpoint, resulting in a milder profile which approaches the condition of uniform wave energy dissipation per unit volume. Similar to this process, for a beach with a milder slope than equilibrium, sediment will be moved from offshore to onshore.

Based on these concepts, Kriebel and Dean (1985) proposed that the cross-shore sediment transport rate per unit beach width, Q, could be approximated according to the deviation of actual wave energy dissipation per unit volume from the equilibrium at a particular location across surf zone as

$$Q = K(D - D_*) \tag{3.5}$$

in which, D represents the actual total destructive force,

$$D = \frac{5}{24}\rho g^{3/2}\kappa^2 \frac{\partial h^{3/2}}{\partial y} \tag{3.6}$$

The transport parameter, K, was considered as a dimensional constant. The following scaling relationship is established from Eq. (3.5)

$$Q_r = \frac{[K(D-D_*)]_{model}}{[K(D-D_*)]_{prototype}} = K_r(D-D_*)_r \tag{3.7}$$

where the subscript r denotes scale ratios. For an undistorted model with same density fluid, according to the definition of D, the disequilibrium scale $(D-D_*)_r$ can be expressed in terms of the length scale, L_r,

$$(D-D_*)_r = \sqrt{L_r} \tag{3.8}$$

On the other hand, according to the Froude relationship the time scale, T_r, is expressed as

$$T_r = \sqrt{L_r} \tag{3.9}$$

Following this relationship, the cross-shore sediment transport per unit beach width should be scaled as

$$Q_r = \frac{L_r^2}{T_r} = L_r^{\frac{3}{2}} \tag{3.10}$$

This equation provides a basis for evaluation of transport models. If K is independent of the length scale, Eq. (3.7) does not provide a valid scaling of transport.

Based on field observations, Dean (1973) hypothesized that sediment was suspended during the wave crest phase position and if the fall time were less or greater than one half

wave period, the net transport would be landward or seaward, resulting in a bar formation for the latter case. This mechanism would exist in the region of wave breaking. Considering the height of suspended sediment to be proportional to the breaking wave height, H_b, resulted in identification so-called fall velocity parameter, $\frac{H_b}{wT}$. By examining small scale wave data for which only deep water reference wave heights, H_0, were available, the following relationship for net seaward sediment transport and bar formation was found

$$\frac{H_0}{wT} \geq 0.85 \tag{3.11}$$

Later, Kriebel et al. (1986) examined only prototype and large scale laboratory data and found a constant of 2.8 instead of 0.85 in Eq. (3.5). Kraus (1988) examined only large tank data and proposed the following relationship for bar formation

$$\frac{H_0}{L_0} \leq 0.0007 \left(\frac{H_0}{wT} \right)^3 \tag{3.12}$$

Several model studies have confirmed that $\frac{H_0}{wT}$ is a valid modeling parameter such that if this parameter is the same in model and prototype, they are scaled versions of each other and the fall velocity is scaled by the length scale as $w_r = \sqrt{L_r}$. Two examples from Hughes et al. (1990) and Kriebel et al. (1986) are presented in Figures 3.2 and 3.3, respectively.

It is of interest to develop and test a transport model which can ensure convergence to the target (equilibrium) beach profile and also satisfy the scale relationship given by Eq.(3.10). One approach is to consider the following form for the sediment transport

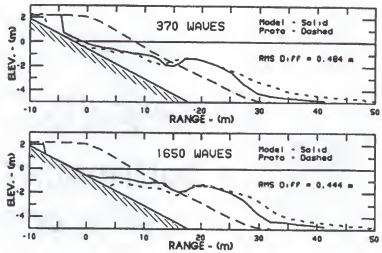

Figure 3.2 Comparison of beach profiles from medium and large scale wave tank, Scaling according to $(H_0/wT)_r=1$ (from Hughes et al. 1990). Note concrete bore underlaying initial sloping sand beach.

$$Q = K(D-D_*)|D-D_*|^{n-1} \tag{3.13}$$

Which results in the scale relationship

$$Q_r = K_r(D-D_*)_r|D-D_*|_r^{n-1} \tag{3.14}$$

Substituting Eqs. (3.8) and (3.10) to Eq. (3.14) yields

$$K_r L_r^{\frac{n}{2}} = L_r^{\frac{3}{2}} \tag{3.15}$$

If K is only a function of the fall velocity parameter, K_r equals unity and n=3 is determined such that both the scaling relationship and convergence to the equilibrium profile can be satisfied. Otherwise, if K_r is related to the length scale as $K_r = L_r^m$, the relationship, $m+\frac{n}{2}=\frac{3}{2}$,

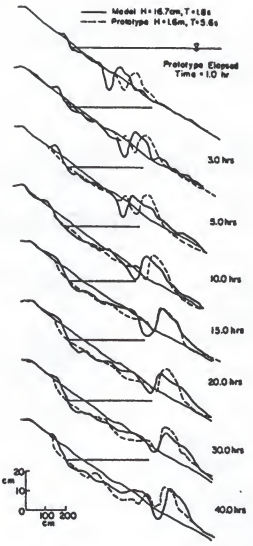

Figure 3.3 Comparison of beach profile from medium and large scale wave tank, Scaling according to $(H_0/wT)_f=1$ (from Kriebel et al. 1986).

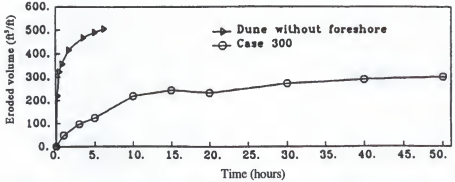

(a) Eroded volumes versus time for the German "dune without foreshore" case and Savill's Case 300.

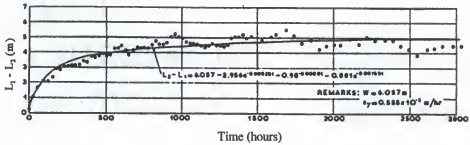

(b) (L_1 - L_2) versus time for Swart's flume B Case with $\delta_1 = 0.15$m and $\delta_2 = 0.10$m

Figure 3.4 Time history of beach evolution in three different experiments.

must hold to satisfy Eq. (3.10). In this case, there is an infinite number of combinations of m and n would satisfy the scaling requirement.

3.3 Discussion of Transport Relationship

Sediment transport in the nearshore region is a complicated process. Under different conditions, some beaches reach equilibrium very fast, but others may vary slowly. The time scale of beach evolution may vary from tens to thousands of hours for different experiments. Figure 3.4 presents the results from the German "dune without foreshore" case (Dette and Uliczka 1987), Saville's Case 300 (Kraus 1988), and Flume B case in Swart's experiments

(Swart 1974a). In these tests, the eroded volume at any time is determined as the cumulative volume of material displaced between initial and current profiles, and L_1 and L_2 are schematized profile lengths at water depth δ_1 and $(\delta_1 + \delta_2)$, respectively. Comparing these three cases in Figure 3.4, a question arises as to the causes of the greatly different profile response times.

In an attempt to understand the causes of the different time scale, we examine the following equation

$$\frac{dx}{dt} = K(x-x_*)\,|x-x_*|^{n-1} \tag{3.16}$$

where x_* is the equilibrium value of x. Eq. (3.16) is reminiscent of the transport relationship discussed above. Non-dimensionalizing with $x' = \frac{x}{x_*}$ and $t' = \frac{t}{Kx_*^{n-1}}$ yields

$$\frac{dx'}{dt'} = (x'-1)\,|x'-1|^{n-1} \tag{3.17}$$

with the initial condition $x'(t'=0) = x_0'$, the normalized solution of Eq. (3.17) is given by

$$\begin{aligned} \frac{x'-1}{x_0'-1} &= e^{-t'} && \text{for } n=1 \\ \frac{x'-1}{x_0'-1} &= \frac{1}{\left[(n-1)\,|x_0'-1|^{n-1}\,t'+1\right]^{\frac{1}{n-1}}} && \text{for } n\neq 1 \end{aligned} \tag{3.18}$$

Figure 3.5 presents the results of $\frac{x'-1}{x_0'-1}$ versus t' for n=1, 2 and 3, and x_0'=2 and 10 respectively. It appears that the time scale of the linear system (n=1) is independent of the initial conditions and the two lines in Figure 3.5 (a) are coincident. However, for the nonlinear

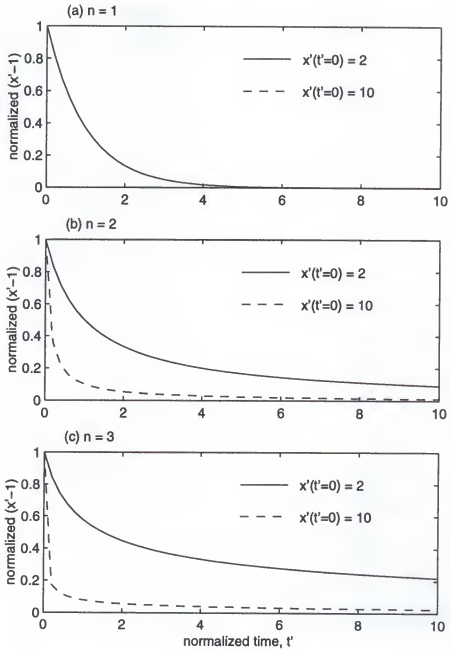

Figure 3.5 The solution of Eq. (3.16).

systems, the initial conditions affect the time scale by the factor $(n-1)|x_0'-1|^{n-1}$. As n increases, this factor becomes more and more significant.

As demonstrated in the solution of Eq. (3.16), a nonlinear transport equation provides an explanation for the range of time scales observed in laboratory experiments of beach profile evolution. In such nonlinear systems, the greater variation of initial condition from equilibrium corresponds to smaller time scales of profile response. Returning to the question raised about Figure 3.4, it appears the time scale differences in the three cases may be caused by the different initial conditions and non-linearity of the transport relationship. Among three cases, the "dune without foreshore" had a sand size of 0.33 mm and a initial slope of 1:4 with a wave height of 1.5 m and period of 6 s, and its initial condition is farthest from its equilibrium and the beach takes the shortest time to approach relative equilibrium. For Case 300, the sand size was 0.22 mm and the initial profile slope was 1:15 with a wave height of 1.68 m and period of 11.33 s. Swart's flume B Case had a sand size of 0.17 mm and an initial slope of 1:10 with a wave height of 0.07 m and period of 1.04 s. Its initial condition is hypothesized closest to the equilibrium and takes the longest time to arrive at relative equilibrium. In the next chapter, the transport relationship, Eq. (3.13) with n=1 and n=3, is applied to three sets of large tank experiment data. Time dependent profile response is then determined by the numerical solution of the transport equation and continuity equation, which is

$$\frac{\partial y}{\partial t} = -\frac{\partial Q}{\partial h} \tag{3.19}$$

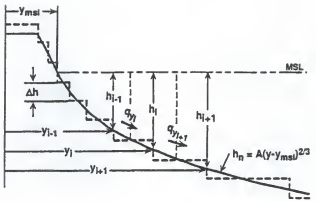

Figure 3.6 Grid with h and t as the independent variables and y dependent.

3.4 Modeling Process

3.4.1 Numerical Method

The sediment transport and continuity equations are solved by a finite difference method. The computational physical domain with the staggered grid is presented in Figure 3.6. The cells are finite increments of the depth variable, h. Thus the depth is the independent variable and the dependent variable is the distance, y, which varies with time. For each time step, the transport and continuity equations are solved simultaneously. After applying Eq. (3.6) as the formula of the actual wave energy dissipation per unit water column, the finite difference form of the transport equation (3.13) at the (m+δ)th time step, $t=(m+\delta)\cdot\Delta t$, becomes

$$Q_i^{m+\delta} = K\left[\frac{\frac{5}{24}\rho g^{3/2}k^2(h_i^{3/2}-h_{i-1}^{3/2})}{y_i^{m+\delta}-y_{i-1}^{m+\delta}} - D_*\right]\cdot\left|\frac{\frac{5}{24}\rho g^{3/2}k^2(h_i^{3/2}-h_{i-1}^{3/2})}{y_i^{m+\delta}-y_{i-1}^{m+\delta}} - D_*\right|^{n-1} \qquad (3.20)$$

where the superscript $m+\delta$ denotes the values at (m+δ)th time step, and δ is a value between

0 and 1. After rewriting the distance variable at the time, $t=(m+1)\cdot\Delta t$, as $y_i^{m+1}=y_i^m+\Delta y_i^{m+1}$, Eq. (3.20) becomes

$$Q_i^{m+1}=K\left[\frac{\frac{5}{24}\rho g^{3/2}k^2(h_i^{3/2}-h_{i-1}^{3/2})}{(y_i^m-y_{i-1}^m)\left(1+\frac{\Delta y_i^{m+1}-\Delta y_{i-1}^{m+1}}{y_i^m-y_{i-1}^m}\right)}-D_*\right]\cdot\left|\frac{\frac{5}{24}\rho g^{3/2}k^2(h_i^{3/2}-h_{i-1}^{3/2})}{(y_i^m-y_{i-1}^m)\left(1+\frac{\Delta y_i^{m+1}-\Delta y_{i-1}^{m+1}}{y_i^m-y_{i-1}^m}\right)}-D_*\right|^{n-1} \quad (3.21)$$

For a small time increment Δt, the value $\epsilon=\frac{\Delta y_i^{m+1}-\Delta y_{i-1}^{m+1}}{y_i^m-y_{i-1}^m}$ is much less than 1. Therefore Eq. (3.21) is linearized as

$$Q_i^{m+1}=K\left[\frac{\frac{5}{24}\rho g^{3/2}k^2(h_i^{3/2}-h_{i-1}^{3/2})}{y_i^m-y_{i-1}^m}(1-\epsilon)-D_*\right]\cdot\left|\frac{\frac{5}{24}\rho g^{3/2}k^2(h_i^{3/2}-h_{i-1}^{3/2})}{y_i^m-y_{i-1}^m}(1-\epsilon)-D_*\right|^{n-1} \quad (3.22)$$

When n is an odd number, the absolute sign in the equation can be dropped. Neglecting higher order terms, the linearized finite difference transport equation is expressed as

$$A_i^*\Delta y_{i-1}^{m+1}+B_i^*Q_i^{m+1}+C_i^*\Delta y_i^{m+1}=D_i^* \quad (3.23)$$

$$A_i^*=-nK\left[\frac{\frac{5}{24}\rho g^{3/2}k^2(h_i^{3/2}-h_{i-1}^{3/2})}{y_i^m-y_{i-1}^m}-D_*\right]^{n-1}\frac{\frac{5}{24}\rho g^{3/2}k^2(h_i^{3/2}-h_{i-1}^{3/2})}{y_i^m-y_{i-1}^m}$$

$$B_i^*=1$$

$$C_i^*=-A_i^*$$

$$D_i^*=K\left[\frac{\frac{5}{24}\rho g^{3/2}k^2(h_i^{3/2}-h_{i-1}^{3/2})}{y_i^m-y_{i-1}^m}-D_*\right]^n$$

For the grid shown in Figure 3.6, the discrete form of the continuity equation (3.19) is

$$\frac{\Delta y_i^{m+1}}{\Delta t} = -\frac{Q_{i+1}^{m+\frac{1}{2}} - Q_i^{m+\frac{1}{2}}}{\Delta h} \tag{3.24}$$

Recalling $Q_i^{m+\frac{1}{2}} \cong \frac{1}{2}\left(Q_i^m + Q_i^{m+1}\right)$, Eq. (3.24) is written as

$$A_i Q_i^{m+1} + B_i \Delta y_i^{m+1} + C_i^{m+1} = D_i \tag{3.25}$$

$$A_i = -\frac{\Delta t}{2\Delta h}$$
$$B_i = 1$$
$$C_i = -A_i$$
$$D_i = -\frac{\Delta t}{2\Delta h}\left(Q_{i+1}^m - Q_i^m\right)$$

Eqs (3.23) and (3.25) are tridiagonal equations and can be solved simultaneously by the standard double sweep method. At each computation time, the active profile domain is determined by the instantaneous incoming wave and water level conditions. Assuming this active domain is the region of $h_{ib} \le h \le h_{ie}$, the boundary conditions, $Q_{ib} = Q_{ie} = 0$ can be applied, which leaves 2×(ie-ib) variables as unknowns. The continuity equation (3.25) is solved from $i=ib$ to $i=ie-1$, and the transport equation (3.23) is solved from $i=ib+1$ to $i=ie$. They provide total 2×(ie-ib) equations. Starting with boundary condition $F_{ie}^* = Q_{ie}$ and $E_{ie}^* = 0$, four new sets of variables are calculated as

$$E_i = -\frac{A_i}{B_i + C_i E_{i+1}^*}, \quad F_i = \frac{D_i - C_i F_{i+1}^*}{B_i + C_i E_{i+1}^*}, \quad E_i^* = -\frac{A_i^*}{B_i^* + C_i^* E_i}, \quad F_i^* = \frac{D_i^* - C_i^* F_i}{B_i^* + C_i^* E_i} \tag{3.26}$$

These coefficients are determined sequentially from i = ie to i = ib. Therefore the current transport rates and the profile changes are determined as

$$\begin{aligned} \Delta y_i &= E_i Q_i + F_i \ , \qquad && ib \le i \le ie \\ Q_i &= E_i^* \Delta y_{i-1} + F_i^* \ , \qquad && ib+1 \le i \le ie-1 \end{aligned} \tag{3.27}$$

3.4.2 Wave Run-up and Set-up

The active profile considered in the numerical model is from the wave run-up limit to the wave breaking point. Outside this active region, the net sediment transport does not result in profile changes. At each time step, the water level is determined by the sum of storm surge, tide and wave set-up, and the elevation contours used in the transport equation are modified according to the change of water level.

The wave induced set-up in the surf zone is calculated according to the balance of pressure gradient and radiation stress. Inside the surf zone, based on the linear wave theory, the set-up, $\bar{\eta}$, is given (Dean and Dalrymple, 1991) as

$$\bar{\eta}(h) = \bar{\eta}_b + \frac{3\kappa^2/8}{1+3\kappa^2/8}(h_b - h) \tag{3.28}$$

where κ is the ratio of breaking wave height to the breaking water depth, and $\bar{\eta}_b$ and h_b are the set-down and the water depth at the breaking point, respectively. For shallow water, the value of $\bar{\eta}_b$ is given by Longuet-Higgins and Stewart (1964) as

$$\bar{\eta}_b = -\frac{k^2 h_b}{16} \tag{3.29}$$

In the numerical model, storm surge and tide are applied to the whole surf zone uniformly, but the set-up is added according to Eq. (3.28) and varies with water depth. At the shoreline, the set-up, $\bar{\eta}_0$ calculated from Eq. (3.28) is

$$\bar{\eta}_0 = \frac{e - 0.0625\kappa^2}{1 - e} h_b \tag{3.30}$$

where $e = \frac{3\kappa^2/8}{1+3\kappa^2/8}$. According to linear wave theory, we have $\kappa = 0.78$, and $\bar{\eta}_0 = 0.18 h_b$ is determined.

In the study of seawalls and breakwaters design, Hunt (1958) proposed wave run-up, R, as a function of bed slope, wave height, and wave steepness, which can be expressed as

$$R = F_R H_b \frac{m}{\sqrt{H_b/L_0}} \tag{3.31}$$

where R is the run-up height measured vertically upward from storm water level, F_R is a non-dimensional coefficient and is approximately 1, m is the average bed slope from the run-up limit to the breaking point, and L_0 is the deep water wave length. Since the wave run-up calculated by Eq.(3.31) is measured from the storm water level, after including wave set-up in water level change, the wave run-up is established as the value calculated from Eq. (3.31) by subtracting the value of wave set-up given in Eq. (3.30).

3.4.3 Dune, Shoreline and Offshore Slopes

In the numerical model, three characteristic slopes must be specified. As shown in Figure 3.7, they are dune slope, m_d, shoreline slope, m_{sl}, and offshore slope, m_{off}. The dune

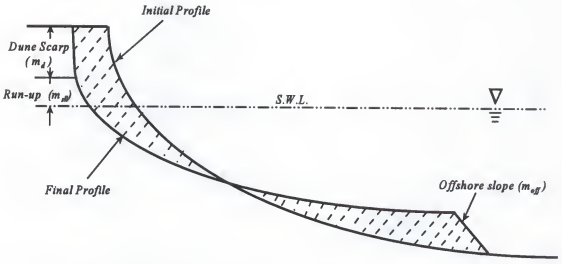

Figure 3.7 Definition sketch for dune, shoreline, and offshore slopes.

slope, which is defined as the averaged dune scarp slope after erosion, is the maximum slope that the profile is allowed to achieve. If the profile reaches an angle steeper than the dune slope at the end of any time step, avalanching occurs and the profile is smoothed to the dune slope.

The shoreline slope, which is the anticipated profile slope between the shoreline and the run-up limit, controls the profile evolution between the shoreline and the run-up limit. In this region, the profile change is caused by the uprush and backrush, and the transport equation discussed in section 3.2 cannot be applied. After each time step, the actual slope is compared with the shoreline slope. If the actual profile is steeper than the given shoreline slope at a point, the following adjustment is made for the distance variables of two adjacent cells

$$\Delta y_i = -0.5\left[y_i - y_{i-1} - \frac{h_i - h_{i-1}}{m_{sl}}\right]\left(1 - e^{-K_y \Delta t}\right)$$
$$\Delta y_{i-1} = 0.5\left[y_i - y_{i-1} - \frac{h_i - h_{i-1}}{m_{sl}}\right]\left(1 - e^{-K_y \Delta t}\right) \quad (3.32)$$

where the subscript i and i-1 denote the indexes of cells, m_{sl} is the shoreline slope, and K_y is a decay parameter and set somewhat arbitrarily to 10 hr^{-1} here, which represents a "folding time" of 0.1 hours.

Sand conservation across the profile is ensured by the continuity equation, so that the volume eroded from the beach face must be deposited offshore. Since the profile change ends at the wave breaking point, there is an unrealistic sudden vertical change in the profile shape. To overcome this problem, the offshore slope is introduced to control the slope at the end of the deposited volume. Under most cases, the value of this slope is between 0.1 to 0.2.

3.4.4 Random Wave Generation

Under random wave conditions, the joint distribution of wave periods and heights developed by Longuet-Higgins (1983) is applied to generate wave height and period series in the time domain. It is convenient to non-dimensionalize wave height and period with the quantities related to the spectral density, $E(\sigma)$. The average frequency is defined as

$$\bar{\sigma} = m_1 / m_0 \quad (3.33)$$

where m_n denotes the nth moment of the spectral density,

$$m_n = \int_0^\infty \sigma^n E(\sigma) d\sigma \quad (3.34)$$

A spectral width parameter ν can then be defined in terms of the variance of E(σ) about the mean as

$$\nu^2 = \int_0^\infty \frac{(\sigma-\bar{\sigma})^2 E(\sigma)\, d\sigma}{\bar{\sigma}^2 m_0} = \frac{m_0 m_2}{m_1^2} - 1 \tag{3.35}$$

For a narrow-banded spectral random wave system, ν is much less than 1. Under severe wave conditions, ν will increase. In practice, ν values are between 0 to 0.6 for ocean waves. After normalizing the wave height, H, and the wave period, T, by

$$R = \frac{H}{2\sqrt{2m_0}}, \qquad \tau = T\frac{\bar{\sigma}}{2\pi} \tag{3.36}$$

the joint probability density function, p, is expressed as

$$p(R,\tau) = L(\nu)\cdot\frac{2}{\sqrt{\pi}\,\nu}\cdot\frac{R^2}{\tau^2}\cdot e^{-R^2\left[1+(1-\frac{1}{\tau})^2\frac{1}{\nu^2}\right]} \tag{3.37}$$

where $L(\nu) = \left[\frac{1}{2}\left(1+\frac{1}{\sqrt{1+\nu^2}}\right)\right]^{-1}$ is a normalization factor introduced to take account of the fact that only positive values of τ are considered.

The marginal probability density of wave height R is found by integrating p(R,τ) with respect to $0 < \tau < \infty$, that is

$$p(R) = L(\nu)\,[1 + erf(R/\nu)]\,R\,e^{-R^2} \tag{3.38}$$

where $erf(R/\nu) = \frac{2}{\sqrt{\pi}}\int_0^{R/\nu} e^{-t^2}dt$ is the error function. Eq. (3.38) states that the density of R

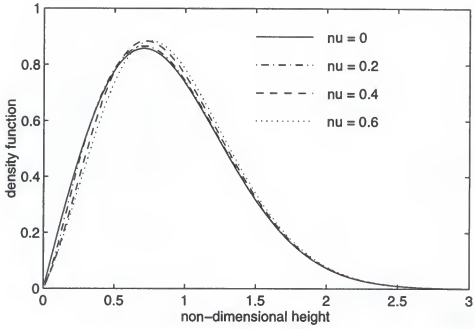

Figure 3.8 The probability density of wave height R when ν = 0.2, 0.4 and 0.6 compared with the Rayleigh distribution (ν = 0).

is almost Rayleigh distributed, but must be corrected by the factor $\frac{1}{2}L(\nu)[1+erf(R/\nu)]$. For large waves and small ν values, the correction is exponentially small. Some examples are presented in Figure 3.8. For the current application, the Rayleigh distribution is used as an approximation of Eq. (3.38). Therefore, the cumulative probability of the wave height becomes

$$P(R) = 1 - e^{-R^2} \tag{3.39}$$

and the root mean square wave height, H_{rms}, is related to the spectral density as $H_{rms} = 2\sqrt{2m_0}$.

The distribution of wave period at fixed values of the wave height R is found by dividing $p(R,\tau)$ in Eq.(3.37) by $p(R)$ in Eq. (38), that is

$$p(\tau/R) = \frac{2}{\sqrt{\pi}\nu[1+erf(R/\nu)]}\frac{R}{\tau^2}\exp\left[-\left(1-\frac{1}{\tau}\right)^2\frac{R^2}{\nu^2}\right] \tag{3.40}$$

Integrating $p(\tau/R)$ with respect to τ results in the cumulative probability

$$P(\tau/R) = \frac{1+erf\left(\frac{R}{\nu}(1-\frac{1}{\tau})\right)}{1+erf\left(\frac{R}{\nu}\right)} \tag{3.41}$$

By approximating $erf(x) \approx \tanh(1.2x)$ (shown in Figure 3.9), Eq.(3.41) is simplified as

$$P(\tau/R) = \frac{1+\tanh\left(\frac{1.2R}{\nu}(1-\frac{1}{\tau})\right)}{1+\tanh\left(\frac{1.2R}{\nu}\right)} \tag{3.42}$$

To simulate an irregular wave condition, a random number P_1 uniformly distributed from 0 to 1 is generated. A random non-dimensional wave height, R_1 is obtained from Eq. (3.39)

$$R_1 = \sqrt{-\ln(1-P_1)} \tag{3.43}$$

To obtain the corresponding wave period, a value of ν is assumed according to the severity of wave conditions. A second random number P_2 with uniform density distribution over (0,1), is generated. Substituting P_2 and R_1 into Eq. (3.42) yields

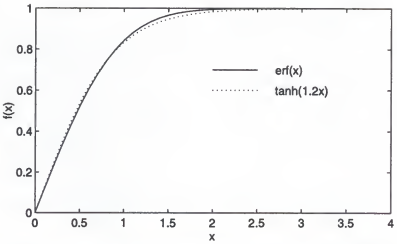

Figure 3.9 Comparison of the error function erf(x) with tanh(1.2x).

$$\tau_1 = \frac{1}{1 - \frac{\nu}{2.4R} \ln\left[\frac{P_2\left(1+\tanh\frac{1.2R_1}{\nu}\right)}{2-P_2\left(1+\tanh\frac{1.2R_1}{\nu}\right)}\right]} \tag{3.44}$$

Given a root mean square wave height, H_{rms}, and an average wave period, $\bar{T}$, the dimensional wave height and period are

$$H_1 = H_{rms} R_1 , \qquad T_1 = \bar{T}\tau_1 \tag{3.45}$$

The random wave heights and periods generated numerically are compared with Longuet-Higgins's joint density distribution in Figure 3.10 and Figure 3.11 for narrow band ($\nu = 0.1$) and wide band ($\nu = 0.5$) spectra, respectively. It appears that the numerical results agree with Longuet-Higgins theory very well.

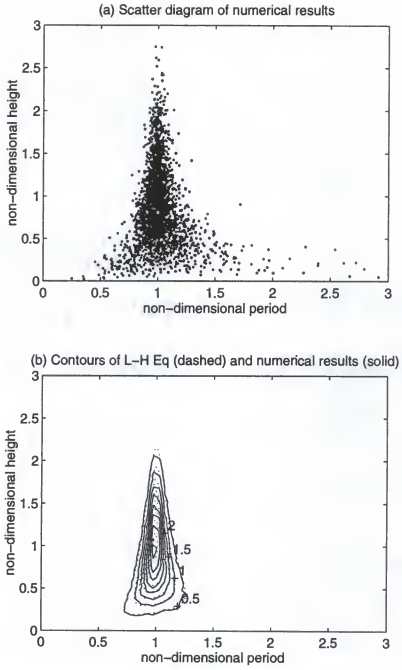

Figure 3.10 Comparisons of the numerical results with the density function (Eq. (3.37)) of Longuet-Higgins for $\nu = 0.1$.

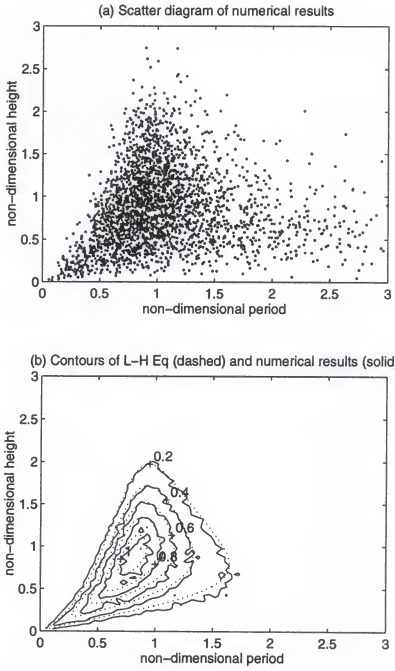

Figure 3.11 Comparisons of the numerical results with the density function (Eq. (3.37)) of Longuet-Higgins for $\nu = 0.5$.

CHAPTER 4
CALIBRATION OF CROSS MODEL WITH LABORATORY EXPERIMENTS

4.1 Introduction

The cross-shore sediment relationships discussed in Chapter 3 have two coefficients requiring quantification. They are the transport coefficient, K and the exponent, n. Based on the scaling analysis, n=3 was proposed in the last chapter. In this section, the proposed nonlinear transport model with n=3 will be compared with the linear transport relationship, n=1, for seven laboratory experiments. Calibrations of the two models are accomplished by a series of simulations in which a trial K value is used to simulate profile development for each experiment. The eroded volume at any time is defined as the cumulative volume of material eroded between the initial and current profiles. The errors between the predicted and observed eroded volume are obtained at the times for which profile information is available. The best-fit K value is determined as the value yielding the overall least square error. The calibrations utilize 3 sets of different laboratory data, involving a total of seven large scale wave tank experiments. Among these, five cases were carried out with monochromatic wave conditions, and the other two were conducted under random waves. According to the wave tank facilities, the seven experiments are divided into three groups: Saville's experiments which were operated by the Beach Erosion Board in the "Large Wave Tank" in 1956-1957 and 1962 (Saville 1957, Saville and Watts 1969, and Kraus 1988); the German "Large Wave

Flume" experiments, which were carried out in Hannover in 1987 (Dette and Uliczka 1987, Dette and Rahlf 1992, and Dette et al. 1992); and SUPERTANK laboratory data collection project, which was conducted at O.H. Hinsdale Wave Research Laboratory, Oregon State University, in 1991 (Kraus and Smith 1994, and Smith and Kraus 1995).

4.2 Saville's Experiments

4.2.1 General Description

Saville's experiments (Saville and Watts 1969, and Kraus 1988) described here were conducted during 1956-1957 and 1962 in the "Large Wave Tank" located at Dalecarlia Reservation in Washington, DC. The concrete tank was 194 m long, 4.6 m wide, and 6.1 m deep. Prior to the start of most new experiments, sand was emplaced to form a 1 on 15 slope. A fine sand of median diameter 0.22 mm was used in the experiment performed during 1956-1957, and a coarse sand of median diameter 0.40 mm was used in the experiment performed in 1962. Since beach erosion is the process of interest in this study, only the set with a sand size of 0.22 mm will be discussed here.

Seven experiments were conducted under constant wave conditions with sand size of 0.22 mm. They were referred as Case 100, 200, 300, 400, 500, 600, and 700. The corresponding fall velocity for the sand at a temperature of 20 °C is 3 cm/s and the profile scale parameter, A, is 0.106 $m^{1/3}$. Since the profile eroded back to the end of the tank during the experiment in Case 100, this case will not be discussed. The wave and water level conditions for the other six cases are listed in Table 4.1. The initial and the final profiles for each of these experiments are presented in Figure 4.1 in the order of the fall velocity parameter, H/wT. Since the wave heights were small in Case 600 and Case 200, there was

Table 4.1 Wave height, period, and water depth in horizontal section of the tank.

Case No.	Wave Height (m)	Wave Period (s)	Water Depth (m)	H/wT
200	0.55	11.33	4.57	1.62
300	1.68	11.33	4.27	4.94
400	1.62	5.60	4.42	9.64
500	1.52	3.75	4.57	13.51
600	0.61	16.00	4.57	1.27
700	1.62	16.00	4.11	3.38

almost no beach erosion. In the other four cases, beaches eroded and offshore bars formed near the break points. It appears that as the fall velocity parameter increases the offshore bar becomes more and more significant. In Case 500, the height of the offshore bar became about 1.5 m. According to observations recorded during the experiment, a second wave breaking position occurred in this case. The time histories of observed eroded volume for the four erosion cases are shown in Figure 4.2. It appears that the variation of eroded volume with time is not consistent in Case 700. Although constant wave conditions were run during the experiment, the eroded volume reached a maximum at 30 hours instead of increasing monotonically. Therefore, for the calibration of CROSS model, only Case 300, Case 400 and Case 500 will be used.

4.2.2 Calibration

The sediment relationship, Eq. (3.13) with both n=1 and n=3, are applied. The active water depth is determined as the breaking water depth, which is 1.28 times of the breaking wave height according to McCowan (1894) theory. Based on the wave heights listed in Table

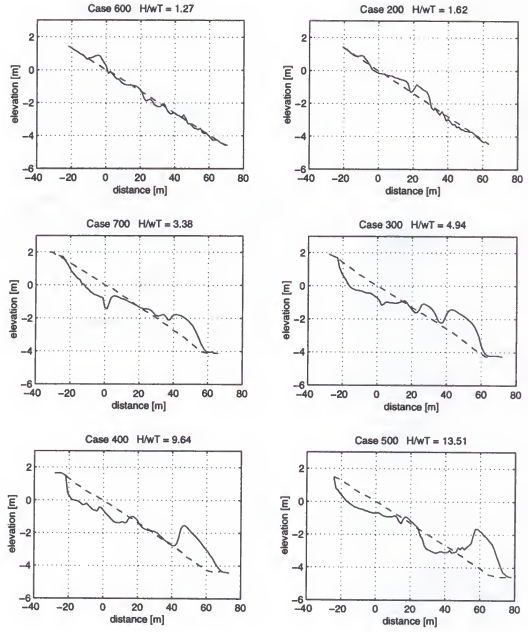

Figure 4.1 The initial (dashed) and the finial (solid) profiles of Cases 200, 300, 400, 500, 600, and 700 in Saville's experiments.

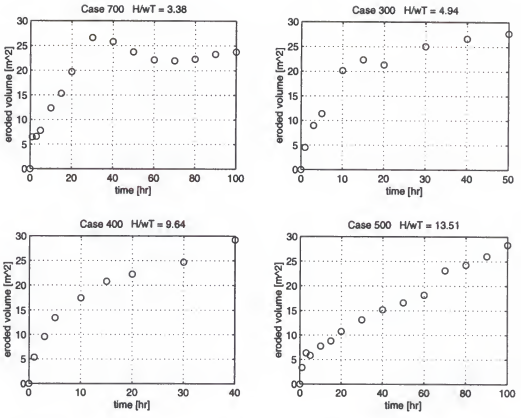

Figure 4.2 The time histories of the observed eroded volume for Cases 700, 300, 400 and 500.

4.1, the active water depths are 2.15 m, 2.08 m and 1.95 m for Case 300, Case 400 and Case 500, respectively. The eroded volume error is defined as

$$Err = \sqrt{\frac{1}{n}\sum_{i=1}^{n}\left[(Vol_p(t_i) - Vol_m(t_i)\right]^2} \qquad (4.1)$$

where the Vol_p and Vol_m are the predicted and measured eroded volumes, respectively, and t_i denotes the time at which the measurements are available. In each case, the dune, shoreline and offshore slopes used in the numerical model are determined according to the observed

Table 4.2 The numerical model inputs and best-fit results for Saville's experiments.

Case	Slope			Best-fit K		Error* [m^2]	
No.	dune	shoreline	offshore	n=3 [m^8s^2/N^3]	n=1 [m^4/N]	n=3	n=1
300	0.50	0.15	0.20	8.55×10^{-10}	3.45×10^{-6}	2.08	3.37
400	1.00	0.17	0.15	7.97×10^{-10}	3.71×10^{-6}	1.78	2.40
500	0.50	0.13	0.30	5.77×10^{-10}	1.57×10^{-6}	3.99	1.88

* Error represents the root mean square between predicted and observed eroded volume as shown in Eq. (4.1).

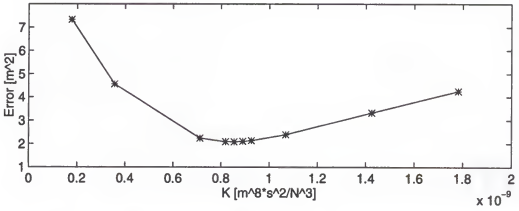

Figure 4.3 Root mean square error of eroded volume as a function of transport coefficient K for the non-linear model (n=3) simulation of Case 300.

final profile. The values of these slopes are shown in Table 4.2. The calibration process for the non-linear transport model simulation of Case 300 is shown in Figure 4.3. Based on the results, a best-fit K value of 8.55×10^{-10} is adopted which gives the overall minimum error for the eroded volume. The best-fit K values and the corresponding errors of eroded volume for the three cases are presented in Table 4.2. The best-fit K values vary from 5.77×10^{-10} to 8.55×10^{-10}, a factor of 1.48 for n=3. The corresponding factor for the best-fit K values for n=1 is 2.36. Comparisons of predicted and measured eroded volumes are shown in Figure 4.4

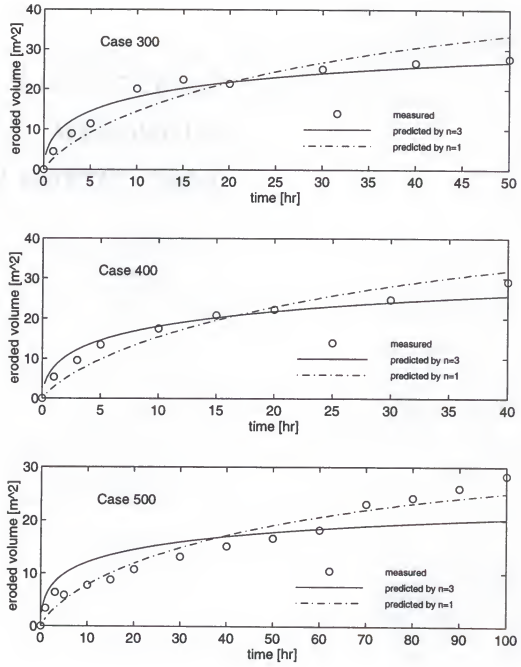

Figure 4.4 Comparisons of prediction with best-fit K value to observed eroded volumes for Cases 300, 400 and 500 in Saville's experiments.

for the predictions of both the linear (n=1) and the non-linear (n=3) sediment transport relationships. It appears that the non-linear transport relationship with n=3 provides a better fit for Case 300 and Case 400, while the linear transport relationship, n=1, predicts better results for Case 500. As discussed before, Case 500 had a very significant offshore bar (Figure 4.1) formed during beach erosion. Waves first broke at the offshore bar, then reshaped in the offshore trough area and broke again in the nearshore region. It is not appropriate to calculate wave energy dissipation per unit volume according to the offshore incident wave height. The vortex caused by the first wave breaking also played an important role in the sediment transport in the area shoreward of the bar.

The beach profile evolutions predicted by the non-linear (n=3) and the linear (n=1) transport relationship are compared in Figures 4.5, 4.6 and 4.7 for Cases 300, 400, and 500, respectively. In each case, the profiles at four different times are compared. Among three cases, the proposed non-linear relationship presents overall better agreement for the profile evolution in Case 300 and Case 400. Owing to the significant offshore bar in Case 500, the numerical models which predict a smooth monotonic profile form have some difficulties in representing the profile around the offshore trough and bar area.

4.3 German "Large Wave Flume"

4.3.1 General

The German "large wave flume" is 324 meters long, 7 meters deep and 5 meters wide. Three series of experiments were carried out in the flume (Dette and Uliczka 1987, Dette and Rahlf 1992, and Dette et al. 1992). Two of these experiments had the same constant wave conditions and different initial profiles. Regular waves with a wave height of 1.5 meters and

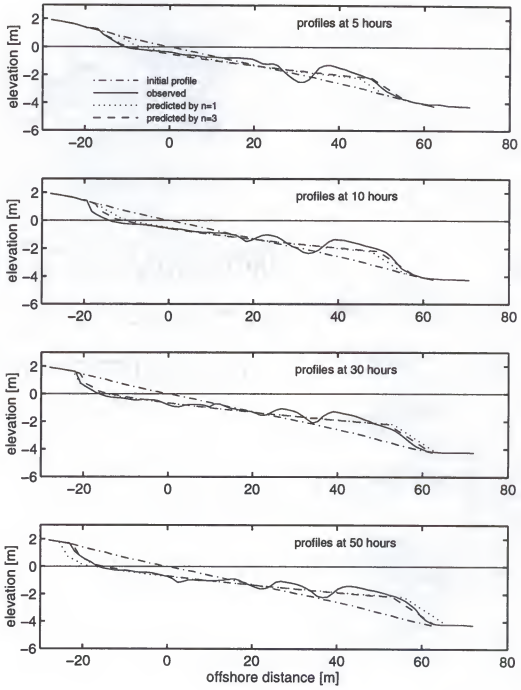

Figure 4.5 Case 300 from Saville's experiments. Comparisons of predicted to observed profiles at different times for the best-fit K values for each transport relationships.

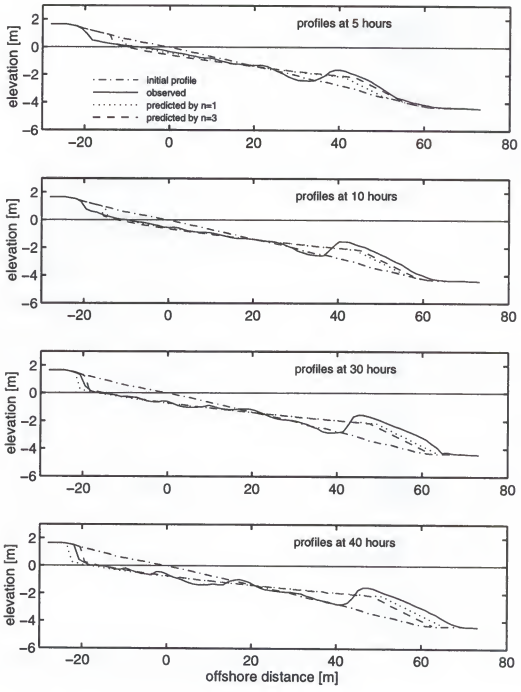

Figure 4.6 Case 400 from Saville's experiments. Comparisons of predicted to observed profiles at different times for the best-fit K values for each transport relationships.

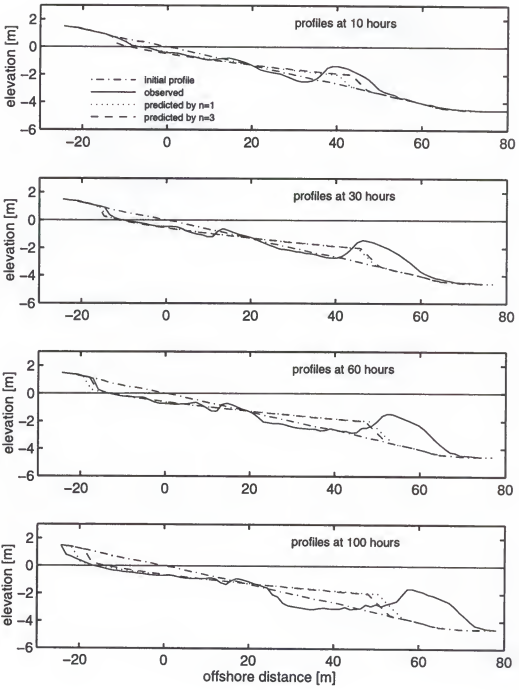

Figure 4.7 Case 500 from Saville's experiments. Comparisons of predicted to observed profiles at different times for the best-fit K values for each transport relationships.

a period of 6 seconds were generated in a water depth of 5 meters. The sand used for both experiments had a mean diameter of 0.33 mm, which corresponding to a fall velocity of 5 cm/s at a temperature of 20 °C and a profile scale parameter, A, of 0.131 $m^{1/3}$. Two initial profiles, termed "dune without foreshore" and "dune with foreshore", were used. The "dune without foreshore" had a dune crest of 2 meters above still water level and a seaward slope of 1:4 down to the channel floor. The "dune with foreshore" had a slope of 1:4 from the dune crest of 2 meters above still water level to 1 meter water depth followed by a slope of 1:20 down to the channel floor. The third experiment, a "dune without foreshore" was conducted with the same sediment as the other two but irregular waves. A JONSWAP-Spectrum was applied to generate random waves with a significant wave height of 1.5 meters and peak spectral wave period of 6 seconds in a water depth of 5 meters.

4.3.2 Experiments With Constant Waves

Two tests with the same constant wave conditions and different initial profiles were carried out in the German "Large Wave Flume" in 1986. They are denoted by their initial profiles as the "dune without foreshore" and the "dune with foreshore". During the experiments, a test was stopped generally whenever the wave height in the horizontal bottom portion (water depth of 5 meters) of the flume exceeded ± 20% of the originally generated wave height so that the breaking point could stay in its original position. After motions in the tank subsided, the tests were resumed.

Based on McCowan (1894) theory, waves break when the ratio of water depth to wave height becomes 1.28. The active water depth, which is the water depth at the breaking point, is determined as 1.92 meters for the numerical model according to the incident wave

Table 4.3 The numerical model inputs and best-fit results for the two constant wave cases in German "large wave flume'.

Case	Slope			Best-fit K		Error* [m^2]	
	dune	shoreline	offshore	n=3 [m^8s^2/N^3]	n=1 [m^4/N]	n=3	n=1
Dune without foreshore	3.00	0.20	0.20	7.64×10^{-10}	2.03×10^{-5}	0.74	8.08
Dune with foreshore	3.00	0.20	0.162	1.03×10^{-9}	8.13×10^{-6}	0.46	1.11

* Error represents the root mean square between predicted and observed eroded volume as shown in Eq. (4.1).

height of 1.5 meters. The input of the dune, shoreline and offshore slopes in the models are adopted based on the finial profiles in the two tests and are presented in Table 4.3. The best-fit K values and the corresponding errors of eroded volume resulting from the calibrations are also shown in Table 4.3. For the two cases, the non-linear transport relationship (n=3) produces much less error for the eroded volume than the linear transport relationship (n=1), especially in the case "dune without foreshore". Of relevance is that the best-fit K values for the non-linear transport equation (n=3) in the calibrations of the two cases here are close to those in Saville's experiments with a difference of less than a factor of 2. However the difference in the best-fit K value for the linear transport equation (n=1) is about a factor of 10 in Saville's experiments and German tests. The predicted eroded volumes as a function of time are compared with measurements in Figure 4.8 for the two cases. The predictions from the non-linear transport model (n=3) agree very well with the measured eroded volume over the whole test time for both cases with the same wave and sediment conditions but different initial profiles. This result supports the discussion in Chapter 3 that the non-linear model has

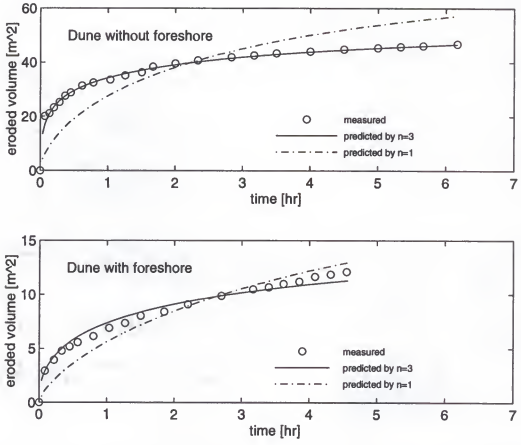

Figure 4.8 Comparisons of predictions with best-fit K values to observed eroded volumes for the two tests with constant waves in German "large wave flume".

capabilities to handle different initial conditions, whereas the linear transport relationship (n=1) cannot represent well the difference in time scale of profile evolution caused by the different initial conditions. Figure 4.8 clearly shows that the linear transport relationship has a difficulty in simulating the rapid response in the case of "dune without foreshore", although it could provide an acceptable predictions for the case "dune with foreshore".

Comparisons of the profiles predicted by the non-linear and the linear transport models and the measurements are presented in Figures 4.9 and 4.10 for the two cases,

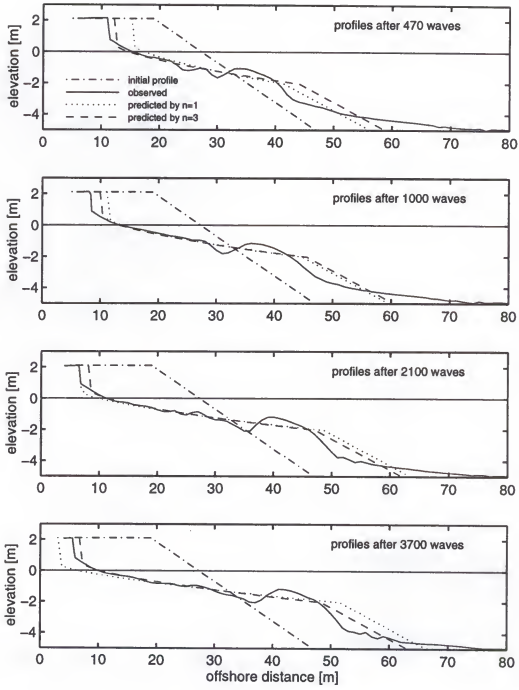

Figure 4.9 Case "dune without foreshore" under regular wave conditions. Comparisons of predicted to observed profiles at different times for the best-fit K values for each transport relationships.

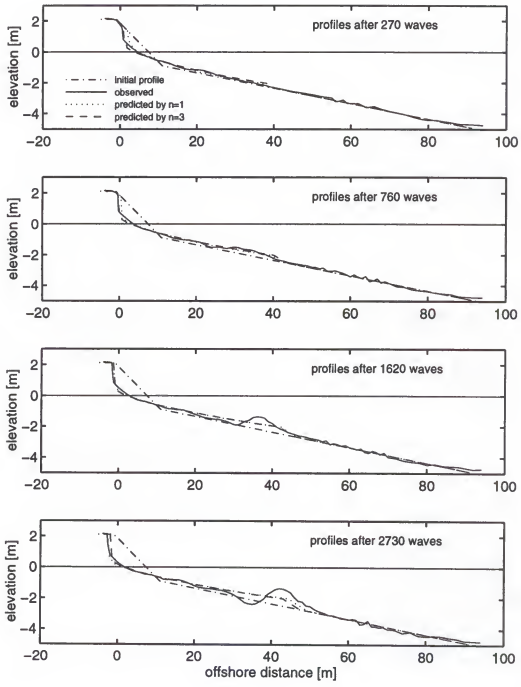

Figure 4.10 Case "dune with foreshore" under regular wave conditions. Comparisons of predicted to observed profiles at different times for the best-fit K values for each transport relationships.

respectively. To represent the profile evolution process, the profiles at four different times are presented. As shown in Figure 4.10, both the non-linear and linear transport relationships can simulate the profile evolution reasonably for the case "dune with foreshore" with corresponding best-fit K values. While in Figure 4.9, only the nonlinear model provides acceptable predictions for the profiles at different times for the case of "dune without foreshore". The linear model under-predicts beach erosion at the early stage and over-predicts it at later times.

4.3.3 Experiment With Irregular Waves

The initial profile "dune without foreshore" was conducted with irregular waves of a 1.5 meter significant wave height, 6 second peak spectral wave period and a water depth of 5 meters. The JONSWAP wave spectrum was applied to generate random waves with a repeating interval of 256 seconds. To reduce the wave reflection effects, the experiment was interrupted after three repetition intervals (i.e. every 768 seconds). The time series of water surface elevation for an interval in the flat part of the tank is presented in Figure 4.11(a). The corresponding zero-crossing wave heights and periods are shown in Figures 4.11(b) and (c), respectively. A total of 45 waves was included in each interval.

During numerical simulation, the wave heights and periods presented in Figure 4.11 are applied. The active water depth at each time step is determined as 1.28 times the incident wave height. The wave set-up and run-up are calculated by Eqs. (3.28) and (3.31), respectively, according to the instantaneous wave height. The desired dune, shoreline and offshore slopes presented in Table 4.4 are determined based on the final profiles. The best-fit K values and the corresponding errors of eroded volume for the non-linear and the linear

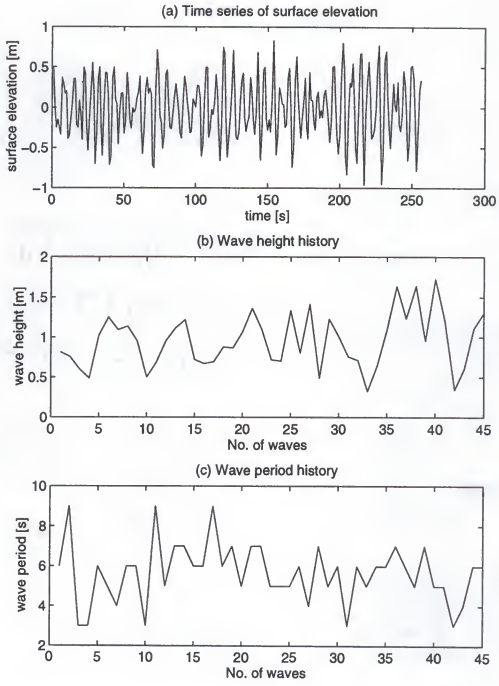

Figure 4.11 The irregular waves generated in the "large wave flume" for the experiment "dune without foreshore".

Table 4.4 The numerical model inputs and best-fit results for the German irregular wave case. Error represents the root mean square between predicted and observed eroded volume.

Case	Slope			Best-fit K		Error [m^2]	
	dune	shoreline	offshore	n=3 [m^8s^2/N^3]	n=1 [m^4/N]	n=3	n=1
Dune without foreshore	3.00	0.18	0.50	4.51×10^{-10}	2.11×10^{-5}	1.58	2.48

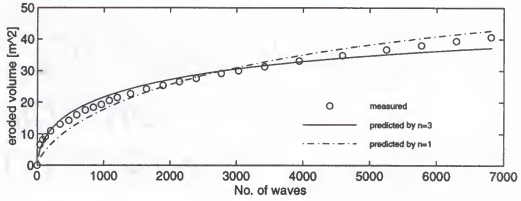

Figure 4.12 Comparisons of predictions with best-fit K values to observed eroded volumes for the German irregular wave experiment.

transport relationships are also shown in Table 4.4. It is noticed that the range of best-fit K value for the non-linear model is smaller than that in the five experiments with constant waves calibrated above. The time histories of the observed eroded volumes is compared with the predictions from the two transport relationships in Figure 4.12. It appears that the nonlinear model provides a better overall fit for the eroded volume at different times. The comparisons of the predicted and observed profiles at four different times are shown in Figure 4.13. The agreements between the predictions for n=3 and the measurements are acceptable.

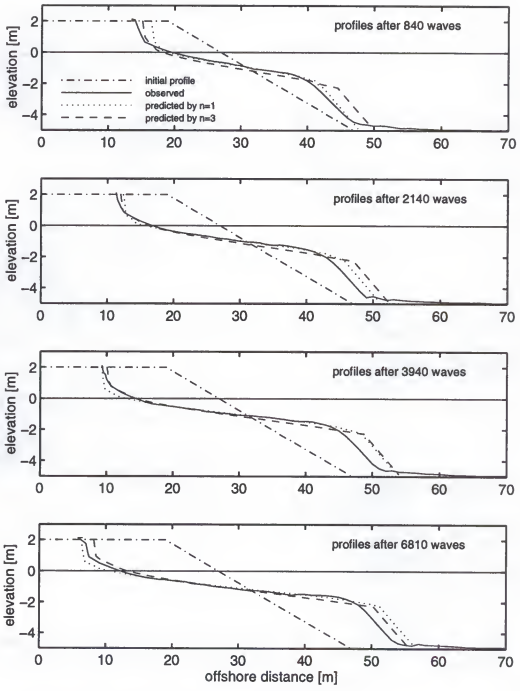

Figure 4.13 Test of "dune without foreshore" with irregular waves. Comparisons of predicted to observed profiles at four different times for the best-fit K values for each transport relationship.

4.4 SUPERTANK Experiments

The SUPERTANK Laboratory Data Collection Project, or, simply "SUPERTANK" was conducted in the large wave tank at the O.H. Hinsdale Wave Research Laboratory, Oregon State University (Kraus and Smith 1994, Smith and Kraus 1995). The project ran for the 8-week period from 29 July to 20 September 1991. The wave tank channel is 104 meters long, 3.7 meters wide, and 4.6 meters deep, into which a 76-meter-long beach was constructed. Among the 20 major data collection tests performed during SUPERTANK, ST-10 was the longest test (21 hours of wave action) and conducted to observe beach response to erosive random waves. The test was run with combinations of random and monochromatic waves with random waves used for most of the experiment duration. The time histories of significant wave height and peak spectral wave period at a water depth of about 2.6 meters are shown in Figure 4.14, where "mon" represents the intervals with monochromatic wave conditions. The constant wave heights and periods are plotted for the period when monochromatic waves were generated. The beach sediment consisted primarily of very uniform sand with median grain-size diameter of 0.22 mm.

During the numerical simulation, a random wave series was generated according to the input of significant wave heights and peak spectral wave periods shown in Figure 4.14. The input dune, shoreline and offshore slopes determined from the measured finial beach profile are presented in Table 4.5 with the best-fit K values and the corresponding errors of eroded volume together. The time histories of predicted eroded volumes are compared with the observations in Figure 4.15. It appears that the linear transport model presents a somewhat smaller error for the beach erosion process. The comparisons of predicted and

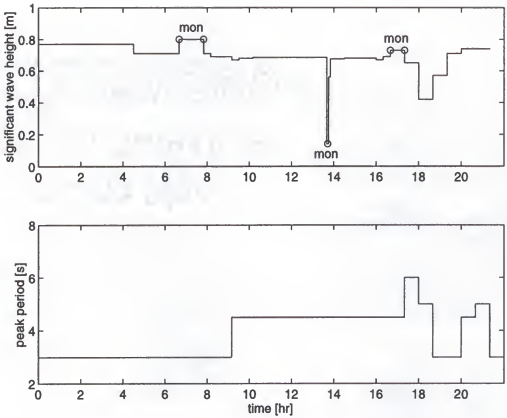

Figure 4.14 Significant wave height and peak spectral wave period time history of ST-10 test in SUPERTANK.

Table 4.5 The numerical model inputs and best-fit results for the test ST-10 in SUPERTANK. Error represents the root mean square between predicted and observed eroded volume.

Case	Slope			Best-fit K		Error [m^2]	
	dune	shoreline	offshore	n=3 [m^8s^2/N^3]	n=1 [m^4/N]	n=3	n=1
ST-10	0.6	0.22	0.16	5.26×10^{-10}	3.03×10^{-6}	0.55	0.37

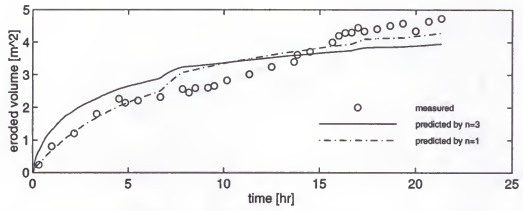

Figure 4.15 Comparisons of predicted with best-fit K values to observed eroded volumes for the test ST-10 in SUPERTANK .

measured profiles at four different time are shown in Figure 4.16. In this case, the measured profiles are steeper than the profiles predicted by non-linear and linear models.

4.5 Results of Laboratory Calibration and Comparison

A total of seven experiments conducted in three different large tanks are employed for the calibration and comparison of the proposed non-linear transport relationship versus the linear transport relationship. Five of these tests were conducted with regular wave conditions and the other two were carried out with random waves. Different sediment sizes, initial profiles, incident wave heights and fall velocity parameters characterized the experiments.

The summary of the experimental parameters, wave conditions, critical profile slopes and the best-fit results of the two numerical relationships are presented in Table 4.6. It appears that the fine sediment generally has a relative mild dune, shoreline and offshore slopes and the coarse sand corresponds to relative steep slopes, consistent with early findings by Bascom (1951). The eroded volume errors, which are used as the objective in the fitting process, are defined as the root mean square values of the deviations of predicted and

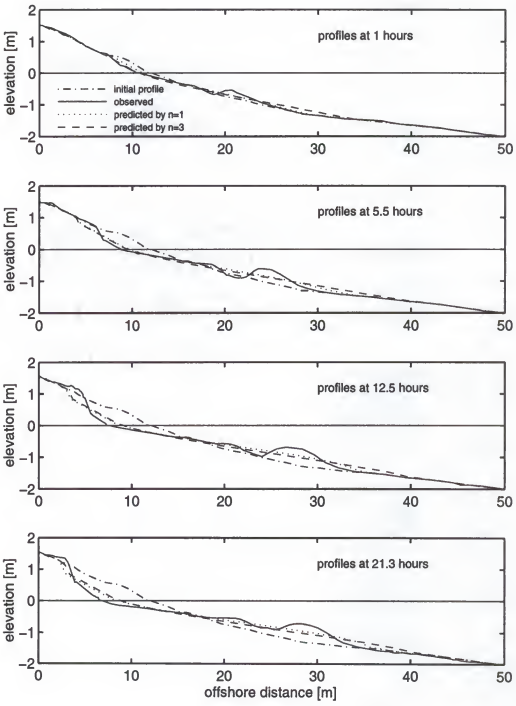

Figure 4.16 Test ST-10 in SUPERTANK. Comparisons of predicted to observed profiles at four different times for the best-fit K values for each transport relationship.

Table 4.6 Summary of laboratory calibration.

Case		Saville's Experiment			SUPERTANK
		Case 300	Case 400	Case 500	ST-10
Tank Size	Length (m)	194	194	194	104
	Width (m)	4.6	4.6	4.6	3.7
	Depth (m)	6.1	6.1	6.1	4.6
Wave Height, H, (m)		1.68	1.62	1.52	0.8 [1]
Wave Period, T, (s)		11.33	5.60	3.75	3 ~ 4.5 [2]
Sediment Size, d_{50} (mm)		0.22	0.22	0.22	0.22
A [3] ($m^{1/3}$)		0.106	0.106	0.106	0.106
Active Water Depth, h_*, (m)		2.15	2.08	1.95	H/0.78 [4]
H / wT		4.96	9.64	13.52	Varies
Slope	Dune	0.50	1.00	0.50	0.60
	Shoreline	0.15	0.17	0.13	0.22
	Offshore	0.20	0.15	0.30	0.16
Best-fit K	n=3 (m^8s^2/N^3)	8.55×10^{-10}	7.97×10^{-10}	5.77×10^{-10}	5.26×10^{-10}
	n=1(m^4/N)	3.45×10^{-6}	3.71×10^{-6}	1.57×10^{-6}	3.03×10^{-6}
Error of Eroded Vol. (m^2)	n=3	2.08	1.78	3.99	0.55
	n=1	3.37	2.40	1.88	0.37

[1] Wave heights varied during the test. The representative significant wave height is 0.8 m.

[2] Wave periods varied during the test. The representative peak wave periods are 3 and 4.5 seconds.

[3] A is the profile scale parameter.

[4] The active water depth is determined according each individual wave height.

Table 4.6 (Continued) Summary of laboratory calibration.

Case		German "Large Wave Flume"			Average of Seven Tests
		Constant Waves		Irregular Waves	
		Dune W/O Foreshore	Dune With Foreshore	Dune W/O Foreshore	
Tank Size	Length	324	324	324	
	Width	5	5	5	
	Depth	7	7	7	
Wave Height, H, (m)		1.5	1.5	1.5 [1]	
Wave Period, T, (s)		6	6	6 [2]	
Sediment Size, D_{50} (mm)		0.33	0.33	0.33	
A [3] ($m^{1/3}$)		0.131	0.131	0.131	
Active Water Depth, h., (m)		1.92	1.92	H/0.78 [4]	
H / wT		5.00	5.00	Varies	
Slope	Dune	3.00	3.00	3.00	1.66
	Shoreline	0.20	0.20	0.18	0.18
	Offshore	0.20	0.16	0.50	0.22
Best-fit K	n=3 (m^8s^2/N^3)	7.64×10^{-10}	1.03×10^{-9}	4.51×10^{-10}	7.14×10^{-10}
	n=1(m^4/N)	2.03×10^{-5}	8.16×10^{-6}	2.11×10^{-5}	6.07×10^{-6}
Error of Eroded Vol. (m^2)	n=3	0.74	0.46	1.58	1.58
	n=1	8.08	1.11	2.48	2.81

[1] The significant wave height is used.

[2] The peak wave period is used.

[3] A is the profile scale parameter

[4] The active water depth is determined according each individual wave height.

measured eroded volumes over the time of each experiment. It is noticed that the best-fit transport coefficient K in the non-linear relationship has a much narrower range than that for the linear relationship. The average best-fit K value of the non-linear relationship is 7.14×10^{-10} m^8s^2/N^3 with a variation from -37% to +44%, whereas the best-fit K values of the linear relationship range between -74% to +248% of the average value of 6.07×10^{-6} m^4/N. On average, the non-linear relationship yields an error of 1.58 m^2 for the eroded volumes and the linear relationship yields 2.81 m^2.

Based on these results, it is determined that the non-linear transport relationship with n=3 is more appropriate in the cross-shore sediment transport model (CROSS). The transport coefficient $K = 7.14\times10^{-10}$ m^8s^2/N^3 is adopted according to the average of the best-fit K values in the seven tests. The input dune slope, which is used to establish the equilibrium post-storm profile slope above the run-up limit, is usually quite steep and may be considered as 1 for most cases, although it can be much steeper for a laboratory experiment with coarse sediment. The offshore slope, which controls the slope at the end of deposited volume, may be taken as 0.15. In laboratory experiments, this offshore slope may be steeper than the value of 0.15 for a steep initial profile. The shoreline slope, which is the anticipated profile slope between the shoreline and the run-up limit, is usually steep for laboratory experiments and mild for field storm erosion. The value of 0.18 may be used for the shoreline slope for laboratory data. In field storm erosion, the measured pre-storm shoreline slope may be applied as the input of shoreline slope. For the more general case in which there is no measured equilibrium shoreline slope available, the results of Bascom (1951) may be used to determine a shoreline slope according to the sediment size and wave height.

CHAPTER 5
EVALUATION OF CROSS WITH LABORATORY EXPERIMENTS

Chapter 4 provided the results of the calibration of the CROSS model in which the profile parameter, A, was selected according to sediment size, and the dune, shoreline and offshore slopes were based on observed values for each experiment, and the best-fit transport coefficient, K, was determined as the value yielding the overall least squares error for the eroded volume in each experiment. For the seven experiments used in the calibration, the best-fit K values vary from 4.51×10^{-10} to 1.03×10^{-9} m^8s^2/N^3. Based on the calibration results, the K value of 7.14×10^{-10} m^8s^2/N^3 which is the average of the best-fit K values was recommended for the applications of CROSS. The purpose of this chapter is to evaluate the CROSS model with sediment size dependent A values, recommended average K value and fixed dune, shoreline and offshore slopes by using the same laboratory data. The CROSS model with the average K value and fixed input slopes is applied to the seven experiments used in Chapter 4 for calibration, and the results of the fixed parameters are compared with those of the best-fit K and slope values. The comparisons include the time history of eroded volume and the profile evolution for each experiment.

5.1 Application of CROSS to Laboratory Experiments

The seven experiments described in Chapter 4 are included in the evaluations of the CROSS model. The input slopes and the K value of CROSS for all seven experiments are

shown in Table 5.1, where the dune, shoreline and the offshore slopes are averaged slopes listed in Table 4.6. The profile parameter, A, is determined according to the sand size in each individual test.

Table 5.1 The input K value and dune, shoreline and offshore slopes in CROSS.

K (m^8s^2/N^2)	Slope		
	Dune	Shoreline	Offshore
7.14×10^{-10}	1.66	0.18	0.22

5.1.1 Saville's Experiments

The CROSS model with the fixed values in Table 5.1 is applied to Cases 300, 400 and 500 of Saville's experiments. The wave conditions of the three cases are presented in Table 4.1. The profile parameter, $A = 0.106\ m^{1/3}$, is determined based on the median sand size of 0.22 mm for all three cases. The eroded volumes predicted with fixed and best-fit values are compared with the measurements in Figure 5.1. There are slight differences in the eroded volumes predicted by the two bases. It is shown that the CROSS model with fixed K and slope values yields less erosion for Cases 300 and 400 and more erosion for Case 500 than the model with the individual best-fit values. The corresponding beach profile evolutions observed and simulated are shown in Figures 5.2, 5.3 and 5.4 for Cases 300, 400, and 500, respectively. The profiles predicted by the two different K values at different times are quite similar for all three cases. The slight difference in the dune and offshore area is mostly caused by the difference in the input dune, shoreline and offshore slopes. Overall, it appears that the predictions of CROSS with fixed parameters are quite close to these predicted by the best-fit K and slope values.

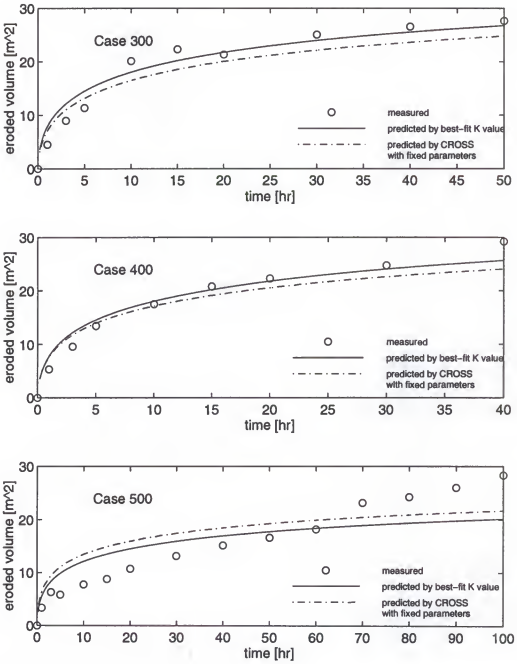

Figure 5.1 Comparisons of predictions of CROSS with fixed and best-fit K and slope values to observed eroded volumes for Cases 300, 400, and 500 in Saville's experiments.

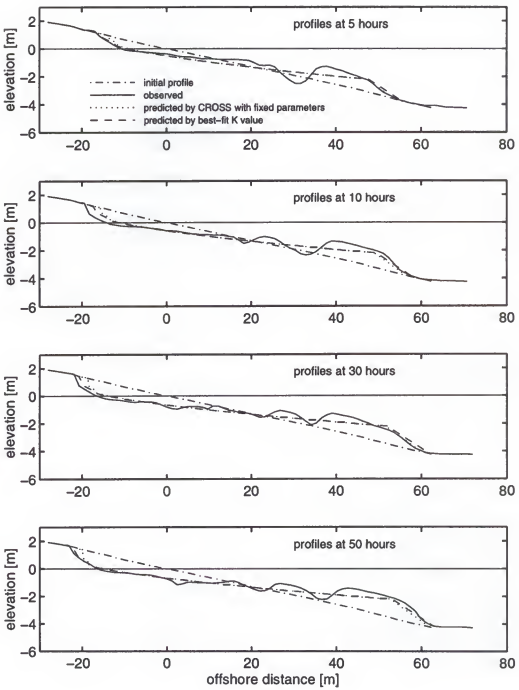

Figure 5.2 Case 300 from Saville's experiments. Comparisons of the measured and predicted profiles by CROSS with fixed and best-fit K and slope values.

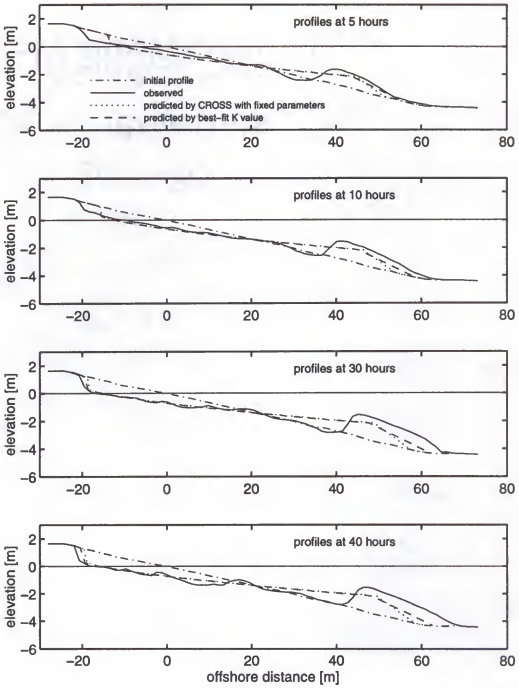

Figure 5.3 Case 400 from Saville's experiments. Comparisons of the measured and predicted profiles by CROSS with fixed and best-fit K and slope values.

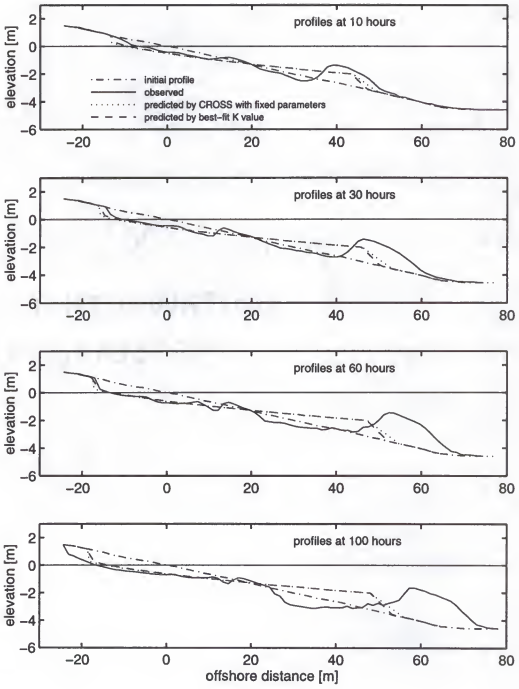

Figure 5.4 Case 500 from Saville's experiments. Comparisons of the measured and predicted profiles by CROSS with fixed and best-fit K and slope values.

5.1.2 German "Large Wave Flume"

Three experiments carried out in the German "large wave flume" are investigated. The sand used in the experiments had a mean diameter of 0.33 mm, which corresponding to a profile scale parameter, A = 0.131 $m^{1/3}$. Two of these experiments had the same monochromatic wave conditions and different initial profiles. Regular waves with a wave height of 1.5 meters and a period of 6 seconds were generated in a water depth of 5 meters. The two initial profiles are "dune without foreshore" and "dune with foreshore" described in Chapter 4. The third experiment, a "dune without foreshore" was conducted with random wave conditions of a significant wave height of 1.5 meters and a peak spectral wave period of 6 seconds.

The observed eroded volumes as a function of time are compared with the numerical results for the two monochromatic wave experiments in Figure 5.5, where both CROSS with the fixed and best-fit K values are applied for the predictions. The differences between the two models are very insignificant. CROSS with fixed parameters predicts slightly less erosion in both tests than the best-fit K and slope values. The corresponding beach profile evolutions are presented in Figures 5.6 and 5.7 for the cases "dune without foreshore" and "dune with foreshore", respectively. In both experiments, the profiles predicted with fixed and best-fit values are almost identical at all times presented in the figures. Overall, it appears that the predictions with fixed values are quite close to those of the best-fit values.

In the third experiment with irregular wave conditions, the time series of wave heights and periods presented in Figure 4.11 is applied in the simulations. The observed eroded volumes and the predictions of CROSS and the best-fit K values are shown in Figure 5.8.

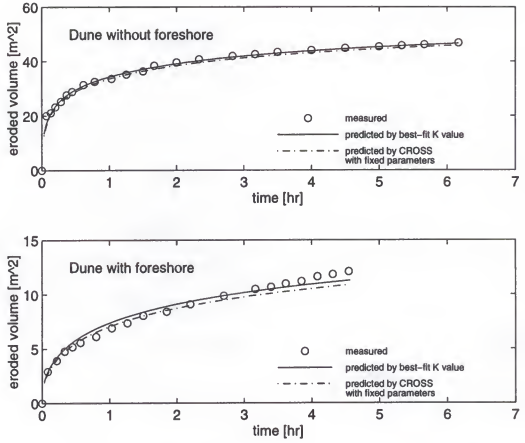

Figure 5.5 Comparisons of observed eroded volumes to predictions of CROSS with fixed and best-fit K and slope values for the two experiments with regular waves in German "large wave flume".

Compared with the measurements and the results of the best-fit K value, much more beach erosion is presented for the fixed values. Comparisons of the measured and the predicted profiles are presented in Figure 5.9. It appears that the overprediction of erosion with fixed values is mainly caused by the mild input offshore slope. In the experiment, the eroded material deposited offshore with a steep slope of 0.5 (corresponding to an angle of 26.6°) compared to the fixed offshore slope of 0.22 used in the model which is much milder than the measured value. In this experiment, since the initial profile is very steep and quite far away

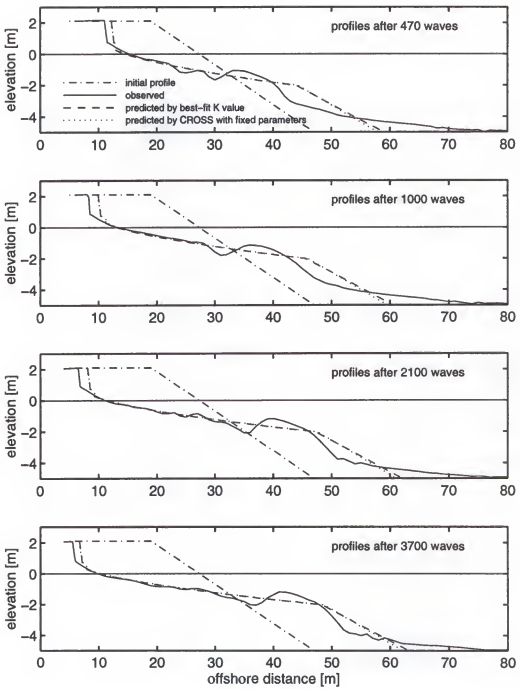

Figure 5.6 Case "dune without foreshore" under regular wave conditions. Comparisons of measured and predicted profiles by CROSS with fixed and best-fit K and slope values.

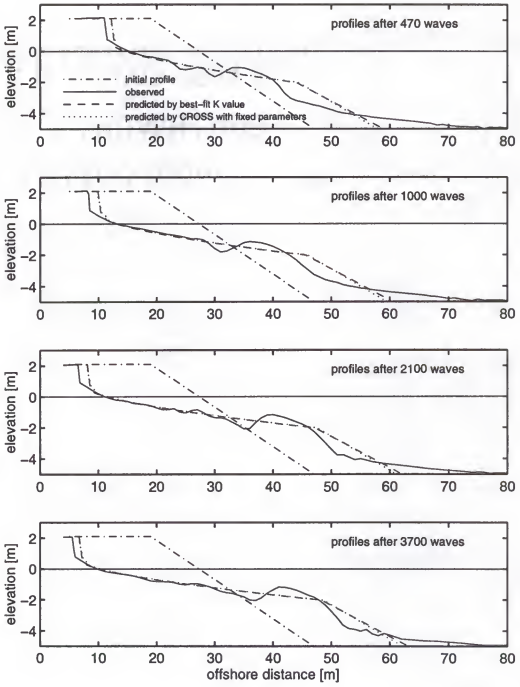

Figure 5.7 Case "dune with foreshore" under regular wave conditions. Comparisons of measured and predicted profiles by CROSS with fixed and best-fit K and slope values.

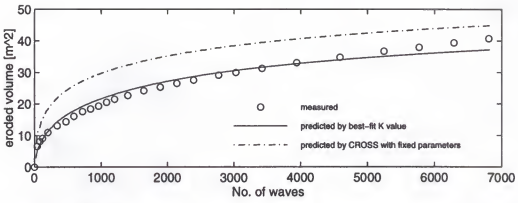

Figure 5.8 Comparisons of observed eroded volumes to the predictions of CROSS with fixed and best-fit K and slope values for German irregular wave experiments. The fixed offshore slope of 0.22 is used in CROSS.

from equilibrium, the volume difference caused by the two different offshore slopes is significant. The results of numerical models are quite sensitive to the offshore slope used in models. However, the sensitivity of CROSS to the offshore slope becomes much less in field applications, since in most cases the initial beach profiles in the field are much milder and thus closer to equilibrium. To evaluate the effects of the offshore slope in the CROSS model, an offshore slope of 0.5, which is determined according to the observed finial profile, is applied. The results of eroded volumes and the profile evolution are compared with the measurements and the predictions of best-fit K and slope values in Figures 5.10 and 5.11, where it is seen that the two results are quite close. The results with the fixed K value predicts slightly more beach erosion than the best-fit K value. Comparing results in Figures 5.10 and 5.11 with those in Figures 5.8 and 5.9, it appears that most of the overprediction in Figures 5.8 and 5.9 is caused by the mild offshore slope used in the model.

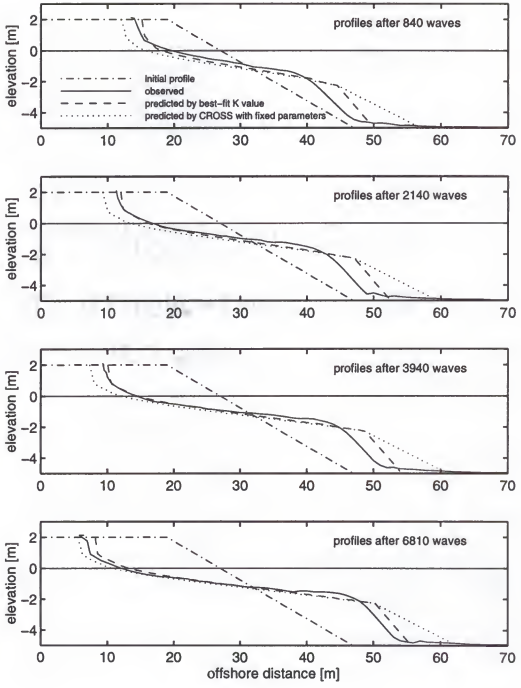

Figure 5.9 Case "dune without foreshore" with irregular waves. Comparisons of measured and predicted profiles by CROSS with fixed and best-fit K and slope values. The fixed offshore slope of 0.22 is used in CROSS.

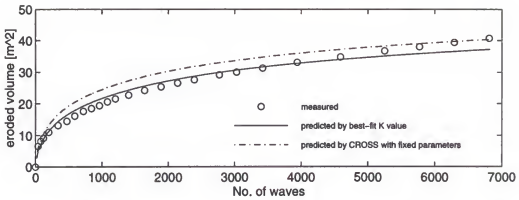

Figure 5.10 Comparisons of observed eroded volumes to predictions of CROSS with fixed and best-fit K and slope values for German irregular wave experiments. An offshore slope of 0.50 is used in CROSS.

5.1.3 SUPERTANK Experiments

The test "ST-10" was conducted in the SUPERTANK laboratory data collection project to observe beach response to erosive wave conditions. The test was run with combinations of random and monochromatic waves. The random waves were conducted for most of the experimental times and the monochromatic waves were used only for three short intervals. The detailed wave conditions during the test are presented in Figure 4.14. The beach sediment consisted primarily of very uniform sand with a median grain-size diameter of 0.22 mm. The profile parameter, A, of 0.106 $m^{1/3}$ is determined based on the median sand size. The eroded volumes predicted by the CROSS model with fixed and best-fit K and slope values are compared with measurements in Figure 5.12. It is noticed that the differences between the two numerical results are insignificant with slightly more erosion predicted by the fixed parameters. The measured profiles observed at four different times during the experiments are compared with the predictions by the two bases in Figure 5.13. At each time, the two predicted profiles have almost identical subaqueous portions. The slight difference

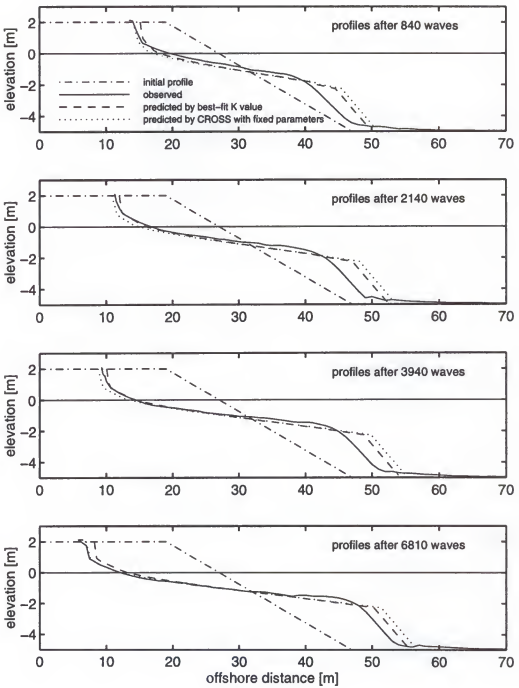

Figure 5.11 Case "dune without foreshore" with irregular waves. Comparisons of measured and predicted profiles by CROSS with fixed and best-fit K and slope values. An offshore slope of 0.50 is used in CROSS.

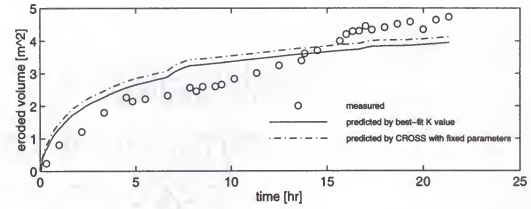

Figure 5.12 Comparisons of observed eroded volumes to predictions of CROSS with fixed and best-fit K and slope values for the test ST-10 in SUPERTANK.

in the dune erosion area is caused mainly by the difference in the anticipated equilibrium dune and shoreline slopes. It appears the profiles predicted by the two bases are in good agreement.

5.2 Results of Evaluation

The predictions of CROSS with fixed parameters evaluated for the seven experiments are quantified in terms of the non-dimensional deviation of the eroded volume root-mean-square error defined in Eq. (4.1). The deviation is expressed as

$$Dev = \frac{Err_F - Err_B}{Err_B} \tag{5.1}$$

where Dev denotes a non-dimensional deviation, Err is the error of eroded volume, the subscript F and B represent the results of the CROSS model with fixed and best-fit K and slope values, respectively. If the predictions of CROSS with fixed values are exactly identical to those of the best-fit values, the deviation defined in Eq.(5.1) is zero. Generally, the sign of

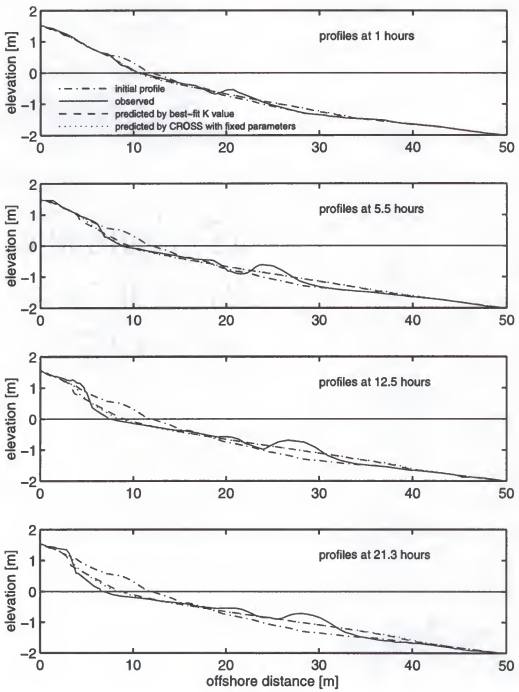

Figure 5.13 Test ST-10 in SUPERTANK. Comparisons of measured and predicted profiles by CROSS with fixed and the best-fit K and slope values.

Table 5.1 The root mean square errors of eroded volumes predicted by CROSS with fixed and best-fit K and slope values, and the corresponding non-dimensional deviations.

Test	Best-fit values					Fixed values	
	K (m^8s^2/N^3)	Slope			Error (m^2)	Error (m^2)	Deviation of fixed vs. best-fit values
		dune	shoreline	offshore			
Case 300	8.55×10^{-10}	0.50	0.15	0.20	2.08	2.62	0.26
Case 400	7.97×10^{-10}	1.00	0.17	0.15	1.78	2.30	0.29
Case 500	5.77×10^{-10}	0.50	0.13	0.30	3.99	4.20	0.05
"D w/o F", mon[1]	7.64×10^{-10}	3.00	0.20	0.20	0.74	1.14	0.54
"D w F", mon[2]	1.03×10^{-9}	3.00	0.20	0.16	0.46	0.57	0.24
"D w/o F", Irr[3]	4.51×10^{-10}	3.00	0.18	0.50	1.58	8.03	4.08
ST-10	5.26×10^{-10}	0.60	0.22	0.16	0.55	0.60	0.09

[1] "D w/o F" denotes the initial profile of "dune without foreshore" and "mon" means monochromatic wave conditions.
[2] "D w F" represents the initial profile of "dune with foreshore".
[3] "Irr" corresponds to irregular wave conditions.

Dev is positive since the model with best-fit K and slope values should yield less error for eroded volumes than that with fixed values.

The root mean square errors of CROSS with the fixed and the best-fit K and slope values are presented in Table 5.1 for the seven experiments. It is seen that, with the exception of the case "dune without foreshore" with irregular waves, the predictions with fixed K and slope values provide fits to the measured profiles which are nearly as good as those with the best-fit values for each experiment. As shown in Table 5.1, there are four experiments have the best-fit K values greater than the average K value of 7.14×10^{-10} m^8s^2/N^3 used in CROSS. They are Saville's Cases 300 and 400, and German "dune without foreshore" and "dune with

foreshore" with regular waves. In these four experiments, CROSS with fixed values predicts less beach erosion than that with best-fit values. In the other three experiments, which are Saville's Case 500, German irregular wave experiment and the test ST-10 in SUPERTANK, the best-fit K values are smaller than the average K value and the CROSS model with fixed values presents more erosion than that with best-fit K values.

Among the seven experiments, the case "dune without foreshore" with irregular waves in German large wave flume has significantly large deviations. As discussed in the section 5.1.2, the overprediction of CROSS with fixed values is mainly due to the mild offshore slope (0.22) used in the model. After using the observed offshore slope of 0.5, the predictions become quite close to those of the best-fit K value. The error of eroded volume decreased from 8.03 to 3.43 m^2, and the corresponding deviation is equal to 1.17.

In the experiment of German "dune without foreshore" with monochromatic waves, the deviation of 0.54 is the second highest in all seven tests. However, as clearly shown in Figures 5.5 and 5.6, the predictions with fixed and best-fit values are rather close to each other. The relatively large deviation in this case is caused by the small error of the best-fit K value. Since the initial profile was quite steep, the beach eroded rapidly during the experiment. After 6 hours, the measured eroded volume is about 43 m^2. The error of eroded volume predicted with fixed and best-fit K and slope values are 1.14 and 0.74 m^2, which are only 2.7% and 1.7% of the total eroded volume, respectively.

Except for the two cases discussed above, the deviations with fixed parameters are less than 30% in the other five tests. Overall, the results with fixed and best-fit K and slope values agree reasonably well.

CHAPTER 6
APPLICATION OF CROSS FOR NOVEMBER 1991 AND JANUARY 1992 STORMS EROSION AT OCEAN CITY, MARYLAND

6.1 Background

Ocean City, Maryland, is located on Fenwick Island, a north-south oriented sandy barrier island of the central Delaware-Maryland-Virginia coast. The island extends from Indian River Inlet, Delaware, on the north to Ocean City Inlet on the south and is backed by Isle of Wight and Assawoman Bays. The Ocean City beach was nourished by the State of Maryland in 1988, and the Federal Government in 1990 and 1991 to protect the city against storm damage (Stauble et al. 1993, Grosskopf and Stauble 1993). A map of the project layout is given in Figure 6.1. The fill constructed by the State of Maryland consisted of approximately 2.7 million cubic yards (2.1 million cubic meters) of material placed along the entire project area. The total amount of material placed in the Federal project was 3.8 million cubic yards (2.9 million cubic meters). Both State and Federal fill material were taken from Borrow Areas 2 and 3 (Figure 6.1). The representative grain sizes from Borrow Areas 2 and 3 are 0.25 mm and 0.35 mm, respectively. The entire project was finished in August 1991.

After the project, a series of storms occurred in late 1991 and early 1992. Among these 1991-1992 winter storms, the January 4, 1992 was very severe with a peak storm surge of 2 meters (Jensen and Garcia 1993). The initial pre-storm beach profiles were surveyed on November 2-4, 1991, and the post-storm profiles were surveyed on January 11, 1992. In this

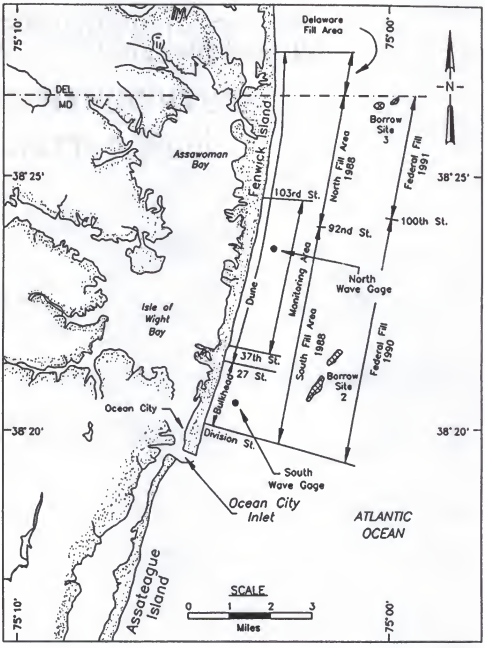

Figure 6.1 The Ocean City beach nourishment project layout.

period, an additional storm occurred on November 11, 1991. To be consistent with the measured pre-storm and post-storm profiles, both November 1991 and January 1992 storms are included in the numerical simulations. The data for seven survey lines located from the southern (37th Street) to northern (124 Street) portions of the project are available for both pre- and post-storm surveys (Stauble et al. 1993 and Kraus & Wise 1993).

In this chapter, the CROSS model developed in Chapters 3 and 4 is compared with three commonly used "closed loop" cross-shore sediment transport models for the simulations of beach erosion at Ocean City during the November 1991 and January 1992 storms. The three models are

- CCCL (Coastal Construction Control Line Model, Chiu & Dean 1984,1986)
- EDUNE (Equilibrium DUNE, Kriebel & Dean 1985, Kriebel 1986,1989,1990)
- SBEACH (Shore and BEAch CHange, Larson & Kraus 1989, Larson et al. 1989)

Two versions (2.0 and 3.0) of the SBEACH model will be included in the following comparisons. Version 3.0 was released in September 1994 by the US Army Corps of Engineers after a study of storm erosion at Ocean City during 1991-1992 winter storms. Three measures are proposed to compare model performance quantitatively. After model comparisons, the sensitivity of the CROSS model to transport coefficient, active water depth, storm surge, and wave height are evaluated.

6.2 Brief Description of Three Commonly Used Models

All three models discussed here are of the "closed loop" type and based on equilibrium beach profile concepts. They are the three most commonly used cross-shore erosion models

in the United States. Each of these three models is discussed briefly in the following paragraph.

6.2.1 CCCL Model

Under erosive water level and wave conditions, the time dependent beach recession, R(t), is given by

$$R(t) = R_{\infty}(1-e^{-Kt}) \tag{6.1}$$

Where R_{∞} is the equilibrium recession (i.e. the recession if the conditions were held constant for an infinite time) and K is a decay parameter (0.075/hour). At each time step, for a given storm surge, breaking wave height and initial profile, the equilibrium profile and recession are calculated by considering the following two facts: (1) sand conservation: the erosion sand volume is equal to that deposited; and (2) the subaqueous equilibrium profile about the instantaneous water level follows Eq.(3.2) and the subaerial part, up to the dune crest, is characterized by a uniform slope. The offshore limit of profile modification is the break point. The actual profile response at the end of the time step is determined by Eq.(6.1). After the final time step computation, a factor of 2.5 is applied to the recession to incorporate variability of beach erosion at different locations.

6.2.2 EDUNE Model

The cross-shore sediment transport rate per unit beach width, Q, is determined by the deviation of local wave energy dissipation per unit volume from the equilibrium as:

$$Q = K(D-D_{*}) \tag{6.2}$$

Where K is an empirical transport parameter (8.73×10^{-6} m^4/N) and D is the local wave energy dissipation per unit volume,

$$D = \frac{5}{24}\rho g\sqrt{g}\,\kappa^2\sqrt{h}\,\frac{\partial h}{\partial y} \tag{6.3}$$

Since D is proportional to the product of the square root of the local water depth and the bottom slope, a beach with a steeper or milder slope than the equilibrium will have sediment transported offshore or onshore, respectively. During a storm, an increased water level increases the degree of disequilibrium. As a result, the beach will erode.

Since the transport Eq. (6.2) has two variables, the continuity equation is used to close the system, which is written as:

$$\frac{\partial y}{\partial t} = -\frac{\partial Q}{\partial h} \tag{6.4}$$

An implicit finite difference scheme is applied to solve Eqs.(6.2) and (6.4) simultaneously. Profile change is bounded onshore by the wave run-up limit and offshore by the break point.

6.2.3 SBEACH Model

The distribution of transport across the nearshore active zone is calculated using different relationships in four distinct zones identified as follows:

- Zone I: Pre-breaking zone, extending offshore from the breaking point.
- Zone II: Transition zone, from the break point to the plunge point.
- Zone III: Broken wave zone, from the plunge point to the seaward limit of swash zone.
- Zone IV: Swash zone, from the seaward swash zone limit to the run-up limit.

A summary of the four zones and corresponding transport relationships is presented in Fig.6.2.

Zone I: The sediment transport rate is expressed as

$$Q = Q_{BP} \exp[-\lambda_1 (y - y_{BP})] \tag{6.5}$$

Where Q_{BP} is the sediment transport at the break point, λ_1 is the spatial decay coefficient and y_{BP} is the break point location. The quantity λ_1 is equal to 0.11 m^{-1} for accretionary conditions. For erosional conditions λ_1 is given by

$$\lambda_1 = 0.4 \left(\frac{d_{50}}{H_b} \right)^{0.47} \tag{6.6}$$

Where d_{50} is the median grain size in mm while the breaking wave height, H_b, is in m and λ_1 is in m^{-1}.

Zone II: The sediment transport is given by

$$Q = Q_{PP} \exp[-\lambda_2 (y - y_{PP})] \tag{6.7}$$

Where Q_{PP} is the transport rate at the plunge point located at y_{PP} and the decay coefficient λ_2 is approximately 0.20 - 0.25 of the value of λ_1.

Zone III: The sediment transport rate is determined by

$$\begin{aligned} Q &= \pm K \left| D - D_* + \frac{\epsilon}{\kappa} \frac{\partial h}{\partial x} \right|, && D > D_* - \frac{\epsilon}{\kappa} \\ &= 0, && D \le D_* - \frac{\epsilon}{\kappa} \end{aligned} \tag{6.8}$$

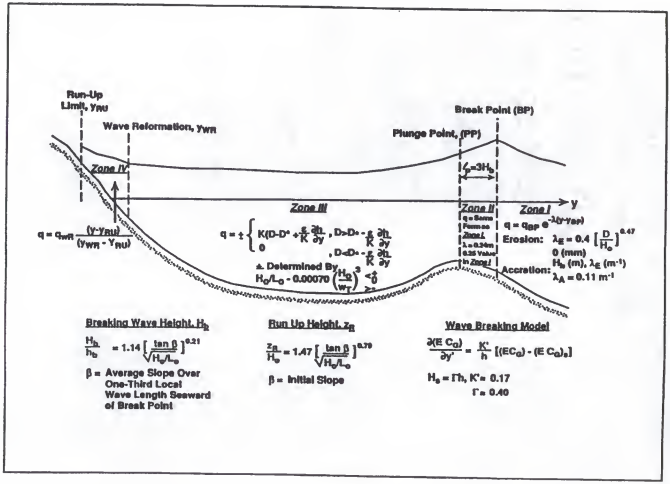

Figure 6.2 Sketch of the transport relationships in SBEACH model.

Where ϵ is an empirical constant (about 0.0006 m^2/s) and K is a transport rate coefficient. The relationship in this zone is similar to EDUNE except for the last term which incorporates the effect of local slope.

Zone IV: The transport equation is a linear function of offshore distance,

$$Q = Q_{WR} \frac{y - y_{RU}}{y_{WR} - y_{RU}} \tag{6.9}$$

Where subscript RU and WR denote run-up limit and landward end of surf zone (wave reformation point) respectively.

The direction of transport rate in all four zones is determined by the ± sign in Equation (6.8) according to the following criterion

$$\frac{H_0}{L_0} < 0.0007\left(\frac{H_0}{wT}\right)^3 \qquad \textit{Offshore transport}$$

$$\frac{H_0}{L_0} \geq 0.0007\left(\frac{H_0}{wT}\right)^3 \qquad \textit{Onshore transport}$$

Where H_0 and L_0 are the deep water wave height and length respectively, w is the sediment fall velocity and T is the wave period. The beach profile evolution is solved by combining the transport relationships in the four zones with the continuity equation , which is

$$\frac{\partial h}{\partial t} = \frac{\partial Q}{\partial y} \tag{6.10}$$

6.3 Storm and Beach Profile Characteristics

6.3.1 Storm Assessment

Water depths and profile elevations used here are referenced to the NGVD (National Geodetic Vertical Datum), which lies 2 cm below mean water level for Ocean City. The wave height, wave period and storm surge time history during the two storms were measured by two gages located directly offshore of Ocean City in a water depth of 10 meters. The gages were installed by the Coastal Engineering Research Center, U.S. Army Engineers Waterways Experiment Station. The measured significant wave height, peak spectral wave period and storm surge are shown in Figures 6.3 and 6.4 for the November 11, 1991 and January 4, 1992 storms (Stauble et al. 1993), respectively. Since the storm surge was measured in a water depth of 10 meters, wave induced set-up was not incorporated in these measurements.

Within a radial distance of 480 km offshore from Ocean City, there are seven buoys operated by the National Data Buoy Center (NDBC). These buoys provide hourly measurements of wind and wave climate. The wave and wind climate for the January 1992 storm was presented by Jensen and Garcia (1993). To the south of Ocean City between NDBC Buoys 44014 and Chesapeake Light (Figure 6.5), the wave heights were strongly attenuated by dissipation during the January 1992 storm. The maximum energy based significant wave height for Buoy 44014 (water depth of 48 m) was about 7.5 m, whereas at Chesapeake Light (water depth of 12 m) the wave height was 5 m. To the north of Ocean City at NDBC Buoy 44025 and Ambrose Light (Figure 6.6), the magnitudes of the storm waves were diminished too. The maximum wave heights decreased from 6.3 at Buoy 44025 to 4.8 m at Ambrose Light with a decrease of water depth from 40 m to 25 m.

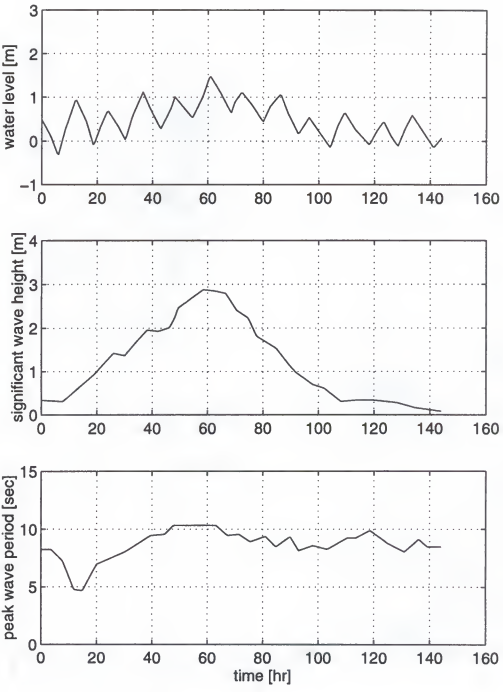

Figure 6.3 Water level, significant wave height and peak spectral wave period time history for the November 11, 1991 storm at Ocean City, MD (From Stable et al. 1993). Note : zero time corresponds to 0:00 on November 8, 1991.

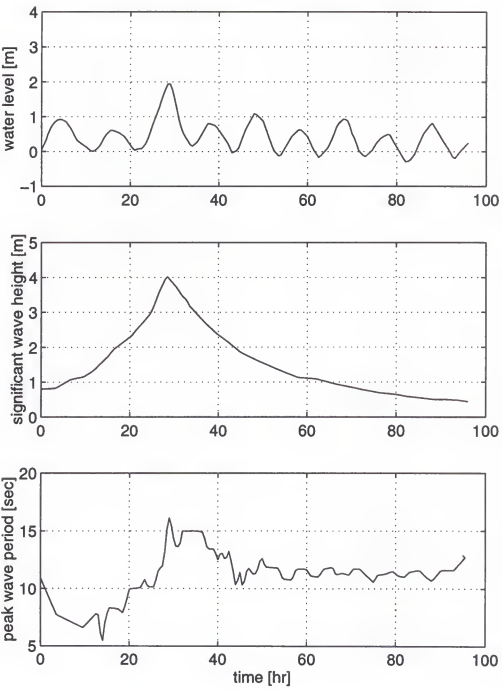

Figure 6.4 Water level, significant wave height and peak spectral wave period time history for the January 4, 1992 storm at Ocean City, MD (From Stauble et al. 1993). Note : zero time corresponds to 0:00 on January 3, 1992.

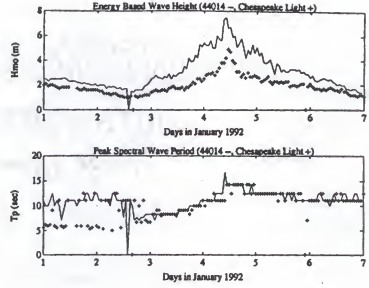

Figure 5 Energy-based wave height and peak spectral period for NDBC Buoy 44014 (h = 48 m) and Chesapeake Light (h = 12 m) (From Jensen and Garcia [1993].

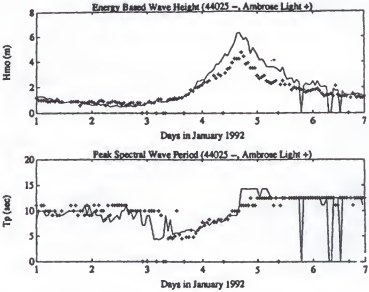

Figure 6 Energy-based wave height and peak spectral period for NDBC Buoy 44025 (h = 40 m) and Ambrose Light (h = 12 m) (From Jensen and Garcia [1993].

In the numerical simulations, the significant wave heights and peak spectral wave periods presented in Figures 6.3 and 6.4 are applied to generate random waves according to the Longuet-Higgins joint probability density function discussed in Chapter 3. Since the wave heights in the two figures were measured at water depths of 10 meters, wave shoaling effects are not included. On the other hand, as mentioned in the above paragraph, the wave heights decayed remarkably from deep to shallow water during the January 1992 storm. Therefore the significant wave heights presented in Figures 6.3 and 6.4 may differ slightly from the significant wave heights which impacted the beaches.

6.3.2 Beach Profile Characteristics

Seven survey lines located at 37th, 45th, 56th, 63rd, 74th, 103rd and 124th Streets have both pre-storm and post-storm measured profiles available and are simulated. In this study area, sediment samples along six profiles located at 37th, 56th, 66th, 81st, 92nd and 103rd Streets were collected during the June 1988 pre-State fill beach profile survey, the September 1988 post-State fill surveys, and the first three State fill monitoring surveys of January, April, and June 1989. The analyzed results were presented by Stauble et al. (1993). An average value was computed for the mean grain size within each of the 11 morphologic zones and is shown in Table 6.1. It is noticed that the four survey lines located at 45th, 63rd, 74th, 124th Streets have no sediment data available. Therefore, the grain size of the profile at 103rd Street is used for the profile at 124th Street, and the grain size at the other three profiles is determined by interpolation. Since the Federal fill project was conducted with the same borrow material, the grain size listed in Table 6.1 is applied in the numerical simulations of beach erosion during the November 1991 and January 1992 storms.

Table 6.1 Average mean grain size in millimeters.

Sample Location	37th St.	45th St.*	56th St.	63rd St.*	66th St.	74th St.*	81st St.	92nd St.	103rd St.**
Dune base	0.35	0.34	0.33	0.39	0.41	0.39	0.38	0.36	0.44
Berm crest	0.29	0.31	0.34	0.35	0.36	0.35	0.34	0.42	0.38
Mean-tide line	0.32	0.30	0.27	0.27	0.27	0.29	0.30	0.38	0.38
Swash zone	0.34	0.38	0.44	0.47	0.48	0.48	0.48	0.48	0.39
Nearshore trough	0.31	0.33	0.36	0.45	0.49	0.47	0.46	0.39	0.81
Nearshore bar	0.29	0.36	0.46	0.44	0.43	0.46	0.49	0.34	0.34
- 1.52 m contour	0.29	0.26	0.21	0.26	0.28	0.32	0.35	0.28	0.23
- 3.05 m contour	0.21	0.21	0.22	0.22	0.22	0.21	0.21	0.21	0.21
- 4.57 m contour	0.20	0.22	0.24	0.21	0.19	0.22	0.23	0.12	0.21
- 6.10 m contour	0.29	0.23	0.14	0.15	0.16	0.28	0.38	0.13	0.17
- 7.62 m contour	0.34	0.25	0.13	0.12	0.11	0.17	0.23	0.19	0.16

* The grain size at each morphologic zone is determined by interpolations.
** The grain size in this column is also used as the grain size of the profile at 124th St.

The seven measured pre-storm and post-storm profiles are shown in Figure 6.7 with the two surveys taken on November 2, 1991 and January 11, 1992, respectively. It appears that the storm-caused erosion is quite different for profiles at different locations. After two storms, the profiles at 37th and 56th Streets had almost no erosion, whereas the other profiles experienced quite severe losses in the dune area. To represent general profile change, an average profile is calculated by first matching all measured pre-storm or post-storm profiles at their respective shorelines and averaging the seven elevations at different cross-shore distances. Based on the measured profiles, the total volumes gained and lost from the pre-storm and post-storm profiles are calculated for each profile and presented in Table 6.2. It is

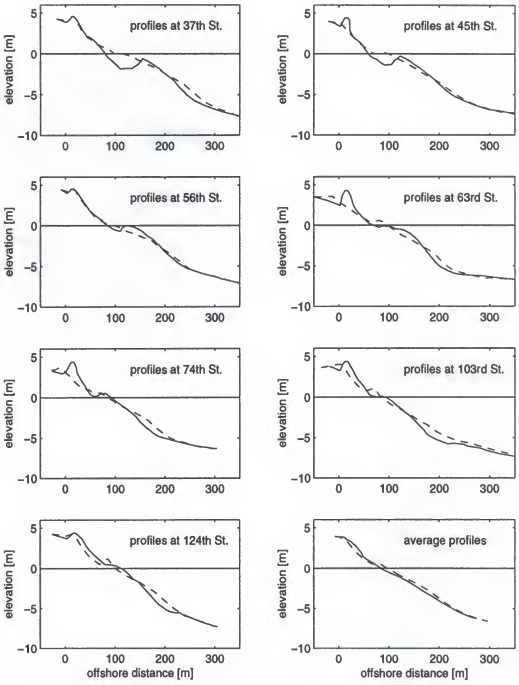

Figure 6.7 Measured pre-storm (solid line) and post-storm (dashed line) profiles.

Table 6.2 Measured volume change during the storm and adjustment Δy.

Street	Volume change (m^3 / m)			Adjustment	h_{total} (m)
	Gain	Loss	Net	Δy (m)	
37th	158.77	20.78	137.99	-11.29	12.22
45th	81.01	49.42	31.59	-2.83	11.16
56th	27.71	47.96	-20.25	1.97	10.28
63rd	82.34	83.99	-1.65	0.16	10.31
74th	80.53	59.61	20.92	-2.19	9.55
103rd	136.06	56.33	79.73	-7.09	11.25
124th	75.74	56.10	19.64	-1.80	10.91
Average	55.71	24.97	30.74	-3.04	10.11

clear that net volume changes during the two storms are quite different from zero for the profiles. To remove this effect, which is due to the gradients in longshore sediment transport, each post-storm profile is adjusted by shifting the profile horizontally a distance Δy to yield zero net volume change. The value of Δy can be calculated by

$$\Delta y = \frac{1}{h_{total}} \int_{y_0}^{y_\infty} (h_{mb} - h_{ma})\, dy = \frac{Vol_{loss} - Vol_{gain}}{h_{total}} \qquad (6.11)$$

where subscripts mb and ma denote profile elevation measured before and after storms, respectively, y_0 and y_∞ are the offshore distance coordinates at the baseline and offshore profile change limit, respectively, h_{total} represents the total elevation of the active storm profile, and Vol_{loss} and Vol_{gain} are the total volume lost or gained from the pre-storm to post-storm profiles. The sign of Δy is positive for a seaward translation. The profile retreat at the 3 meter

Table 6.3 Measured eroded volumes and beach retreat at the 3 m contour.

Street	Eroded volume (m^3 / m)		Retreat at 3 m contour (m)	
	without adjust.	with adjust.	without adjust.	with adjust.
37th	6.75	48.50	2.10	13.39
45th	20.36	29.42	8.30	11.13
56th	9.12	2.72	2.30	0.33
63rd	44.76	44.46	29.78	29.62
74th	50.05	54.66	21.65	23.84
103rd	42.40	62.51	13.59	20.68
124th	40.08	46.17	10.11	11.91
Average	24.97	34.49	8.19	11.23

contour and the eroded volume with and without the shifting adjustments are shown in Table 6.3. These parameters will be used as measures of the storm erosion and of the performance of the numerical models.

6.4 Comparisons of CROSS Model With Three Commonly Used Models

6.4.1 Input Case Design

The predictions of the proposed CROSS model and three existing models : CCCL (Chiu and Dean 1984, 1986), EDUNE (Kriebel & Dean 1985, Kriebel 1986,1989,1990) and two versions of SBEACH (Larson and Kraus 1989, Larson et al. 1989), are compared with the storm erosion measured at Ocean City, Maryland. The input parameters for each model in this study are selected to represent the conditions for which each model was calibrated. Among the four models, CROSS model is the only one which can incorporate variable

sediment size along a profile. The conditions run for each model are described briefly as follows.

6.4.1.1 CROSS Model

The dune slope (beach slope above instantaneous wave run-up limit) and the offshore slope are set equal to 1 and 0.15, respectively, as default conditions, and the shoreline slope is set to the average shoreline value of the measured pre-storm profiles (0.05). Two different profile parameters are compared in this model. First, along each measured profile the variable profile parameter, A, is determined according to the variable sediment size listed in Table 6.1. The mean sediment size of the average profile within each of the 11 morphologic zones is given by the average of the seven measured profiles. Second, as a basis for comparison with the other three models, a constant grain size of 0.35 mm, which was recommended by Kraus and Wise (1993) and corresponds to a profile parameter, A, of 0.135 $m^{1/3}$, is used. During each storm, a random wave series is generated according to the time history of the measured significant wave height and spectral peak wave period. The wave set-up is given by Eq. (3.28) and the wave run-up limit is established from Hunt's model, Eq. (3.31). The active water depth is 1.28 times the instantaneous incoming individual wave height. Since the breaking wave heights are not available, the wave heights measured in a water depth of 10 m are applied. As discussed in Chapter 4, the average transport coefficient, K, of 7.14×10^{-10} m^8s^2/N^3 is used for this field application.

6.4.1.2 CCCL Model

This model has been used in establishment of the Coastal Construction Control Line (CCCL) in Florida. The CCCL is a line which depicts the landward limit of impact of a 100

year return period storm event. The default dune slope is set to 1. Since this model cannot handle variable sediment size along a profile, a constant grain size of 0.35 mm is applied. At each time, the significant wave height input is used as the regular wave height. The set-up at the shoreline is calculated by Eq. (3.30) as 0.23 times that of the incoming wave height. The input water level during a storm is given by adding the set-up at the shoreline to the measured storm surge. No wave run-up is included in the model. After running the two storms, consistent with model calibration, a factor of 2.5 is applied to those contours which receded. This model does not incorporate a transport equation, but rather considers the profile to approach equilibrium with a folding time scale of 13 hours.

6.4.1.3 EDUNE Model

The default input dune slope is set to 1 and the input shoreline slope is taken as 0.05 which is the average shoreline slope of the measured pre-storm profiles. For the same reason as described for the CCCL model, a sediment size of 0.35 mm is used. The input significant wave height is applied as a regular wave height for each time step. In EDUNE, the wave run-up is a constant value throughout the erosion simulation and is used to control the location of the dune scarp above the peak still water flood level. According to the EDUNE Users Manual (Kriebel 1989), the value of run-up should be based on field data or experience from a particular location and does not necessarily simulate a realistic wave run-up limit at each time step. For the Ocean City storm erosion simulation, based on the dune erosion level of post-storm profiles and the run-up calculated by Hunt's formula of Eq. (3.31) for the maximum significant wave height in each storm, the run-up is fixed as 0.91 and 1.52 meters for the November 1991 and January 1992 storms over the entire storm simulation time,

respectively. No set-up is included in the simulations. The transport coefficient for this application is the program default value of 8.73×10^{-6} m^4/N.

6.4.1.4 SBEACH Model

Both versions (2.0 and 3.0) of SBEACH model are believed to incorporate wave run-up and set-up. The maximum slope that a predicted profile is allowed to achieve is required and is set to 17.5° as a default condition; this corresponds to a beach slope of 0.32. A constant sediment size of 0.35 mm is applied here. The wave conditions used in the SBEACH model simulations are the same as the measurements shown in Figures 6.3 and 6.4. Both versions of SBEACH model provide a choice of wave type (monochromatic or irregular). The option of irregular waves which requires an input of significant wave height time history is chose for this study. The version 3.0 of SBEACH, which became available in September 1994, is not documented to the same degree as the earlier version. The default value for the transport coefficient in both versions is 1.50×10^{-6} m^4/N.

6.4.2 Numerical Results and Comparisons

The numerical results from the four models are quantified in terms of several parameters. A comparison of measured and predicted entire active profile changes is provided by the residual parameter, Res, defined in non-dimensional form as:

$$Res = \frac{\sum_{i=1}^{n} (h_{pi} - h_{mai})^2}{\sum_{i=1}^{n} (h_{mbi} - h_{mai})^2} \qquad (6.12)$$

Where h is the profile elevation, the subscripts "p" and "m" denote predicted and measured,

respectively, "b" and "a" indicate before and after storm conditions, respectively, i represents the "i" th location on the profile and the sums extend across the entire active profile. The minimum possible value of Res is zero, which would correspond to a perfect simulation. If no changes occurred, the value of Res is 1. The dune erosion agreement between calculated and measured is quantified by the eroded volume and the beach retreat at the 3 meter contour. To provide a measure of erosion and retreat, two different errors are presented: the root mean square error, ERR_{rms}, and the algebraic average error, ERR_{ave}. These are expressed as:

$$ERR_{rms} = \frac{\sum_{j=1}^{n} (S_{pj} - S_{mj})^2}{\sum_{j=1}^{n} S_{mj}^2} \tag{6.13}$$

$$ERR_{ave} = \frac{\sum_{j=1}^{n} (S_{pj} - S_{mj})}{\sum_{j=1}^{n} S_{mj}} \tag{6.14}$$

Where S is an eroded volume or beach retreat, the subscripts "p" and "m" again represent the predicted and measured values, respectively, and j means the "j" th beach profile. ERR_{rms} represents a factor of simulation accuracy and ERR_{ave} provides a measure of over or under-prediction of erosion. The measure, Res, is based on local differences across the entire active profile whereas ERR_{rms} and ERR_{ave} are based on total differences of eroded volume or beach retreat at a particular elevation.

Comparisons between predicted and measured profiles are presented in Figures 6.8-6.14 for the seven survey lines. Figure 6.15 shows the results of the average pre-storm and post-storm profiles and the predictions, in which the average pre-storm profile is used as the initial input profile for the four models. The ridge features of the measured post-storm profiles suggest that there was some beach recovery even though the post-storm profiles were measured only a week after the second storm. The predictions of CROSS model with both variable and constant sand size are presented. It appears that the results predicted by variable sand size provide more reasonable simulations for dune erosion while the predictions with the constant sand size fit for the entire profiles better. After applying the factor of 2.5 to those contours which receded, the CCCL model tends to overpredict erosion for most profiles. Since the application purpose of CCCL is to establish the coastal construction control line, the 2.5 factor is included to incorporate the variability of beach erosion at different locations. For example, the profile at 63rd Street experienced very severe erosion during two storms. Although the other three models underpredict the dune erosion at 63rd Street, CCCL with a factor of 2.5 yields very reasonable simulations. As mentioned in Section 6.4.1 for the EDUNE model, the wave run-up at the peak storm is used throughout the entire time of the numerical simulation. Since beach erosion is quite sensitive to water level, the numerical results of EDUNE will depend greatly on the storm duration time and the input of wave run-up used in the numerical simulations. Calm wave conditions before or after a storm can cause considerable erosion because of the fixed unrealistic high run-up. Among all four models, SBEACH version 2.0 is the only model which can represent the offshore bar feature. The newly modified version 3.0 of SBEACH presents substantial better results than version 2.0.

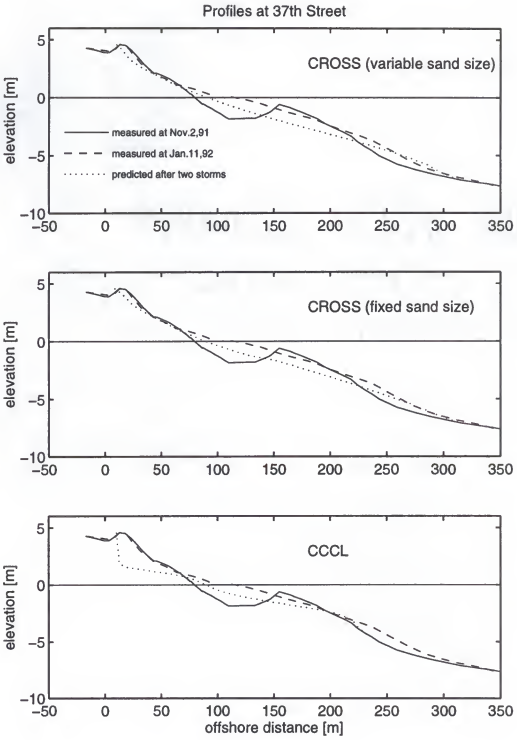

Figure 6.8 Comparisons of predicted and measured profiles at 37th Street.

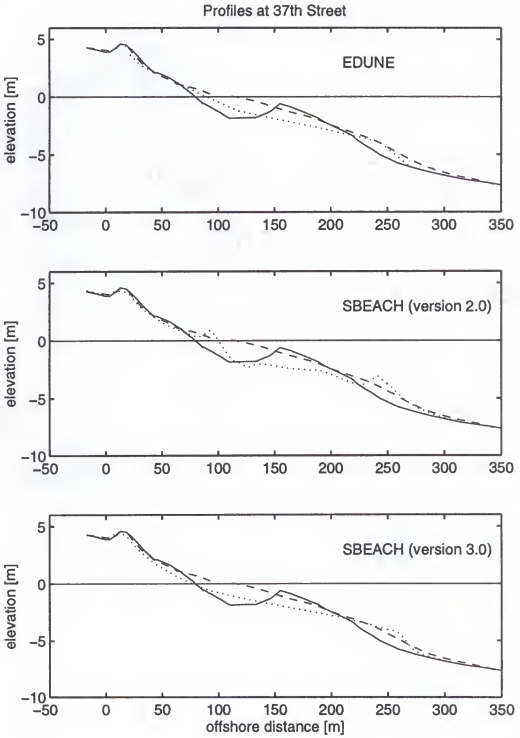

Figure 6.8 Continued.

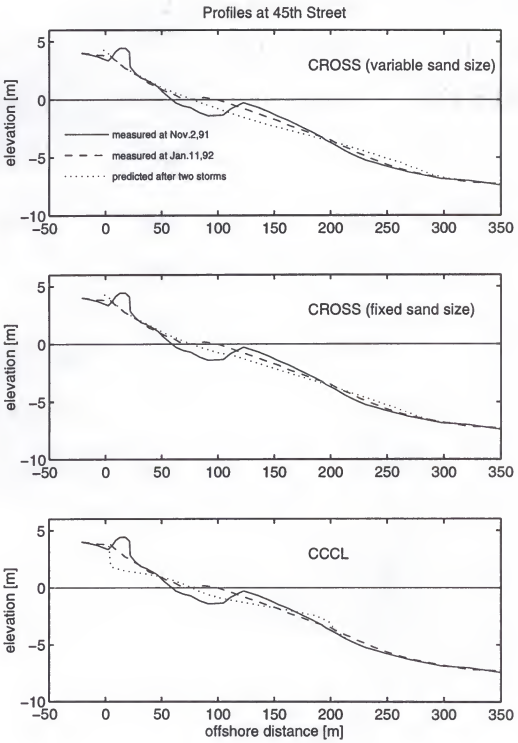

Figure 6.9 Comparisons of predicted and measured profiles at 45th Street.

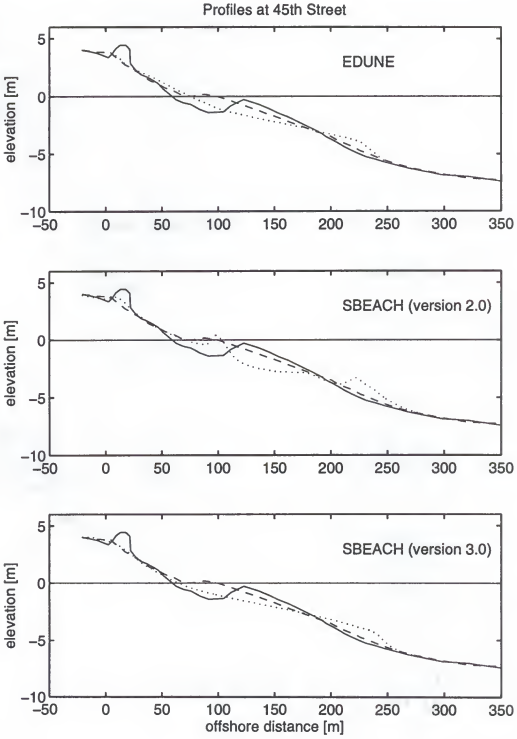

Figure 6.9 Continued.

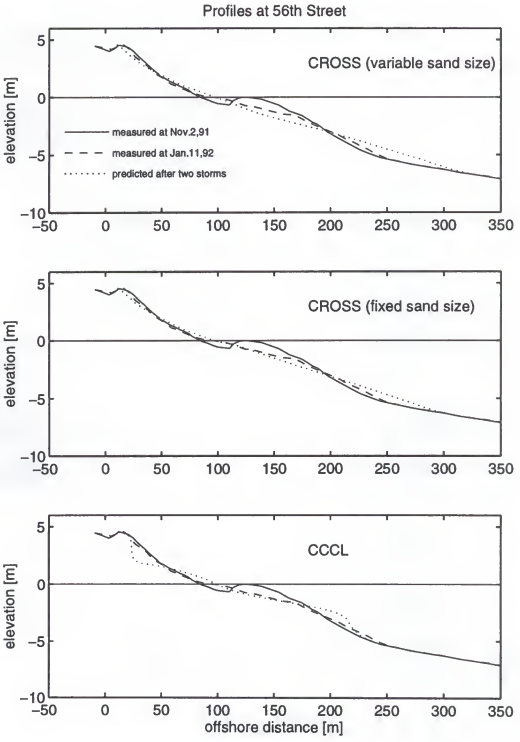

Figure 6.10 Comparisons of predicted and measured profiles at 56th Street.

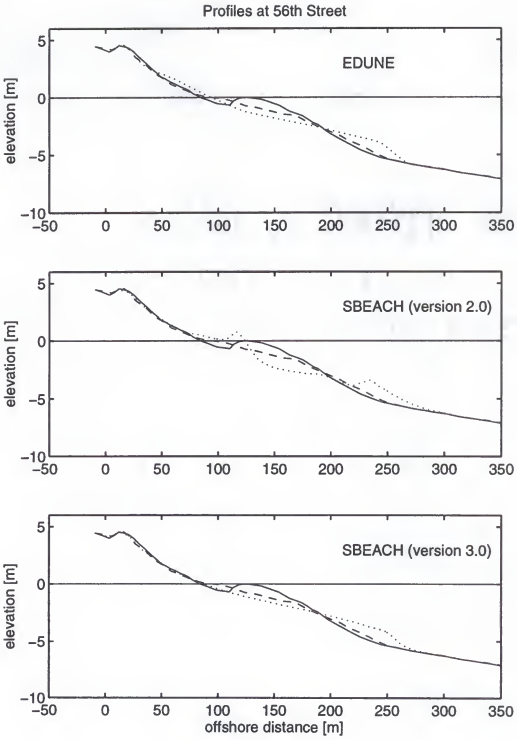

Figure 6.10 Continued.

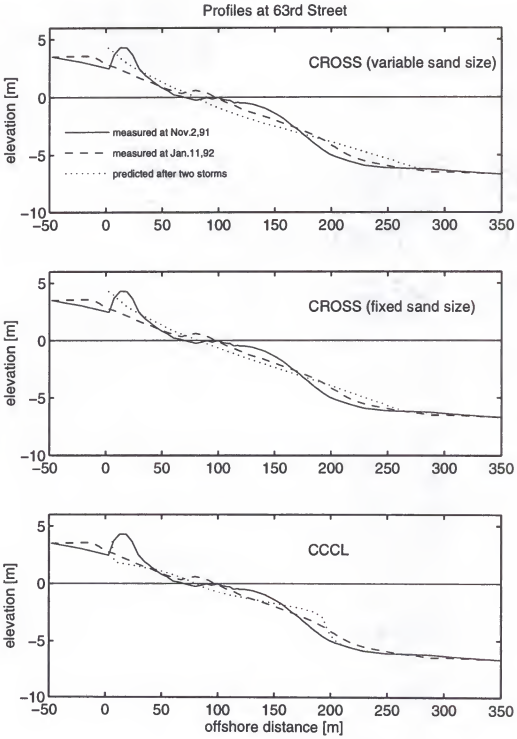

Figure 6.11 Comparisons of predicted and measured profiles at 63rd Street.

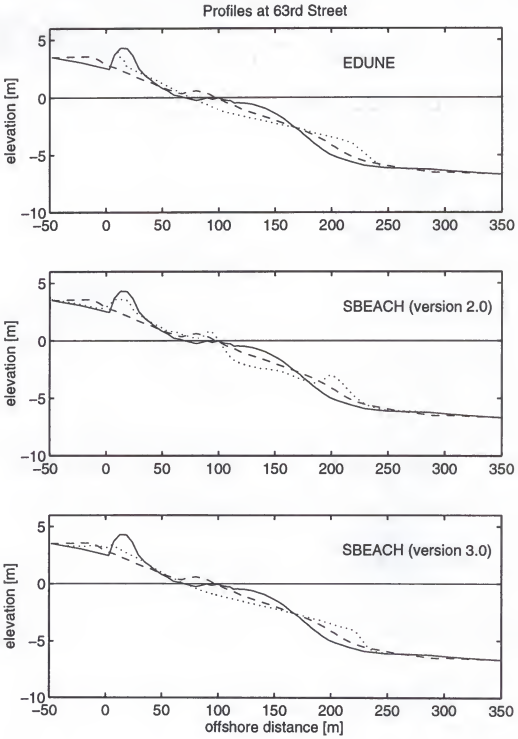

Figure 6.11 Continued

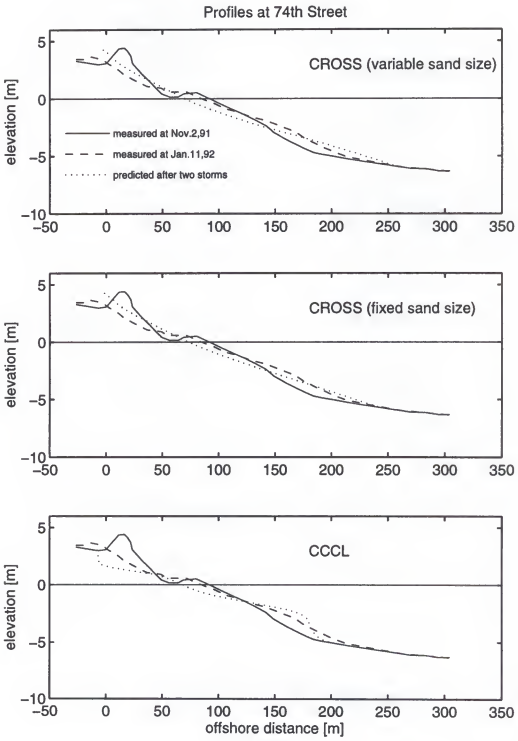

Figure 6.12 Comparisons of predicted and measured profiles at 74th Street.

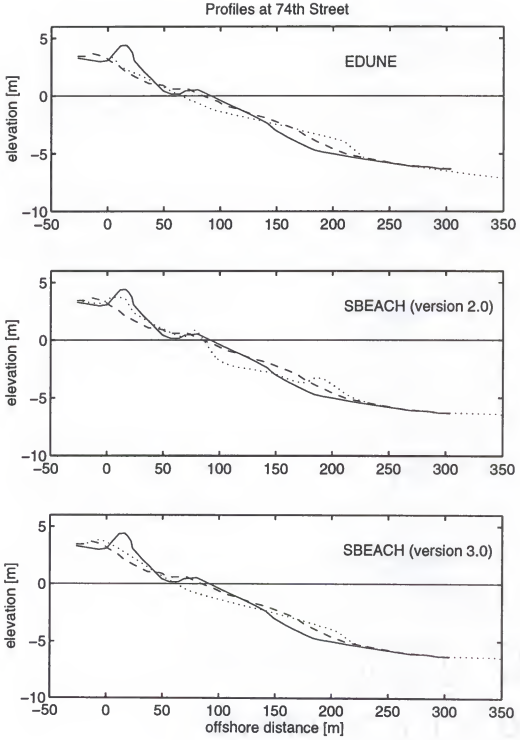

Figure 6.12 Continued

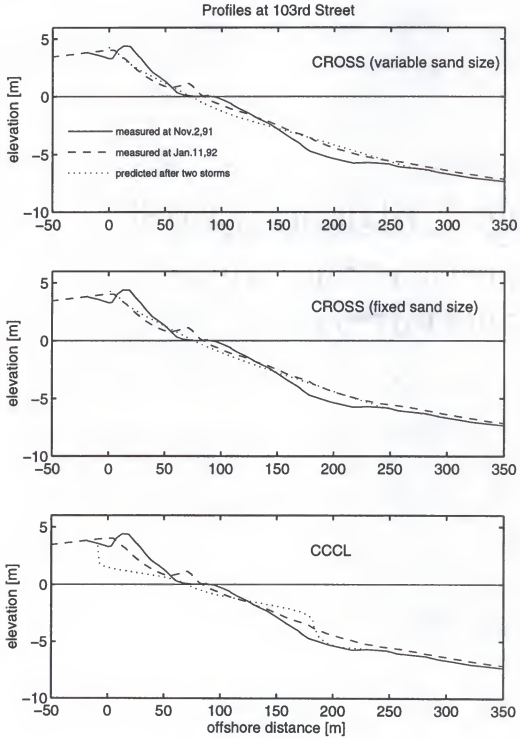

Figure 6.13 Comparisons of predicted and measured profiles at 103rd Street.

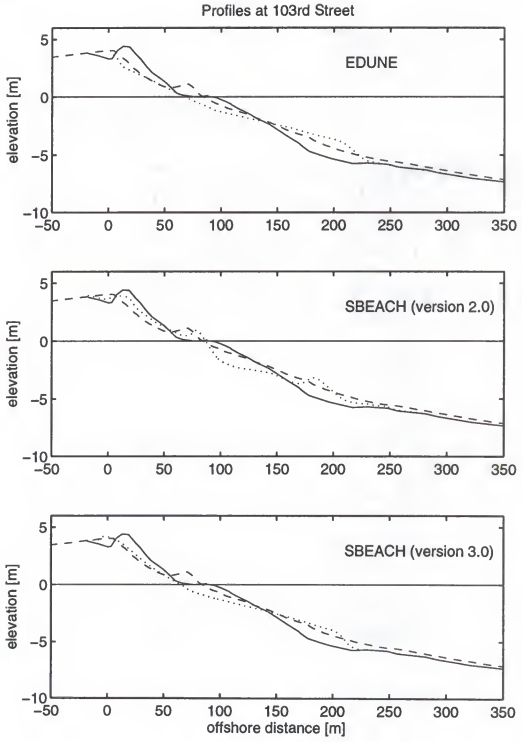

Figure 6.13 Continued.

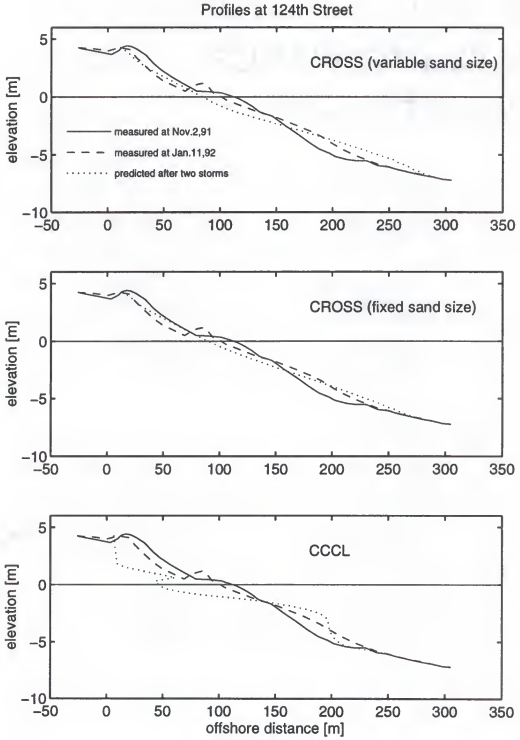

Figure 6.14 Comparisons of predicted and measured profiles at 124th Street.

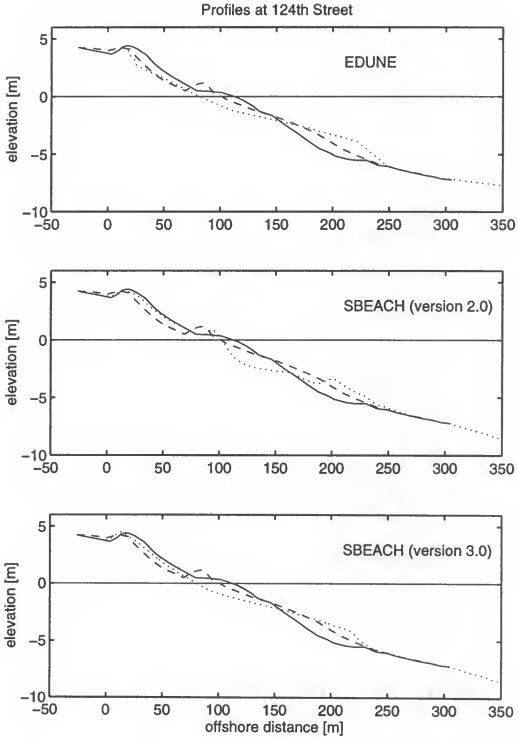

Figure 6.14 Continued

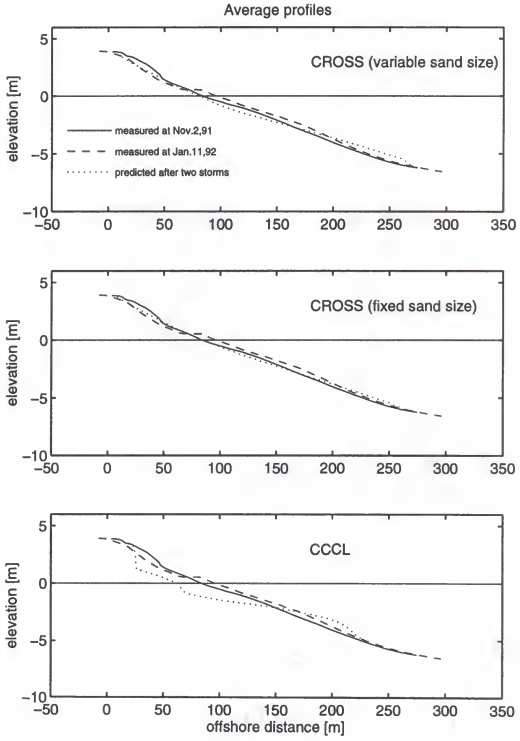

Figure 6.15 Comparisons of predictions and measurements at the average profile.

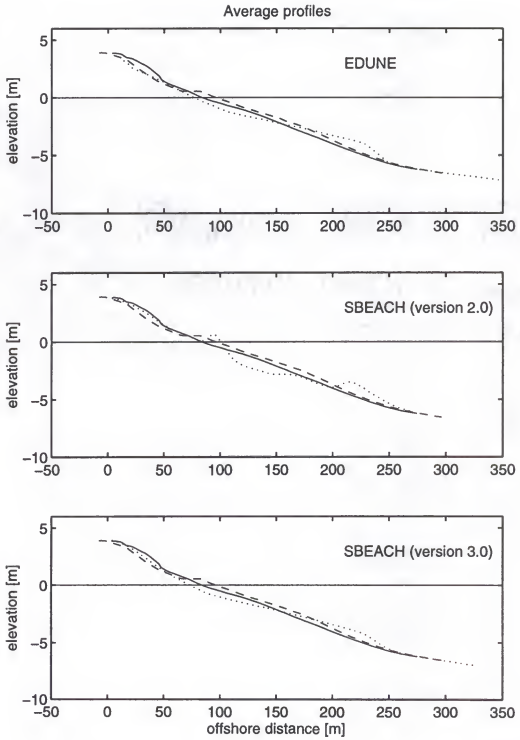

Figure 6.15 Continued

The corresponding residuals, eroded volumes and beach retreat at the 3 meter contour for each individual profile are shown in Table 6.4. Because the net volume changes between measured pre-storm and post-storm profiles are quite different from zero due to gradients of longshore sediment transport, in addition to the measured profiles, a version is included by shifting each post-storm profile the horizontal distance, Δy, to yield zero net volume change. In the tables, "without adjustment" means data given by the original measured post-storm profiles, while "with adjustment" means data resulted from horizontally shifted post-storm profiles. Since all four models discussed here included only cross-shore sediment transport, the data presented "with adjustment" are considered to be the more appropriate results. The onshore limit of predicted eroded volume of each profile is determined by the onshore cross-over point of the predicted post-storm and measured pre-storm profiles, and the offshore limit is determined by the offshore cross over point of the predicted post-storm and measured pre-storm profiles or the shoreline of the predicted profile depending on which is closer. It is noticed that all four models yield large residuals for the profile at 56th Street because the profile had very little change after two storms and the denominator of Eq. (6.12) becomes very small. The average profile is smoother than the individual measured profiles, which also makes the denominator of equation (6.12) small. As a result, the residuals of the average profile are considerably greater than these of the measured profiles. Among the four models, CROSS with fixed sand size yields the smallest residuals. Judged by eroded volume and beach retreat at 3-meter contour, CROSS with variable sand size, EDUNE and SBEACH version 3.0 present comparable predictions for dune erosion. Considering profile residuals and dune

Table 6.4 The predicted residuals, eroded volumes and beach retreat at the 3-meter contour.

Profile	Model	Residual		Eroded vol. (m^2)	Retreat at 3-m contour (m)
		w/o adjust.	With adjust.		
37th St.	CROSS(var. Sand size)	0.614	0.454	22.04	8.04
	CROSS(fixed sand size)	0.508	0.339	19.37	6.75
	CCCL	1.286	0.443	83.22	18.34
	EDUNE	0.588	0.512	9.15	4.80
	SBEACH (ver. 2.0)	1.074	1.075	16.42	3.55
	SBEACH (ver. 3.0)	0.664	0.613	30.01	4.84
45th St.	CROSS(var. Sand size)	0.525	0.496	20.13	8.71
	CROSS(fixed sand size)	0.287	0.280	19.39	8.36
	CCCL	1.067	0.851	60.56	18.34
	EDUNE	0.624	0.604	18.30	6.51
	SBEACH (ver. 2.0)	1.018	0.971	15.21	2.96
	SBEACH (ver. 3.0)	0.736	0.713	23.34	6.79
56th St.	CROSS(var. Sand size)	1.539	1.584	12.36	5.74
	CROSS(fixed sand size)	0.765	0.785	11.48	5.28
	CCCL	1.506	1.761	31.62	11.86
	EDUNE	1.812	1.725	4.68	3.73
	SBEACH (ver. 2.0)	2.971	2.971	4.76	2.28
	SBEACH (ver. 3.0)	1.588	1.526	5.56	3.32
63rd St.	CROSS(var. Sand size)	0.854	0.854	17.71	9.27
	CROSS(fixed sand size)	0.596	0.595	17.12	9.07
	CCCL	1.960	1.966	53.68	20.08
	EDUNE	0.797	0.795	19.88	8.93
	SBEACH (ver. 2.0)	0.803	0.802	14.76	4.59
	SBEACH (ver. 3.0)	0.646	0.645	25.68	14.65

Table 6.4 (continued) The predicted residuals, eroded volumes and beach retreat at the 3-meter contour.

Profile	Model	Residual		Eroded vol. (m^2)	Retreat at 3-m contour (m)
		w/o adjust.	With adjust.		
74th St.	CROSS(var. Sand size)	0.511	0.524	25.41	11.69
	CROSS(fixed sand size)	0.450	0.463	21.33	9.71
	CCCL	0.610	0.515	86.72	30.99
	EDUNE	0.534	0.530	39.20	16.18
	SBEACH (ver. 2.0)	0.936	0.935	16.72	4.11
	SBEACH (ver. 3.0)	0.526	0.527	29.73	12.68
103rd St.	CROSS(var. Sand size)	0.329	0.274	35.18	15.23
	CROSS(fixed sand size)	0.261	0.251	28.88	13.41
	CCCL	2.233	1.499	123.05	28.92
	EDUNE	0.548	0.413	54.66	20.04
	SBEACH (ver. 2.0)	0.596	0.590	19.54	7.03
	SBEACH (ver. 3.0)	0.510	0.433	35.20	10.61
124th St.	CROSS(var. Sand size)	0.931	0.895	40.08	12.45
	CROSS(fixed sand size)	0.503	0.493	23.36	9.08
	CCCL	3.131	2.821	93.83	31.70
	EDUNE	1.000	0.968	48.02	14.79
	SBEACH (ver. 2.0)	1.112	1.136	10.08	3.31
	SBEACH (ver. 3.0)	0.802	0.805	23.88	4.87
Average	CROSS(var. Sand size)	1.622	1.552	20.78	10.24
	CROSS(fixed sand size)	0.968	0.906	12.68	7.97
	CCCL	5.030	4.498	50.30	3.93
	EDUNE	2.132	2.094	27.36	11.75
	SBEACH (ver. 2.0)	3.570	3.547	7.48	3.91
	SBEACH (ver. 3.0)	2.092	2.128	17.15	4.41

erosion together, CROSS with variable sand size provides overall better results for the average profile.

The residuals averaged over seven measured profiles and the two errors defined in Eqs.(6.13) and (6.14) for eroded volume and beach retreat at the 3 meter contour with respect to the original measured profiles and the horizontal shifted profiles are presented in Tables 6.5 and 6.6, respectively. Since the non-zero net volume change between measured pre-storm and post-storm profiles was caused by longshore sediment transport, for comparisons between cross-shore sediment transport models, the results in Table 6.6 are more appropriate. Overall, CCCL overpredicts the dune erosion during the two storms, whereas the other three models underpredict it. It appears that CROSS with fixed sand size produces more under-prediction than CROSS with variable sand size along the profiles. The errors of CROSS with variable sand size, EDUNE and SBEACH version 3.0 are at comparable magnitudes. It is noticed that dune overwash occurred during the January 1992 storm. Among the four models, EDUNE and SBEACH incorporate dune overwash processes, but this effect is not included in CCCL and CROSS . In the CROSS model, the profile shoreward of the dune crest is treated as a horizontal flat beach with the same elevation of the dune crest. Therefore, the numerical simulations of CROSS do not include the dune erosion part caused by overwash. It is expected that the underpredictions of CROSS could be improved by incorporating dune overwash processes in the model. The predicted versus measured eroded volume and beach retreat at the 3-meter contour for seven survey profiles are plotted in Figures 6.16 and 6.17, respectively, where the results from measurements are those based on horizontally shifted measured post-storm profiles. It appears that the results

Table 6.5 The average residuals and errors of eroded volume and beach retreat at the 3-meter contour with respect to the original measured profiles.

Model	Averaged residual	Error of eroded volume		Error of retreat	
		ERR_{rms}	ERR_{ave}	ERR_{rms}	ERR_{ave}
CROSS (variable sand size)	0.758	0.193	-0.190	0.334	-0.190
CROSS (fixed sand size)	0.481	0.262	-0.340	0.350	-0.298
CCCL	1.685	2.222	1.495	1.072	0.971
EDUNE	0.843	0.116	-0.092	0.314	-0.146
SBEACH (ver. 2.0)	1.216	0.423	-0.544	0.617	-0.683
SBEACH (ver. 3.0)	0.782	0.196	-0.188	0.207	-0.342

Table 6.6 The average residuals and errors of eroded volume and beach retreat at the 3-meter contour with respect to the horizontal shifted measured profiles.

Model	Averaged residual	Error of eroded volume		Error of retreat	
		ERR_{rms}	ERR_{ave}	ERR_{rms}	ERR_{ave}
CROSS (variable sand size)	0.725	0.227	-0.401	0.283	-0.359
CROSS (fixed sand size)	0.458	0.319	-0.511	0.327	-0.444
CCCL	1.331	0.707	0.847	0.480	0.561
EDUNE	0.792	0.182	-0.328	0.260	-0.324
SBEACH (ver. 2.0)	1.211	0.470	-0.663	0.623	-0.749
SBEACH (ver. 3.0)	0.752	0.183	-0.399	0.259	-0.479

of each individual profile are consistent with the root mean square and algebraic errors in Table 6.6. Among all models, CCCL overpredicts dune erosion and SBEACH version 2.0 underpredicts most. The results of CROSS, EDUNE and SBEACH version 3.0 are comparable.

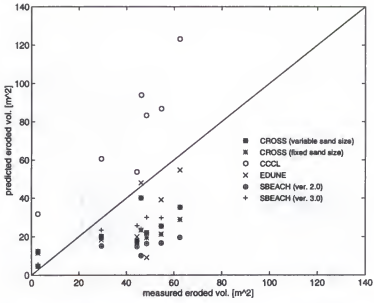

Figure 6.16 Predicted versus measured eroded volumes, all models and all profiles. Profiles adjusted for no net volume change.

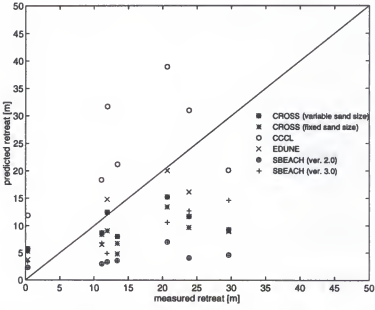

Figure 6.17 Predicted versus measured beach retreat at the 3 meter contour, all models and all profiles. Profiles adjusted for no net volume change.

6.4.3 Average Profile Changes at Different Elevation Contours

During a storm, the portions of a beach at high levels retreat and sediment is deposited offshore. The beach profile change in the subaerial portion is usually used by the public to judge storm erosion. To represent severity of erosion over an entire area of interest, an average profile change at a elevation contour is defined as

$$\Delta\bar{y}(h_i) = \bar{y}_{after}(h_i) - \bar{y}_{before}(h_i) \tag{6.15}$$

where h_i denotes the elevation of the contour, the over bar represents the average over the seven survey lines, $\Delta\bar{y}$ is the average profiles change, the subscript "after" means predicted or measured after the two storms, and "before" means the pre-storm measurements. The corresponding standard deviation of the profile change is calculated as

$$\sigma = \sqrt{\frac{1}{n-1}\sum_{j=1}^{n}\left[\Delta y_j(h_i) - \Delta\bar{y}(h_i)\right]^2} \tag{6.16}$$

where σ is the standard deviation, $\Delta y_j(h_i)$ and $\Delta\bar{y}(h_i)$ are the beach change of the "jth" profile and the average profile at the elevation h_i, respectively, and n is the total number of measured profiles. The measured average profile change and the corresponding standard deviation at different elevation contours are shown in Figure 6.18, where the solid and dashed lines denote the results of the original measured and horizontally adjusted post-storm profiles. After two storms, the average profile retreated and advanced above and below the 1.8 m contour, respectively. The area from the water line to the -1 m contour has a greater standard deviation.

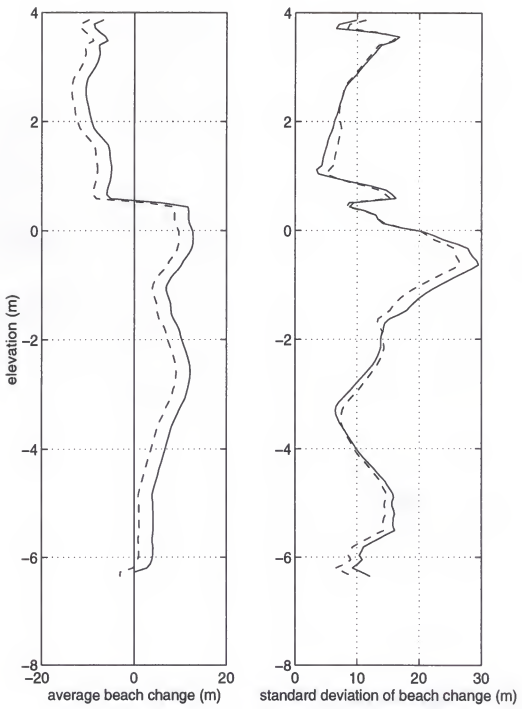

Figure 6.18 The measured average profile changes and the corresponding standard deviations at different elevation contours. The results from both the original measured post-storm profiles (solid lines) and the shifted post-storm profiles (dashed lines) are presented.

The average profile changes at different elevation contours predicted by the four models are presented in Figure 6.19. It appears that CROSS with variable sand size, EDUNE, and SBEACH version 3.0 yield reasonable beach retreat predictions for the dune area. Since all profiles predicted by the three models are monotonic and cannot represent the ridge feature of the measured post-storm profiles. Thus the subaqueous portion of the average profile is not simulated well by them.

6.5 Sensitivity Study of CROSS Model

The transport coefficient, K, and the active water depth are two important factors in the CROSS model. It is interesting to investigate the sensitivity of the model to these two factors. As mentioned in section 6.3, the wave and storm surge conditions used in the numerical simulations were measured at a water depth of 10 meters during the two storms. Due to the wave shoaling and the wave energy dissipation caused by winds and bottom friction, the waves conditions which impacted the beaches might differ from the wave parameters at the 10 meter water depth. Generally, some uncertainties exist in measured field wave conditions during a storm. To evaluate the effects of these uncertainties, the sensitivities of the CROSS model to wave height and storm surge are discussed. To better represent beach sediment characteristics, the variable sand size distributions across the profiles as listed on Table 6.1 are applied for the following studies.

6.5.1 Transport Coefficient

According to the calibrations of seven experiments in three different large wave tanks, a standard average transport coefficient, K, of 7.14×10^{-10} m^8s^2/N^3 is used in the numerical simulations of the two storm erosions. For sensitivity analysis, the transport coefficient of

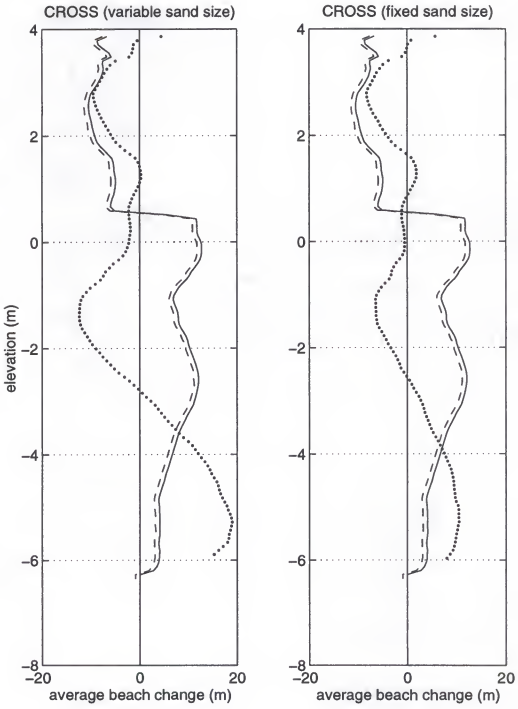

Figure 6.19 The comparisons of the measured and predicted (dotted lines) average profile changes at different elevation contours. The measured results from both the original measurements and the shifted measured post-storm profiles.

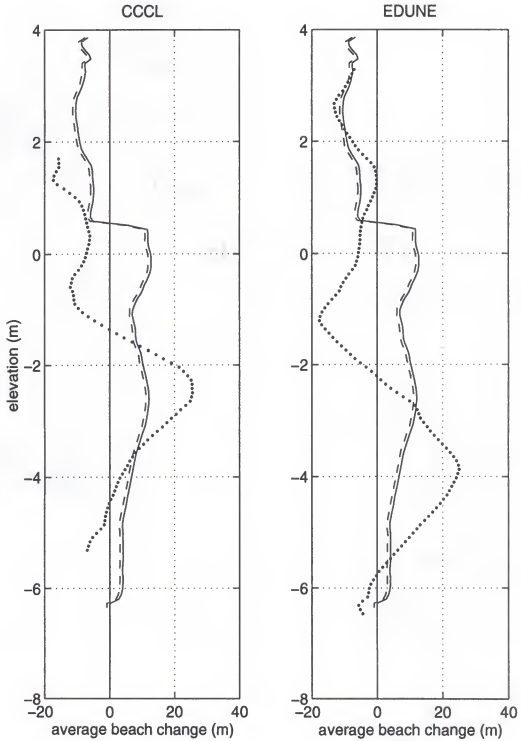

Figure 6.19 Continued.

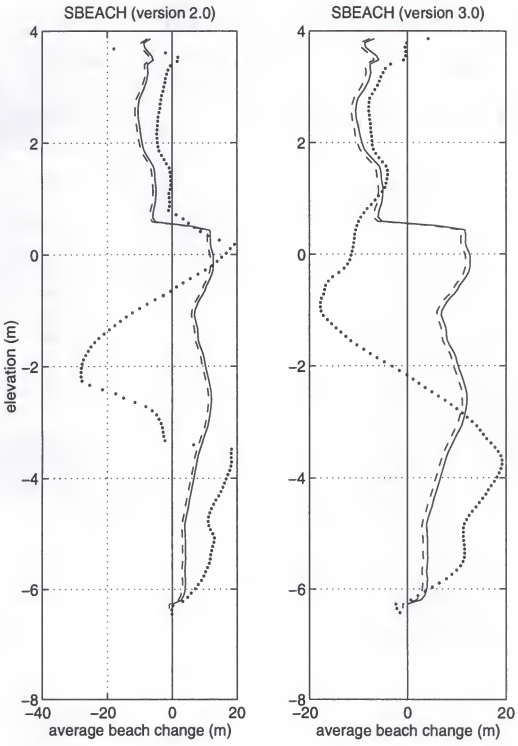

Figure 6.19 Continued.

5.71×10^{-10} and $8.57\times10^{-10}\ m^3s^2/N^3$, which correspond to 20% decrease and increase, respectively, are applied. The predicted profiles with varied K values are compared with the measurements and the predictions of standard K value in Figure 6.20 for the seven survey lines and the average profile. The change of K value has very little effect on the predicted profiles. In most locations, the profiles predicted by the standard K value and the varied K values are almost identical. The residuals, eroded volumes and beach retreat at the 3-meter contour predicted by the varied K value are shown in Table 6.7, in which the results of the standard K are included from Table 6.4 for comparisons. The variations of dune erosion are less than 10% for all the profiles although the change of the K value is 20%. The average residual and the root mean square and the algebraic average errors of the eroded volume and beach retreat at the 3-meter contour over the seven measured profiles are shown in Table 6.8. With a 20% change in K value, the variations of the root mean square error and the algebraic average error are less than 3% and 7 %, respectively. It appears that CROSS model is quite insensitive to the transport coefficient for the beach erosion during the two storms at Ocean City. Since it has non-linear transport relationship, CROSS model is supposed to be less sensitive than a linear model when the initial profile conditions are close to equilibrium.

6.5.2 Active Water Depth

In the CROSS model, the sediment transport rate is related to the wave energy dissipation caused by wave breaking. The active water depth, h_*, is defined as the breaking water depth which is 1.28 times the instantaneous breaking wave height according to McCowan (1894) theory. Depending on different wave conditions and beach slopes, the ratio of the breaking water depth to the breaking wave height may vary from 1.28. In this

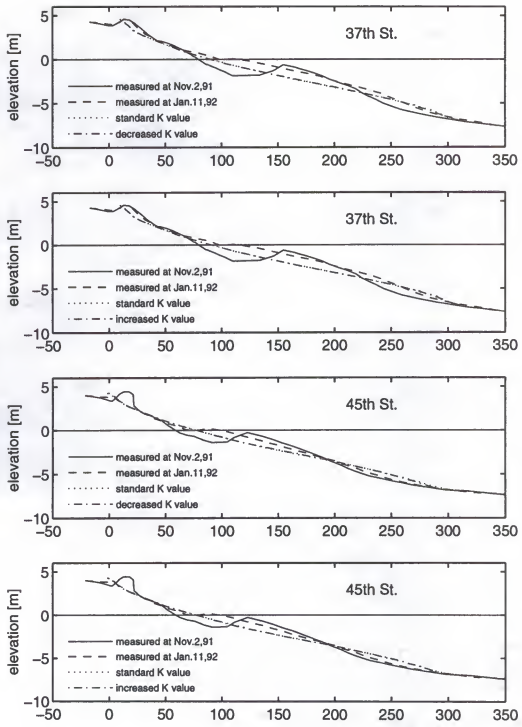

Figure 6.20 Comparisons of the measured profiles and the predictions of CROSS with standard K value, 20% decreased K value and 20% increased K value.

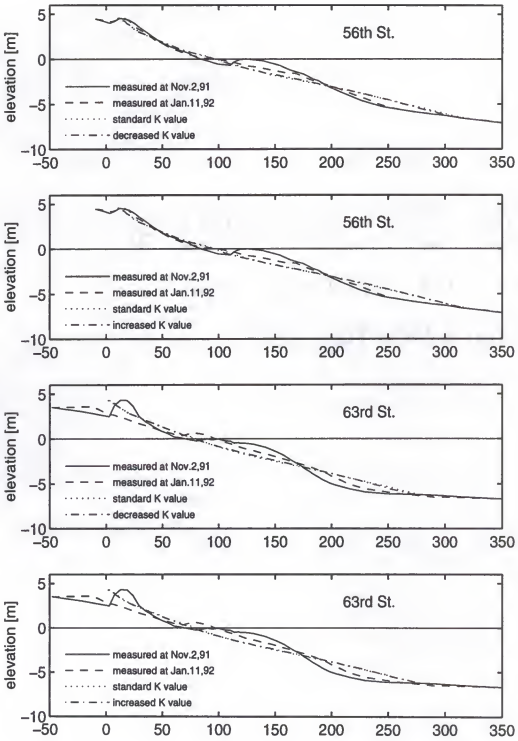

Figure 6.20 Continued.

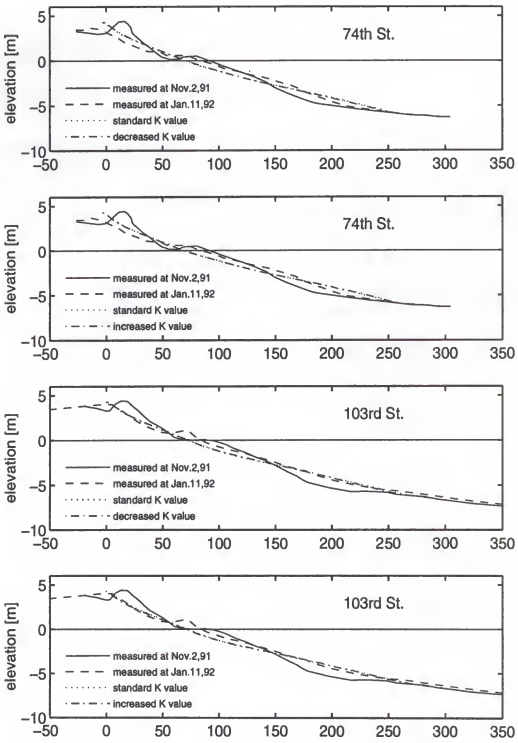

Figure 6.20 Continued.

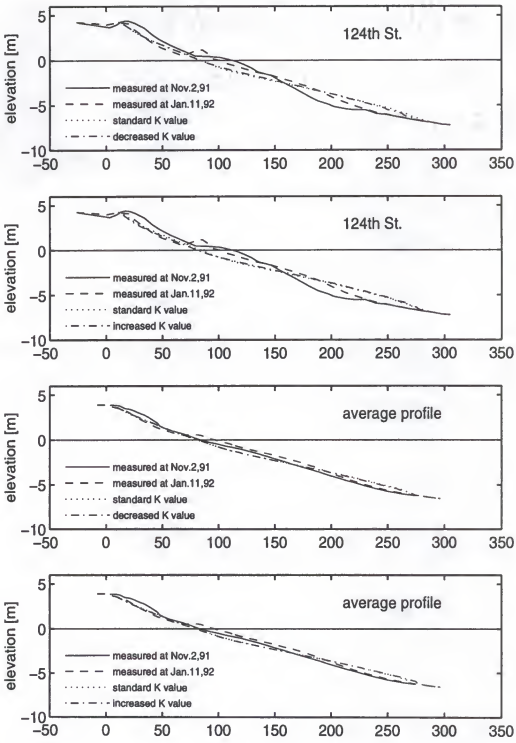

Figure 6.20 Continued.

Table 6.7 Sensitivity study of CROSS. The residuals, eroded volumes and beach retreat at the 3-meter contour predicted by the 20% increased and 20% decreased K values.

Profile	K value	Residual		Eroded vol. (m^2)	Retreat at 3-m contour (m)
		w/o adjust.	with adjust		
37th St.	Standard	0.614	0.454	20.04	8.04
	Decreased	0.582	0.426	20.91	7.53
	Increased	0.643	0.481	22.99	8.47
45th St.	Standard	0.525	0.496	20.13	8.71
	Decreased	0.465	0.444	20.16	9.23
	Increased	0.567	0.535	21.14	9.57
56th St.	Standard	1.539	1.584	12.36	5.74
	Decreased	1.306	1.336	11.94	6.20
	Increased	1.619	1.666	12.90	6.88
63rd St.	Standard	0.854	0.854	17.71	9.27
	Decreased	0.748	0.747	17.81	9.26
	Increased	0.824	0.824	19.39	10.22
74th St.	Standard	0.511	0.524	25.41	11.69
	Decreased	0.498	0.509	23.47	10.39
	Increased	0.502	0.513	27.40	12.40
103rd St.	Standard	0.329	0.274	35.18	15.23
	Decreased	0.311	0.269	33.07	14.24
	Increased	0.346	0.274	39.71	16.50
124th St.	Standard	0.931	0.895	40.08	12.45
	Decreased	0.747	0.722	37.52	12.01
	Increased	0.973	0.932	46.60	14.50
Average	Standard	1.622	1.552	20.78	10.24
	Decreased	1.526	1.460	17.52	9.32
	Increased	1.799	1.709	23.71	11.01

Table 6.8 Sensitivity study of CROSS. The average residuals and errors of eroded volume and beach retreat at the 3-meter contour predicted by the 20% increased and 20% decreased K values.

Adjustment	K	Average residual	Error of eroded vol.		Error of retreat	
			ERR_{rms}	ERR_{ave}	ERR_{rms}	ERR_{ave}
Without adjustment	Standard	0.758	0.193	-0.190	0.334	-0.190
	Decreased	0.665	0.205	-0.228	0.347	-0.216
	Increased	0.782	0.176	-0.110	0.322	-0.113
With adjustment	Standard	0.725	0.227	-0.401	0.283	-0.359
	Decreased	0.636	0.250	-0.428	0.306	-0.379
	Increased	0.746	0.191	-0.341	0.256	-0.297

sensitivity study, an active water depth equal to the incoming wave height is investigated. The comparisons of the two different active water depths (the 1.28 and 1 times the wave height) are shown in Figure 6.21. It appears that the predictions with an active water depth the same as the incoming wave height provide better fits for the entire profiles. The change of the active water depth has less effects on the subaerial portion of a profile than the subaqueous portion. The residuals, eroded volumes and beach retreat at the 3-meter contour predicted by the different active water depths are shown in Table 6.9. The corresponding average residuals and the errors of eroded volume and beach retreat at the 3-meter contour are compared in Table 6.10. It is noticed that there are considerable decreases in profile residuals and errors of the eroded volumes and beach retreat with the ratio of active water depth to incoming wave height changed from 1.28 to 1. Both the predictions of dune erosion and the fitting of the subaqueous portion of the profile improved with decreased active water depth. It seems that the active water depth of 1.28 times wave height, which comes from McCowan theory

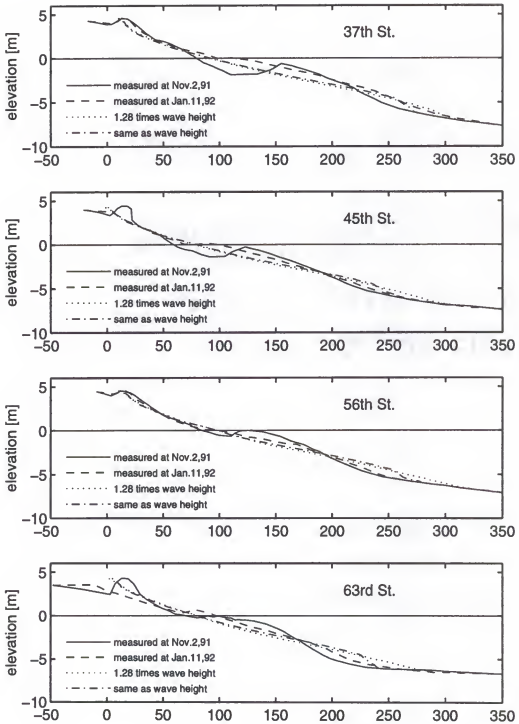

Figure 6.21 Comparisons of the measured profiles and the prediction of CROSS with the active water depth as 1.28 time and the same as instantaneously incoming wave height.

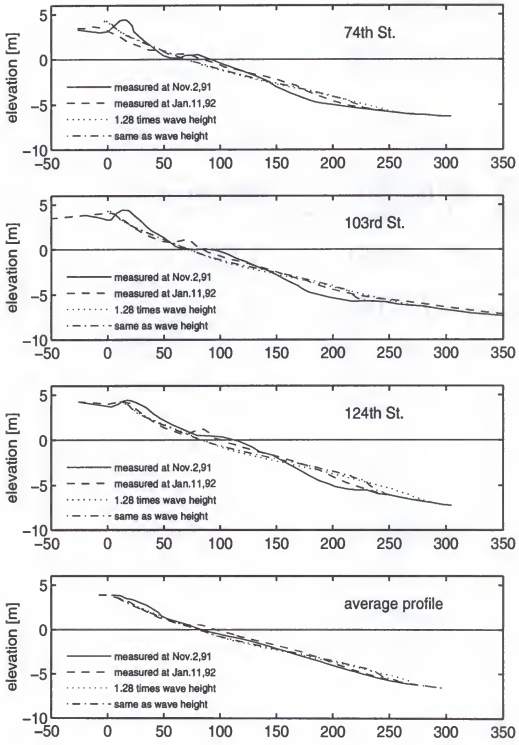

Figure 6.21 Continued.

Table 6.9 Sensitivity study of CROSS. The residuals, eroded volumes and beach retreat at the 3-meter contour predicted by active water depth as 1.28 times and the same as instantaneous incoming wave height.

Profile	Ratio*	Residual		Eroded vol. (m^2)	Retreat at 3-m contour (m)
		w/o adjust.	with adjust		
37th St.	1.28	0.614	0.454	20.04	8.04
	1.00	0.463	0.267	27.13	9.43
45th St.	1.28	0.525	0.496	20.13	8.71
	1.00	0.362	0.349	22.78	10.64
56th St.	1.28	1.539	1.584	12.36	5.74
	1.00	1.248	1.255	13.46	7.39
63rd St.	1.28	0.854	0.854	17.71	9.27
	1.00	0.604	0.602	19.33	10.76
74th St.	1.28	0.511	0.524	25.41	11.69
	1.00	0.408	0.424	27.39	12.06
103rd St.	1.28	0.329	0.274	35.18	15.23
	1.00	0.341	0.310	36.26	15.28
124th St.	1.28	0.931	0.895	40.08	12.45
	1.00	0.682	0.671	42.21	13.55
Average profile basis	1.28	1.622	1.552	20.78	10.24
	1.00	1.219	1.163	26.66	12.00

* This is the ratio of active water depth to incoming wave height.

and the laboratory calibrations of CROSS, may be too large for the Ocean City storm erosion. Recall that five of the seven laboratory experiments used in the calibrations of CROSS were carried out with constant wave conditions, it appears that there are differences in the ratio of active water depth to wave height between monochromatic and irregular waves. The ratio of

Table 6.10 Sensitivity study of CROSS. The average residuals and errors of eroded volume and beach retreat at the 3-meter contour predicted by active water depth as 1.28 times and the same as instantaneous incoming wave height.

Adjustment	Ratio*	Average residual	Error of eroded vol.		Error of retreat	
			ERR_{rms}	ERR_{ave}	ERR_{rms}	ERR_{ave}
Without adjustment	1.28	0.758	0.193	-0.190	0.334	-0.190
	1.00	0.587	0.194	-0.117	0.322	-0.099
With adjustment	1.28	0.725	0.227	-0.401	0.283	-0.359
	1.00	0.554	0.189	-0.346	0.255	-0.287

* This is the ratio of active water depth to incoming wave height.

1.28 provides quite good predictions for profiles under constant wave conditions, while for a profile under irregular wave conditions, the active water depth equal to the instantaneous wave height presents better results. The phenomenon that random waves correspond to relative shallow active water depth was also noticed by Vellinga (1983), who found in his laboratory studies that the active water depth of a profile was equal to approximately 0.75 times the significant wave height.

6.5.3 Storm Surge

During a storm, beach erosion is related to augmented water levels caused by storm surge. A higher surge level and a longer surge duration will cause more severe dune erosion. Generally, it is difficult to reconstruct, from limited measurements, the exact storm surge conditions for numerical simulation purposes. To predict beach erosion during a N-year period return storm, a storm surge hydrograph constructed through numerical modeling and the history of storms at the area of interest is usually applied, although some uncertainties

always exist in these predictions. To investigate the sensitivity of CROSS model to storm surge, the water levels measured in the two storms (Figures 6.3 and 6.4) were increased and decreased 20% respectively. The profiles predicted by standard and modified storm surges are compared with measurements in Figure 6.22 for the seven survey lines and the average profile. It is shown that the dune area is more sensitive to the elevation change of storm surge than the portions of a profile at lower level contours. A higher level storm surge causes greater dune erosion but has little effect on the subaqueous profiles. The residuals, eroded volumes and beach retreat at the 3-meter contour predicted by different storm surges are shown in Table 6.11 for each individual profile. The averaged residual and errors of eroded volume and beach retreat over the seven measured profiles are presented in Table 6.12. With a 20% variation in storm surge, the changes of dune erosion and profile residual for each individual profile are less than 15%. The variation of average residuals and the errors of dune erosion are less than 10% and 15%, respectively. Overall, it appears the 20% increased storm surge provides a better simulation for the beach erosion during the two storms.

6.5.4 Wave Height

As mentioned in section 6.3, the wave heights of the January 4, 1992 storm decayed strongly from offshore to shallow water. South of Ocean City, the storm was stronger than to the north. The wave parameters used in the numerical simulations may differ from the values which impacted the beaches during the storm. In general the exact storm wave parameters will not be available for simulations. The effects of wave heights on a numerical model are one of the most difficult problems in coastal engineering applications since rarely are the wave heights known well.

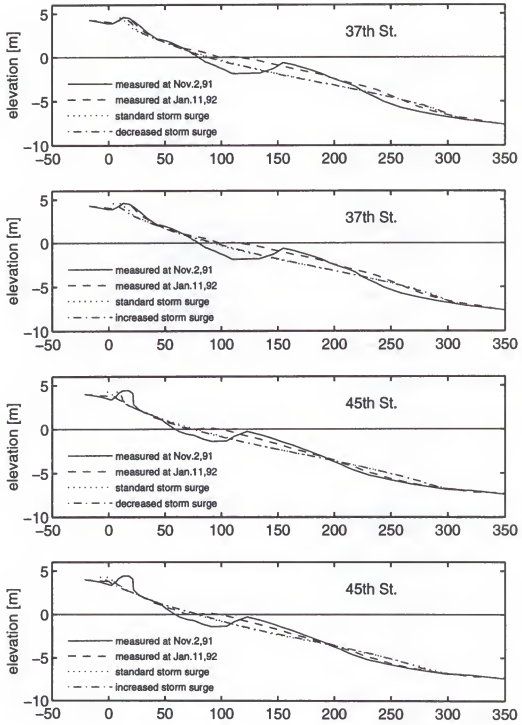

Figure 6.22 Comparisons of the measured profiles and the predictions of CROSS with the standard, 20% decreased an 20% increased storm surge levels.

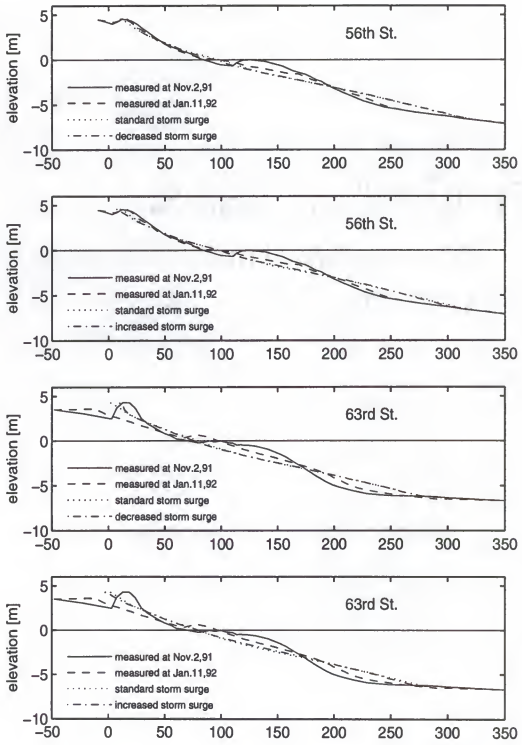

Figure 6.22 Continued

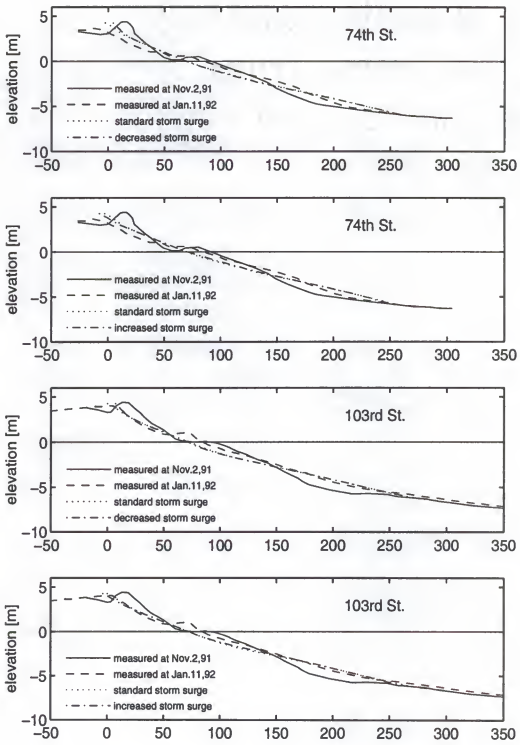

Figure 6.22 Continued

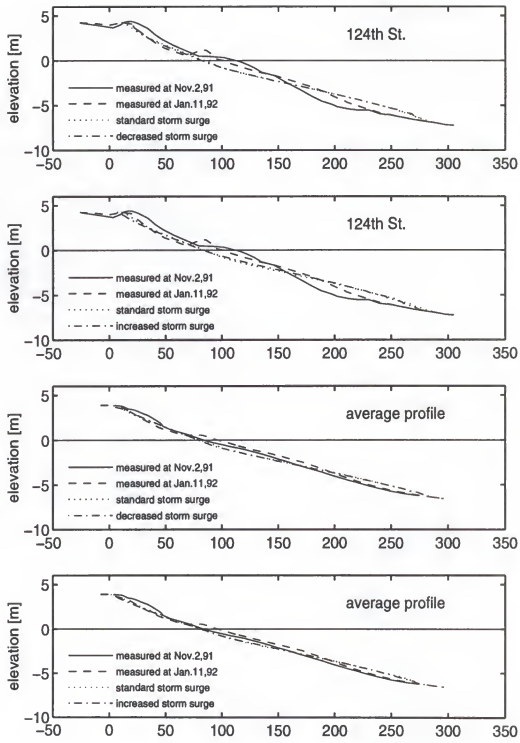

Figure 6.22 Continued.

Table 6.11 Sensitivity study of CROSS. The residuals, eroded volumes and beach retreat at the 3 meter contour predicted by the 20% increased and 20% decreased storm surges.

Profile	Storm surge	Residual		Eroded vol. (m^2)	Retreat at 3 m contour (m)
		w/o adjust.	with adjust		
37th St.	Standard	0.614	0.454	20.04	8.04
	Decreased	0.660	0.560	16.56	6.25
	Increased	0.579	0.372	27.12	9.20
45th St.	Standard	0.525	0.496	20.13	8.71
	Decreased	0.613	0.581	16.84	7.37
	Increased	0.448	0.421	22.93	11.05
56th St.	Standard	1.539	1.584	12.36	5.74
	Decreased	1.503	1.527	8.45	5.60
	Increased	1.463	1.498	16.43	7.32
63rd St.	Standard	0.854	0.854	17.71	9.27
	Decreased	0.868	0.869	15.47	8.60
	Increased	0.713	0.711	20.65	11.28
74th St.	Standard	0.511	0.524	25.41	11.69
	Decreased	0.578	0.576	22.15	9.15
	Increased	0.404	0.424	28.00	13.48
103rd St.	Standard	0.329	0.274	35.18	15.23
	Decreased	0.376	0.300	33.33	13.26
	Increased	0.293	0.238	38.81	17.01
124th St.	Standard	0.931	0.895	40.08	12.45
	Decreased	0.938	0.907	37.68	11.19
	Increased	0.813	0.783	46.02	14.70
Average profile basis	Standard	1.622	1.552	20.78	10.24
	Decreased	1.913	1.841	13.32	8.03
	Increased	1.334	1.248	26.03	12.45

Table 6.12 Sensitivity study of CROSS. The average residuals and errors of eroded volume and beach retreat at the 3 meter contour predicted by the 20% increased and 20% decreased storm surge.

Adjustment	Storm surge	Average residual	Error of eroded vol.		Error of retreat	
			ERR_{rms}	ERR_{ave}	ERR_{rms}	ERR_{ave}
Without adjustment	Standard	0.758	0.193	-0.190	0.334	-0.190
	Decreased	0.791	0.217	-0.296	0.369	-0.301
	Increased	0.673	0.188	-0.064	0.305	-0.043
With adjustment	Standard	0.725	0.227	-0.401	0.283	-0.359
	Decreased	0.760	0.284	-0.479	0.348	-0.446
	Increased	0.635	0.178	-0.307	0.229	-0.242

For the two storms which occurred at Ocean City during November 1991 and January 1992, the wave heights presented in Figures 6.3 and 6.4 are increased and decreased by 20% to test the sensitivity of the CROSS model. The predicted profiles with different wave heights are compared with the measurements in Figure 6.23. The residuals, eroded volumes and beach retreat at the 3-meter contour predicted by different wave heights are shown in Table 6.13 for the seven measured profiles and the average profile. Since the ratio of active water depth to wave height is fixed as 1.28, the active water depth shallows and deepens as wave heights decrease or increase. It appears that the subaqueous part of a profile is quite sensitive to the change of wave heights and the subaerial part is affected less. As a result, the variations of the eroded volume and beach retreat are mostly under 20% with the 20% change of wave heights, while the variations of the profile residual are much more significant. The average residuals and errors of eroded volume and beach retreat at the 3-meter contour predicted by different wave heights are presented in Table 6.14. Due to the variations in wave heights, the changes

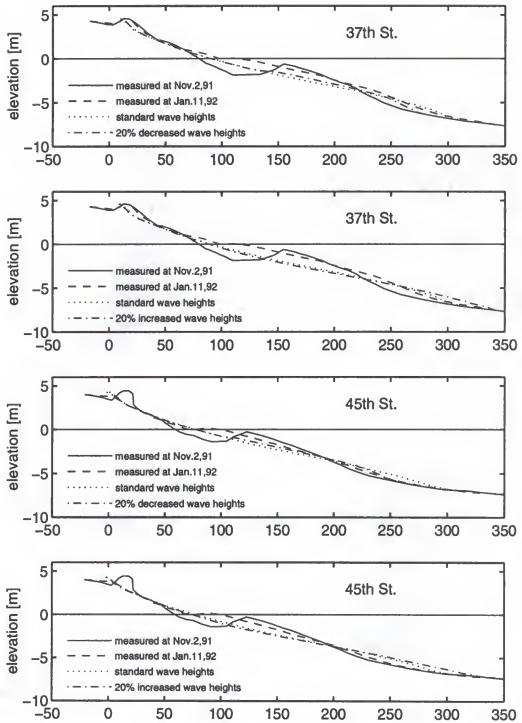

Figure 6.23 Comparisons of the measured profiles and the prediction of CROSS with the standard, 20% decreased an 20% increased wave heights.

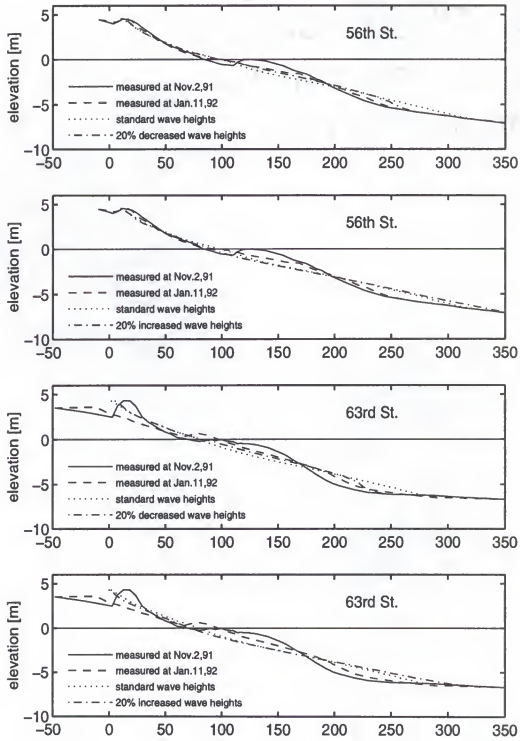

Figure 6.23 Continued.

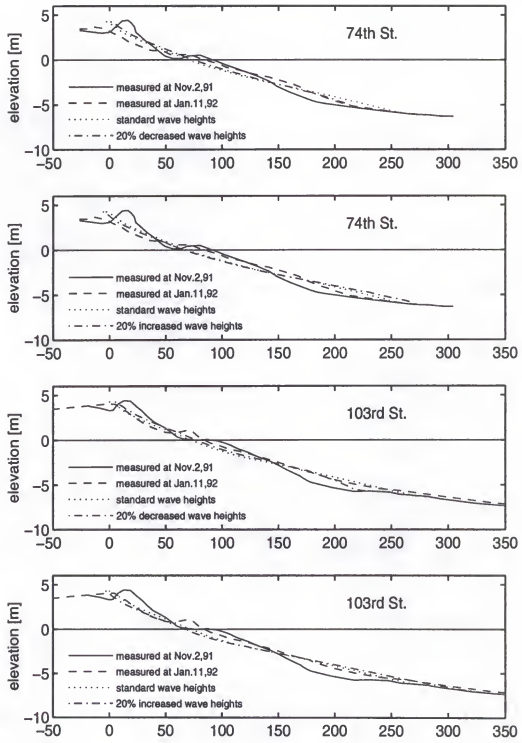

Figure 6.23 Continued.

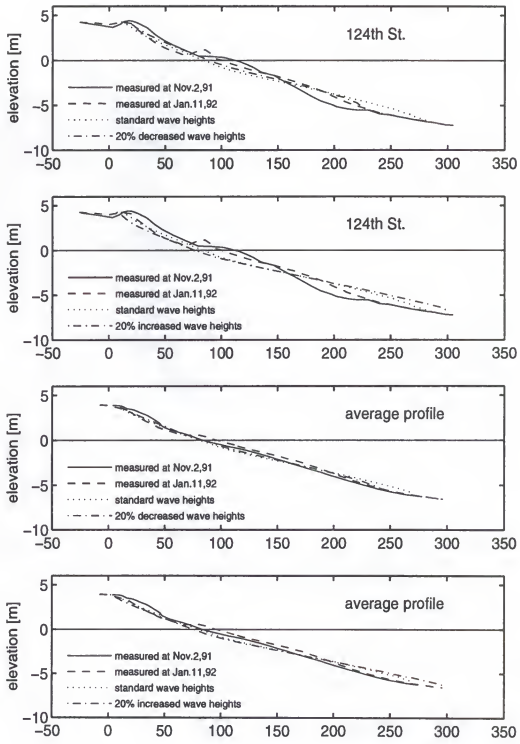

Figure 6.23 Continued.

Table 6.13 Sensitivity study of CROSS. The residuals, eroded volumes and beach retreat at the 3-meter contour predicted by 20% increased and 20% decreased wave heights.

Profile	Wave height	Residual		Eroded vol. (m^2)	Retreat at 3-m contour (m)
		w/o adjust.	with adjust		
37th St.	Standard	0.614	0.454	20.04	8.04
	Decreased	0.434	0.257	20.09	6.83
	Increased	0.936	0.768	24.90	8.68
45th St.	Standard	0.525	0.496	20.13	8.71
	Decreased	0.230	0.235	19.49	8.34
	Increased	0.914	0.845	22.45	10.61
56th St.	Standard	1.539	1.584	12.36	5.74
	Decreased	0.548	0.536	10.98	5.78
	Increased	2.333	2.449	15.41	7.79
63rd St.	Standard	0.854	0.854	17.71	9.27
	Decreased	0.464	0.462	16.56	8.73
	Increased	1.095	1.095	23.99	13.13
74th St.	Standard	0.511	0.524	25.41	11.69
	Decreased	0.462	0.472	18.35	7.47
	Increased	0.587	0.591	33.24	15.48
103rd St.	Standard	0.329	0.274	35.18	15.23
	Decreased	0.339	0.336	21.88	9.72
	Increased	0.466	0.316	51.51	20.38
124th St.	Standard	0.931	0.895	40.08	12.45
	Decreased	0.401	0.405	17.52	7.10
	Increased	1.690	1.601	62.94	18.93
Average profile basis	Standard	1.622	1.552	20.78	10.24
	Decreased	0.925	0.892	11.53	7.44
	Increased	2.524	2.341	32.81	13.68

Table 6.14 Sensitivity study of CROSS. The average residuals and errors of eroded volume and beach retreat at the 3 meter contour predicted by the 20% increased and 20% decreased wave heights.

Adjustment	Wave height	Average residual	Error of eroded vol.		Error of retreat	
			ERR_{rms}	ERR_{ave}	ERR_{rms}	ERR_{ave}
Without adjustment	Standard	0.758	0.193	-0.190	0.334	-0.190
	Decreased	0.411	0.344	-0.416	0.408	-0.386
	Increased	1.146	0.204	0.093	0.301	0.082
With adjustment	Standard	0.725	0.227	-0.401	0.283	-0.359
	Decreased	0.386	0.389	-0.567	0.400	-0.513
	Increased	1.095	0.147	-0.191	0.202	-0.143

of average residuals are higher than 30% and the changes in the errors of eroded volume and beach retreat at the 3 meter contour are about equal to or less than 20%.

6.6 Summary

This chapter has presented comparisons of the predictions of the CROSS model and three other commonly used models (CCCL, EDUNE and SBEACH) for storm erosion at Ocean City, Maryland during the November 1991 and January 1992 storms. The "2.5" factor was exercised in the CCCL model in this application. The wave run-up parameters used in the EDUNE model are determined according to the measured post-storm profiles and the maximum significant wave heights during two storms. Seven survey lines located from the southern (37th Street) to northern (124th Street) portions of the project are selected for evaluation of the four models. In most locations, the net volume changes in profiles are quite different from zero due to gradients in longshore transport. An adjustment is made by shifting

the whole profile horizontally a distance Δy to yield a zero net volume change for each profile.

A residual parameter is proposed to evaluate the agreement between the entire measured and predicted profiles (including subaerial and subaqueous parts). Two kinds of error averaged with different methods (root mean square and algebraic average) are provided to estimate the prediction of dune erosion. It appears that the residuals are less affected by the shifting adjustment, while eroded volumes and beach retreat are affected more significantly by the shift. Among the four models, the CCCL model is the only one which overpredicts average dune erosion. Considering profile residuals and errors of eroded volume and beach retreat together, CROSS, EDUNE and SBEACH version 3.0 present reasonable predictions for both dune erosion and entire profiles.

The sensitivity of CROSS to the transport coefficient, active water depth, storm surge levels and the storm wave heights are studied. It is shown that the CROSS model is quite insensitive to the transport coefficient for the beach erosion during the two storms at Ocean City, Maryland. With 20% change in the transport coefficient, the variations of average profile residuals and dune erosion are less than 9% and 7%, respectively. Since, it is based on a non-linear transport relationship, CROSS is less sensitive than a linear model when the initial profile conditions are close to equilibrium. With the ratio of active water depth to incoming wave height changed from 1.28 to 1, the profile residuals and errors of eroded volumes and beach retreat decrease significantly. It appears that the 1.28 ratio provides quite good predictions for profiles under constant wave conditions, while for a profile under irregular wave conditions, the active water depth equal to the instantaneous wave height presents

better results. To test the sensitivity of CROSS to the storm surge, the measured water levels in the two storm are decreased and increased 20% respectively. Overall, the 20% increased storm surge provide a better simulation for both profile residuals and dune erosion. With a ±20% variation in storm surge, the changes of average residuals and the errors of dune erosion are less than 10% and 15%, respectively. The sensitivity of CROSS to wave heights is investigated by a ±20% change of the measured wave heights. It appear that the subaqueous part of a profile is quite sensitive to the wave heights and the subaerial part is affected less. As a result, the variations of the eroded volume and beach retreat are generally less than 20% with a ±20% change of wave heights. However, the variations of the profile residual are much more significant and the changes of average residuals are higher than 30%.

CHAPTER 7
SUMMARY, CONCLUSIONS AND RECOMMENDATIONS

7.1 Summary

With a goal of providing accurate estimates of beach profile evolution in response to storm waves and high water levels and the adjustment of beach fill to long term wave action, cross-shore sediment transport relationships and models are studied. To better understand the mechanism of sediment transport, time-averaged bottom shear stresses are discussed quantitatively. A non-linear cross-shore sediment transport relationship is proposed based on the concepts of equilibrium beach profile and transport scale analysis. A finite difference method is applied to solve the sediment transport and the continuity equations numerically. The proposed non-linear transport relationship is calibrated and compared with the linear transport relationship for laboratory data. A total of seven large scale wave tank experiments from three different facilities are incorporated. The best-fit transport coefficient, K, is determined as the value yielding the overall least square error of eroded volume in each case. Based on the calibration results, an average transport coefficient and three characteristic profile slopes are determined for the CROSS model. The performance of CROSS is evaluated by the difference between the errors of eroded volume predicted by CROSS with fixed and best-fit K values. It appears that the predictions of CROSS with fixed and best-fit K values are quite close for the seven experiments.

The CROSS model is applied to the November 1991 and January 1992 storm erosion at Ocean City, Maryland. The predictions of CROSS are compared with three other commonly used models (CCCL, EDUNE and SBEACH). Based on the dune erosion level of post-storm profiles, the constant wave run-up parameter used in the EDUNE model is determined according to the maximum significant wave height during a storm. Seven survey lines located from the southern (37th Street) to northern (124th Street) portions of the project are selected. In most locations, the net volume changes in profiles are quite different from zero due to gradients in longshore sediment transport. An adjustment is made by shifting the whole profile horizontally a proper distance to yield a zero net volume change for each profile. A residual parameter is proposed to evaluate the agreement between the entire measured and predicted profiles. Two kinds of error averaged with different methods are given to estimate the predictions of dune erosion. The sensitivity of CROSS to the transport coefficient, active water depth, storm surge levels and the storm wave heights are studied.

7.2 Conclusions

The "closed loop" models, in which the cross-shore sediment transport rate is expressed in terms of the deviation of the actual wave energy dissipation per unit volume from equilibrium, are discussed in this study. The sediment transport is caused by deviations of a beach profile from its equilibrium form. According to scaling analysis, the linear transport relationship (n=1) proposed by Moore (1982) and Kriebel (1982) is modified and a non-linear transport equation (n=3), in which the transport rate is proportional to the cube of the difference of the local wave energy dissipation per unit volume from the equilibrium value, is developed. This non-linear transport relationship can explain the significant time scale

differences of profile evolution between various laboratory experiments. An analytical analysis of a similar process demonstrates that initial conditions cause considerable differences in the time scale of response for nonlinear systems but does not affect that of the linear systems.

The CROSS model is developed based on the non-linear transport relationship. Among the seven experiments used in the calibration of CROSS, five were conducted with regular wave conditions and the other two were carried out with random waves. Different wave conditions, initial profiles and sediment sizes characterized the experiments. The input dune, shoreline and offshore slopes used in the calibration model are determined according to the observed final profile in each experiments. It is noticed that the transport coefficient K in the non-linear transport relationship has a much narrower range than that of the linear. The average best-fit K value of the non-linear relationship is 7.14×10^{-10} m^8s^2/N^3 with a variation from -37% to +44%, whereas the best-fit K values of the linear relationship range from -74% to +248% of the average value of 6.07×10^{-6} m^4/N. On the average, the non-linear model yields much less error for the eroded volumes than the linear model. Based on these results, it appears that the non-linear transport relationship is more appropriate to represent the cross-shore sediment transport. The transport coefficient, K, of 7.14×10^{-10} m^8s^2/N^3 is recommended for applications of CROSS according to the average of the best-fit K values in the seven laboratory experiments.

Since individual best-fit K and dune, shoreline and offshore slopes were used in the calibration of CROSS for each experiment, the difference between the predictions of the calibration model with best-fit K and slope values and CROSS with fixed values is investigated. In the CROSS model, the dune, shoreline and offshore slopes are the average

slopes over the seven cases. CROSS with fixed values yields rather close predictions to the measurements for six of the seven experiments. The case of "dune with foreshore" with irregular waves in German large wave flume is an exception. In this case, the offshore slope formed during the experiment is about 0.5, which corresponds to an angle of 26.6°. This slope is unusually steep for a beach under wave action and is approximately equal to the static angle of repose of the sand material (26 to 34 degrees). The overprediction of CROSS is mainly due to the mild offshore slope (0.22) used in the model. After using the observed offshore slope of 0.5 in CROSS, the predictions of CROSS become quite close to measurements.

The CROSS model is compared with CCCL, EDUNE and SBEACH for the November 1991 and January 1992 storms at Ocean City, Maryland. Among the four models, the CCCL model is the only one which overpredicts average dune erosion; the other three underpredict erosion. The run-up used in EDUNE is constant over the entire simulation time of a storm and is determined according to the dune erosion level of post-storm profiles and the maximum significant wave height during the storm. Considering profile residuals and errors of eroded volume and beach retreat together, CROSS, EDUNE and SBEACH version 3.0 present reasonable predictions for both the dune erosional area and the entire profile. It is shown that CROSS is quite insensitive to the transport coefficient for the beach erosion during the two storms at Ocean City. With a decrease in the ratio of active water depth to incoming wave height from 1.28 to 1, the CROSS predictions are improved. Compared with the results of laboratory experiments, it appears that the ratio of 1.28 provides better predictions for profiles under monochromatic wave conditions and the ratio of 1.0 presents better results for a profile under irregular waves. The sensitivity of CROSS to storm surge

is tested by increasing and decreasing the measured water level by 20%. On average, the 20% increased storm surge provides better agreement for both profiles and dune erosion. As storm surge varies 20%, the changes of average profile residuals and errors of dune erosion are less than 10% and 15%, respectively. The sensitivity of CROSS to wave heights is investigated by a 20% change of the measured wave heights. The subaqueous part of a profile is quite sensitive to the wave heights and the subaerial part is affected less. As a result, the variations of the eroded volume and beach retreat are generally less than 20% with a 20% change of wave heights. However, the variations of the profile residual are much more significant and the changes of average residuals are higher than 30%.

7.3 Discussion and Recommendations

To better represent a profile change between the set-up limit to the run-up limit, swash mechanism and the corresponding sediment transport need to be taken into account in this region. During storms, overwash could affect dune erosion significantly, and thus should be represented.

As shown in the seven laboratory experiments, the eroded sediment was deposited offshore with different slopes during each experiment. In most experiments, the observed offshore slope is around 0.2. But in the case "dune without foreshore" with irregular waves, the offshore slope is 0.5 (corresponding to an angle of 26.6°) which is approximately equal to the static angle of repose for sand material. The explanation for such steep offshore slopes under wave action is not evident. The effects of offshore slope on dune erosion are quite significant when an initial profile is steep and far away from equilibrium.

In cross-shore sediment transport models, the active water depth is determined by incoming wave heights. Under monochromatic wave conditions, an offshore bar usually forms near the breaking point. Seaward of the offshore bar, there is no significant observable profile change in experiments. Therefore, the active water depth is defined as the breaking water depth in CROSS which is 1.28 times of the breaking wave height according to the McCowan (1894) theory. However, in the application of CROSS it appears that the active water depth of 1.28 times wave height is too large for Ocean City storm erosion. Decreasing active water depth to the instantaneous wave height provides improved predictions. It is also seen in the experiment of "dune without foreshore" with random waves in the German large wave flume that the limiting depth of beach profile change is about the same as the incoming significant wave height. It appears that the mechanism of beach erosion under regular and irregular waves is different. More random wave experiments should be conducted in future laboratory studies to evaluate the cause.

REFERENCES

Amos, C.L., Bowen, A.J., Huntley, D. A., and Lewis C.F.M. (1988) Ripple generation under the combined influences of waves and currents on the Canadian continental shelf. *Continental shelf Res.,* Vol. 8, No. 10, pp 1129-11953.

Bagnold, R.A. (1940) Beach formation by waves: Some model experiments in a wave tank. *Journal of the Institution of Civil Engineering*, Vol. 15, pp 27-52.

Bagnold, R.A. (1956) The flow of cohesionless grains in fluids. *Philosophical Transactions,* Royal Society of London, Series A, No.964, Vol.249, pp 235-297.

Bagnold, R.A. (1963) Mechanics of marine sedimentation. *The Sea, Ideas and Observations, Vol. 3, The earth beneath the sea.* Interscience, New York, pp 507-528.

Bagnold, R.A. (1966) An approach to the sediment transport problem from general physics. *Geological Survey Professional Paper 422-I,* U.S. Department of Interior.

Bailard, R.A. (1981) An energetics total load sediment transport model for a plane sloping beach. *Journal of Geophysical Research.* Vol. 86 (c11), pp 10938-10954.

Bailard, R.A. (1982) Modeling on-offshore sediment transport in the surf zone. *Proceedings of the 18th International Conference on Coastal Engineering*, Cape Town, ASCE, New York, pp 1419-1438.

Bailard, J.A. and Inman D.L. (1981) An Energetics bedload model for a plane sloping beach: local transport. *Journal of Geophysical Research,* 86 (c3): pp 2035-2043.

Bakker, M.T. (1968) The dynamics of a coast with a groyne system. *Proceeding of 11st International Conference on Coastal Engineering*, London, ASCE, New York, pp 491-517.

Bascom, W. (1951) The relationship between sand size and beach-face slope. *Transactions, American Geophysical Union,* Vol. 32, No. 6, December 1951, pp 866-874.

Broker Hedegaard, I., Roelvink, J.A., Southgate, H.N., Pechin, P., Nicholson, J. and Hamm, L. (1992) Intercomparison of coastal profile models. *Proceeding of 23rd International Conference on Coastal Engineering*, Venice, Italy, ASCE, New York, pp 2108-2121.

Bruun, P. (1954) Coastal erosion and the development of beach profiles. *Technical Memorandum No. 44,* U.S. Army Corps of Engineering, Beach Erosion Board.

Bruun, P. (1962) Sea level rise as a cause of shore erosion. *Journal of the Waterways and Harbors Division,* ASCE, Vol. 88 (WW1), pp 117-130.

Chiu, T.Y. and Dean, R.G. (1984) Methodology on coastal construction control line establishment. *Technical & Design Memorandum 84-6,* Beaches and Shore Resource Center, Florida State University, Tallahassee, FL.

Chiu, T.Y and Dean, R. G. (1986) Additional comparisons between computed and measured erosion by hurricanes. *Technical Report,* Beaches and Shore Resource Center, Florida State University, Tallahassee, FL.

Dally, W.R. (1980) A numerical model for beach profile evolution. *Master Thesis,* University of Delaware, Newark, DE.

Dally, W.R. and Dean, R.G. (1984) Suspended sediment transport and beach profile evolution. *Journal of Waterway, Port, Coastal , and Ocean Engineering*, ASCE, Vol. 110 (1), pp 15-33.

Dally, W.R., Dean, R.G. and Dalrymple, R.A. (1985) Wave height varication across beaches of arbitrary profile. *Journal of Geophysical Research*, Vol. 90 (c6), pp 11917-11927.

Dean, R.G. (1973) Heuristic models of sand transport in the surf zone. *Proceeding of Conference on Engineering Dynamics in the Surf Zone,* Sydney, Australia.

Dean, R.G. (1977) Equilibrium beach profiles : U.S. Atlantic and Gulf Coasts. *Ocean Engineering Report No. 12,* Department of Civil Engineering, University of Delaware.

Dean, R.G. (1987) Additional sediment input into the nearshore region. *Shore and Beach*, Vol.55: 3-4, pp 76-8.

Dean, R.G. (1994) Chapter III-3: Cross-shore sediment transport processes. *Draft of Coastal Engineering Manual.*

Dean, R.G. and Dalrymple, R. A. (1991) *Water Wave Mechanics for Engineers and Scientists*, World Scientific Publishing Co. Pte. Ltd., Singapore.

Dean, R.G. and Dalrymple, R. A. (1996) *Coastal Processes with Engineering Applications*, book to be published.

Deigaard, R., Fredsoe, J., and Hedegaard, I.B. (1986) Suspended sediment in the surf zone. *Journal of Waterway, Port, Coastal, and Ocean Engineering*, ASCE, Vol. 112 (1), pp 115-128.

Dette, H., Oelerich, J. and Rahlf, H. (1992) Time-dependent dune and beach transformations – prototype experiments with JONSWAP-Spectrum. *LWI-Report,* No. 735, Leichtweiss-Institute of Waterconstruction, Technical University Braunschweig.

Dette, H. and Rahlf, H. (1992) Time-dependent dune and beach transformations – prototype experiments with monochromatic waves. *LWI-Report,* No.734, Leichtweiss-Institute of Waterconstruction, Technical University Braunschweig.

Dette, H. and Uliczka, K. (1987) Prototype investigation on time-dependent dune recession and beach erosion. *Proceeding of Coastal Sediment'87,* Specialty Conference on Advances in Understanding of Coastal Sediment Processes, New Orleans, Louisiana, ASCE, pp 1430-1443.

Edelman, T. (1972) Dune erosion during storm conditions. *Proceeding of 13rd International Conference on Coastal Engineering*, ASCE, New York, pp 1305-1372.

Engelund, F. and Fredsoe, J. (1976) A sediment transport model for straight alluvial channels. *Nordic Hydrology,* Vol. 7, pp 293-306.

Grosskopf, W.G. and Stauble, D.K. (1993) Atlantic coast of Maryland (Ocean City) shoreline-protection plan. *Shore and Beach,* Vol. 61, No. 1, pp 3-7.

Hammond, T.M. And Collins, M.B. (1979) On the threshold of transport of sand-sized sediment under the combined influence of unidirectional and oscillatory flows. *Sedimentology*, Vol. 26, pp 795-812.

Hanes, D.M. and Inman, D.L. (1985) A dynamic yield for granule-fluid flow. *Journal of Geophysical Research*, Vol.90, No. B5, pp 3670-3674.

Hansen, J.B. and Svendsen, I.A. (1984) A theoretical and experimental study of undertow. *Proceeding of 19th International Conference on Coastal Engineering*, Houston, USA, pp 2246-2264.

Hughes, S.A. and Chiu, T.Y. (1978) The variations in beach profile when approximated by a theoretical curve. *UFL/COEL/TR-039,* Coastal and Oceanographic Engineering Department, University of Florida, Gainesville, FL.

Hughes, S.A. and Fowler, J.E. (1990) Validation of movable-bed modeling guidance. *Proceeding of 22nd International Conference on Coastal Engineering,* Delft, The Netherlands, ASCE, New York, pp 2457-2470.

Hunt, I.A. Jr. (1958) Design of seawall and breakwaters. *U.S. Lake Survey,* Corps of Engineers, U.S. Army, January 1958.

Inman, D.L., Elwany, M.H.S. and Jenkins, S.A. (1993) Shorerise and bar-berm profiles on ocean beaches. *Journal of Geophysical Research,* Vol. 98 (c10), pp 18181-18199.

Jensen R.E. and Garcia A. (1993) Wind, wave and water level assessment for the January 4, 1992 storm at Ocean City, *Maryland. Shore and Beach,* Vol. 61, No.1, pp 13-22.

Kraus, N.C. (1988) Beach profile change measured in the tank for large waves 1956-1957 and 1962. *Technical Report CERC-88-6,* CERC, U.S. Army WES, Vicksburg, MS.

Kraus, N.C. and Smith, J.M. (1994) SUPERTANK laboratory data collection project, volume I: Main Text. *Technical Report CERC-94-3,* CERC, U.S. Army WES, Vicksburg, MS.

Kraus, N.C. and Wise R.A. (1993) Simulation of January 4, 1992 storm erosion at Ocean City, Maryland. *Shore and Beach,* Vol. 61, No.1, pp 13-22.

Kriebel, D.L. (1982) Beach and dune response to hurricanes. *Master's Thesis,* University of Delaware, Newark, DE.

Kriebel, D.L (1986) Verification study of dune erosion model. *Shore and Beach,* Vol. 54, No.3, pp 13-21.

Kriebel, D.L (1989) Users manual for dune erosion model EDUNE.

Kriebel, D.L (1990) Advances in numerical modeling of dune erosion. *Proceeding of 22nd International Conference on Coastal Engineering,* Delft, The Netherlands, ASCE, New York, pp 2304-2317.

Kriebel, D.L. and Dean, R.G. (1985) Numerical simulation of time-dependent beach and dune erosion. *Coastal Engineering,* Vol. 9, pp 221-245.

Kriebel, D.L., Dally, W.R. and Dean, R.G. (1986) Undistorted Froude model for surf zone sediment transport. *Proceeding of 20th International Conference on Coastal Engineering,* Taipei, ASCE, New York, pp 1296-1310.

Larson, M. (1988) Quantification of beach profile change. *Report 1008,* Department of Water Resources Engineering, University of Lund.

Larson, M. and Kraus, N.C. (1989) SBEACH: numerical model for simulating storm-induced beach change, Report 1: theory and model foundation. *Technical Report CERC-89-9,* CERC, U.S. Army WES, Vicksburg, MS.

Larson, M., Kraus, N.C., and Byrnes M.R. (1989) SBEACH: numerical model for simulating storm-induced beach change, Report 2: numerical formulation and model tests. *Technical Report CERC-89-9,* CERC, U.S. Army WES, Vicksburg, MS.

Longuet-Higgins, M.S. (1953) Mass transport in water waves. *Philosophical Transactions,* Royal Society of London, Series A, No.903, Vol.245, pp 535-581.

Longuet-Higgins, M.S. (1983) On the joint distribution of wave periods and amplitudes in a random wave field. *Proceedings of the Royal Society of London*, Series A, Vol. 389, pp 241-258.

Longuet-Higgins, M.S. and Stewart, R.W. (1964) Radiation stresses in water waves; a physical discussion with application. *Deep Sea Research,* Vol. 2, pp 529-546, 561-562.

McCowan, J. (1894) On the highest wave theory of permanent type. *Philosophical Magazine and Journal of Science,* Ser. 5th, Vol. 38, 1894.

Moore, B.D. (1982) Beach profile evolution in response to changes in water level and wave height. *Masters's Thesis,* University of Delaware, Newark, DE.

Natarajan, P. (1969) Sand movement by combined action of waves and currents. *Ph.D. dissertation*, University of London.

Nairn, R.B. (1990) Prediction of cross-shore sediment transport and beach profile evolution. *Ph. D.* Dissertation, University of London.

Nielsen, P. (1992) *Coastal Bottom Boundary Layers and Sediment Transport.* World Scientific Publishing Co. Pte. Ltd., Singapore.

Nishimura, H. and Sunamura, T. (1986) Numerical simulation of beach profile changes. *Proceeding of 20th International Conference on Coastal Engineering*, Taipei, ASCE, New York, pp 1444-1455.

Okayasu, A. Shibayama, T. And Horikawa, K. (1988). Vertical variation of undertow in the surf zone. *Proceeding of 21st International Conference on Coastal Engineering*, Malaga, Spain, ASCE, New York, pp 478-491.

Reid, R.O. (1957) Modification of the quadratic bottom-stress law for turbulent channel flow in the presence of surface wind. *Technical Memorandum No. 93,* Beach Erosion Board, Office of the Chief Engineers, Department of the Army Corps of Engineers.

Roelvink, J.A. and Stive, M.J.F. (1989) Bar-generating cross-shore flow mechanisms on the beach. *Journal of Geophysical Research,* Vol. 94 (c4), pp 4785-4800.

Saville, T., Jr. and Watts, G.M. (1969) (Untitled). *PIANC 22nd International Navigation Conference,* Section II, Subject 4, pp 249-271.

Schoonees, J.S. and Theron, A.K. (1995) Evaluation of 10 cross-shore sediment transport morphological models. *Coastal Engineering,* Vol. 25, pp 1-41.

Shibayama, T. And Horikawa, K. (1982) Sediment transport and beach transformation due to waves. *Proceeding of 18th International Conference on Coastal Engineering*, Cape Town, ASCE, New York, pp 1439-1458.

Smith, J.M. and Kraus, N.C.(1995) SUPERTANK laboratory data collection project, volume II: Appendices A-I. *Technical Report CERC-94-3,* CERC, U.S. Army WES, Vicksburg, MS.

Steetzel, H.J. (1993) Cross-shore transport during storm surges. *Ph. D. Dissertation*, Delft Hydraulics.

Stive, M.J.F. (1986) A model for cross-shore sediment transport. *Proceeding of 20th International Conference on Coastal Engineering*, Taipei, ASCE, New York, pp 1550-1564.

Stauble, D.K., Garcia A.W. and Kraus, N.C. (1993) Beach nourishment project response and design evaluation : Ocean City, Maryland; report 1, 1988-1992. *Technical Report,* CERC-93-13, CERC, U.S. Army WES, Vicksburg, MS.

Stive, M.J.F. and Wind H.G. (1982) A study of radiation stress and set-up in the nearshore region. *Coastal Engineering,* Vol. 6, pp 1-25.

Swart, D.H. (1974a) Offshore sediment transport and equilibrium beach profiles. *Publication No. 131,* Delft Hydraulics Laboratory.

Swart, D.H. (1974b) A schematization of onshore-offshore transport. *Proceeding of 14th International Conference on Coastal Engineering*, Copenhagen, ASCE, New York, pp 884-900.

Ting, F.C.K. and Kirby, J.T. (1994) Observation of undertow and turbulence in a laboratory surf zone. *Coastal Engineering,* Vol. 24, pp 51-80.

Trowbridge, J. and Young, D. (1989) Sand transport by unbroken water waves under sheet flow conditions. *Journal of Geophysical Research,* 94 (c8), pp 10971-10991.

Vellinga, P. (1983) Predictive computational model for beach and dune erosion during storm surges. *Proceedings of ASCE Specialty Conference, Coastal Structures 1983,* pp 806-819.

Watanabe, A. (1988) Numerical predictive model of evolution of beach topography. *Nearshore Dynamics and Coastal Processes, Part III.* University of Tokyo.

BIOGRAPHICAL SKETCH

Jie Zheng was born on September 5, 1963 in Nanjing, Jiangsu Province, P.R. China. She earned her bachelor's and master's degrees in applied mechanics from Beijing University of Aeronautics & Astronautics, Bejing, China, in 1985 and 1988, respectively. While studying for her master's degree, she worked in the field of flight dynamics and control. From 1988 to 1991, she worked as a research associate in the Department of Chemical Engineering, Dalian University of Technology, Dalian, China. During this period, a beautiful beach a mile away from her apartment moved her and she fell in love with the ocean. After she came to Gainesville, FL to visit her husband Jian Liu, she found the Department of Coastal and Oceanographic Engineering at the University of Florida. Since fall 1992, she has been pursuing a Ph.D degree in the department under the advisement of Professor Robert G. Dean.

I certify that I have read this study and that in my opinion it conforms to acceptable standards of scholarly presentation and is fully adequate, in scope and quality, as a dissertation for the degree of Doctor of Philosophy.

Robert G. Dean, Chair
Graduate Research Professor
of Coastal and Oceanographic
Engineering

I certify that I have read this study and that in my opinion it conforms to acceptable standards of scholarly presentation and is fully adequate, in scope and quality, as a dissertation for the degree of Doctor of Philosophy.

Hsiang Wang
Professor of Coastal and
Oceanographic Engineering

I certify that I have read this study and that in my opinion it conforms to acceptable standards of scholarly presentation and is fully adequate, in scope and quality, as a dissertation for the degree of Doctor of Philosophy.

Daniel M. Hanes
Associate Professor of Coastal and
Oceanographic Engineering

I certify that I have read this study and that in my opinion it conforms to acceptable standards of scholarly presentation and is fully adequate, in scope and quality, as a dissertation for the degree of Doctor of Philosophy.

Robert J. Thieke
Assistant Professor of Coastal and Oceanographic Engineering

I certify that I have read this study and that in my opinion it conforms to acceptable standards of scholarly presentation and is fully adequate, in scope and quality, as a dissertation for the degree of Doctor of Philosophy.

Ulirich H. Kurzweg
Professor of Aerospace Engineering, Mechanics and Engineering Science

This dissertation was submitted to the Graduate Faculty of the College of Engineering and to the Graduate School and was accepted as partial fulfillment of the requirements for the degree of Doctor of Philosophy.

August, 1996

Winfred M. Phillips
Dean, College of Engineering

Karen A. Holbrook
Dean, Graduate School